

Early conformational changes control spontaneous polyQ-mediated huntingtin polymerization

Dissertation zur Erlangung des akademischen Grades des
Doktors der Naturwissenschaften (Dr. rer. nat.)

Eingereicht im Fachbereich Biologie, Chemie, Pharmazie
der Freien Universität Berlin

vorgelegt von

Anne Sophie Wagner

aus Stuttgart

Oktober, 2011

Die Arbeit wurde im Zeitraum von April 2007 bis Oktober 2011 unter der Leitung von Herrn Prof. Dr. Erich E. Wanker am Max Delbrück Centrum für Molekulare Medizin Berlin-Buch angefertigt.

1. Gutachter: Prof. Dr. Erich E. Wanker

2. Gutachter: Prof. Dr. Fritz G. Rathjen

Disputation am 13. April 2012

Danksagung

Ich danke Herrn Prof. Dr. Erich Wanker für die Überlassung des Themas wie auch der Bereitstellung von finanziellen Mitteln und sein Know-how.

Vielen Dank an „meine“ Mathematiker Jana und Toni, die durch die Erstellung des Modells meine Ergebnisse noch aufgewertet haben und die immer mit neuen Ideen und Denkanstößen mich bei meinem Projekt unterstützt haben. Außerdem möchte ich noch Dr. Bettina Purfürst von der EM-Corefacility am MDC danken. Mit ihrer Unterstützung wurden die Elektronenmikroskopie-Bilder in dieser Arbeit erstellt.

Des Weiteren danke ich allen Kollegen der AG Wanker, besonders allen im 1. Stock des Flachbaus, für ihre Hilfe bei alltäglichen Problemen im Labor sowie für die angenehme Arbeitsatmosphäre.

Dr. Katja Mühlenberg, Dr. Jan Bieschke und Dr. Ralph Friedrich, Anne Möller, Maliha Shah und Anup Arumughan danke ich für ihre Hilfsbereitschaft und Unterstützung bei der Erstellung dieser Arbeit und viele wertvolle Anregungen.

Mein besonderer Dank gilt meinen Eltern und Freunden. Auch wenn ich sie die letzten Monate mitunter etwas vernachlässigt habe waren sie immer für mich da und haben mich stets unterstützt.

Zusammenfassung

In Gehirnen von Patienten mit neurodegenerativen Erkrankungen wurden Ablagerungen von fehlgefalteten Proteinen in neuronalen Einschlüssen gefunden, die als ein gemeinsames pathologisches Merkmal angesehen werden können. Zu diesen Krankheiten gehören die Alzheimer Erkrankung, die Parkinson Erkrankung und die Polyglutaminerkrankungen, zu denen auch Chorea Huntington zählt.

Experimentelle Ergebnisse weisen darauf hin, dass Konformationsänderungen in löslichen amyloiden Proteinen, die der Aggregation voraus gehen, kritisch für den Verlauf der Pathogenese bei Fehlfaltungskrankheiten sind. Obwohl diese Proteine unterschiedliche Aminosäuresequenzen aufweisen, haben die gebildeten unlöslichen Proteinaggregate gemeinsame Charakteristika. Amyloidogene Proteine aggregieren zu fibrillären Aggregaten mit einem hohen Anteil an β -Faltblattstrukturen. Ein besseres Verständnis der molekularen Mechanismen wie Amyloidaggregate in vitro und vivo gebildet werden, ist äußerst wichtig für die Krankheitsforschung und für die Entwicklung von neuen Therapien zur Behandlung von Proteinefehlfaltungs-Erkrankungen.

Es gibt eine Vielzahl von Anhaltspunkten, die darauf hindeuten, dass die Polyglutamin-Domäne in N-terminalen Huntingtin (Htt) Fragmenten für die Aggregation der Proteine in unlösliche fibrilläre Aggregate verantwortlich ist. In dieser Arbeit wurde die spontane Aggregation eines Htt Exon 1 Fragments mit 49 Glutaminen (Ex1Q49) systematisch untersucht. Dazu wurden Zeit-aufgelöste Polymerisationsversuche durchgeführt und Epitop-spezifische Antikörper eingesetzt, um zu zeigen, dass frühe Konformationsänderungen in der polyQ-Domäne von Ex1Q49 den Beginn der Aggregation kontrollieren. Die Stabilisierung einer spezifischen Polyglutamin-Konformation durch die Wirkung des kleinen Moleküls O4 konnte mit Hilfe des monoklonalen Antikörpers 3B5H10 nachgewiesen werden. Außerdem konnte gezeigt werden, dass durch die Stabilisierung dieser Polyglutamin-Konformation die Bildung von unlöslichen Ex1Q49 Aggregaten verzögert wird. Die Ergebnisse lassen vermuten, dass die Bildung dieser Polyglutamin-Konformation eine Voraussetzung dafür ist, dass das Ex1Q49 Protein effizient in amyloide Strukturen polymerisieren kann. Die Wichtigkeit dieser biochemischen Ergebnisse wurde durch mathematische Modellierung des Aggregationsprozesses unterstützt. Das Modell sagt voraus, dass ein autokatalytischer Prozess für die spontane Bildung von fibrillären Ex1Q49 Aggregaten verantwortlich ist.

Weiterhin konnte gezeigt werden, dass durch die Deletion von 15 N-terminalen Aminosäuren im Ex1Q49 Protein ($\Delta N15Ex1Q49$) die spontane Proteinaggregation dramatisch verlangsamt wird. Diese Ergebnisse unterstützen eine kürzlich publizierte Studie, die zeigt dass N-terminale Aminosäuren in Htt für die intermolekulare Interaktion von Ex1Q49 Molekülen wichtig sind.

Durch die Behandlung von Zellen mit der Substanz O4 konnte die relative Menge an Ex1Q49 Molekülen, die mit den Polyglutamin-spezifischen Antikörpern 3B5H10 und MW1 erkannt werden, erhöht werden. In früheren Studien wurde die Immunoreaktivität der Antikörpers 3B5H10 in Zellen mit einer erhöhten Toxizität von pathogenen Htt-Exon1-Fragmenten in Zusammenhang gebracht. Es konnte hier jedoch gezeigt werden, dass die erhöhte Reaktivität des Antikörpers 3B5H10 nicht mit einer Zunahme der Toxizität verbunden ist. Diese Untersuchungen deuten darauf hin, dass lösliche Htt Proteine mit einer für Antikörper zugänglichen Polyglutaminsequenz für Zellen nicht toxisch sind.

Die Ergebnisse erlauben ein besseres Verständnis des molekularen Mechanismus der spontanen Polyglutamin-vermittelten Polymerisation von N-terminalen Htt-Fragmenten. Außerdem helfen sie neue Substanzen zu finden, die die Selbstassoziation von mutierten Htt Fragmenten beeinflussen.

Summary

The deposition of misfolded proteins in inclusion bodies of patient brains has been recognized as a common pathological hallmark of a large number of neurodegenerative diseases, including Alzheimer's disease (AD), Parkinson's disease (PD) and polyglutamine (polyQ) diseases, such as Huntington's disease (HD). Increasing experimental evidence indicates that conformational changes in disease proteins that precede aggregation are critical for pathogenesis in protein misfolding disorders. Despite the distinct primary amino acids of disease-causing proteins, the insoluble protein aggregates share a common characteristic, namely that they are β -sheet-rich amyloid fibrils. A better understanding of the molecular mechanism of how amyloid aggregates are formed *in vitro* and *in vivo* is of high importance for disease research and the development of therapies against amyloid diseases.

Several lines of evidence indicate that polyQ tracts in N-terminal huntingtin (Htt) fragments promote their aggregation into insoluble β -sheet-rich fibrillar aggregates. In this study, the spontaneous self-assembly of Htt-exon 1 fragments with a pathogenic polyQ tract of 49 glutamines (Ex1Q49) was systematically analyzed using time-resolved amyloid polymerization assays and epitope-specific antibodies, to show that early conformational changes in the polyQ tract of Ex1Q49 control the onset of spontaneous amyloid polymerization. Stabilizing a distinct polyQ conformation specifically recognized by the monoclonal antibody 3B5H10 through the action of a small molecule (O4) delays the onset of Ex1Q49 amyloidogenesis, indicating that formation of this polyQ structure is a prerequisite for efficient amyloid assembly. The importance of these observations was emphasized by comprehensive mathematical modeling studies. Based on the data the model predicts that β -sheet-rich Ex1Q49 amyloid fibrils are spontaneously formed by a prion-like autocatalytic process.

Deletion of 15 N-terminal amino acids in the Htt-exon 1 fragment reduces the rate of spontaneous amyloid polymerization without changing the mechanism of aggregation. The results suggest that the N-terminus enhances nucleus formation by forming intramolecular interactions or by promoting intermolecular interactions with other monomers.

Treatment of cells with the compound O4 increases the relative amount of soluble Htt molecules with exposed polyQ tracts that can be recognized by the anti-polyQ antibodies 3B5H10 and MW1. 3B5H10 has been shown before to recognize a toxic Htt conformation in cells. However, no increase in polyQ-induced toxicity was observed in O4 treated SH-EP

cells expressing a Htt-exon 1 fragment with 73 glutamines fused to YFP, indicating that soluble Htt proteins with exposed polyQ tracts are non-toxic for mammalian cells.

Taken together, the experimental and theoretical studies provide a basis for a better understanding of the molecular mechanism by which expanded polyQ tracts promote the spontaneous polymerization of Htt fragments. In addition, the results might help to develop therapeutic small molecules that target different events in the Htt amyloid assembly process.

Contents

1. Introduction	1
1.1 Protein aggregation and conformational diseases	1
1.1.1 Protein folding and misfolding	1
1.1.2 Protein aggregation and amyloid-like inclusions	5
1.2 Chorea Huntington	11
1.2.1 Clinical manifestation and neuropathology	11
1.2.2 Genetics	13
1.2.3 The huntingtin protein	13
1.2.4 Misfolding, aggregation and toxicity of mutant Htt	15
1.2.5 Anti-Htt antibodies are useful tools for the detection of Htt conformations	19
1.3 Aims	21
2. Results	22
2.1 Investigating spontaneous Htt-exon 1 aggregation with time-resolved assays <i>in vitro</i>	22
2.1.1 Generation of the plasmid pGEX-6P1-HttEx1Q49 for the expression of GST-Ex1Q49	22
2.1.2 Production and characterization of GST-Ex1Q49 fusion protein	23
2.1.3 Establishing a filter retardation assay for the detection of SDS-resistant Ex1Q49 aggregates	25
2.1.4 Investigating the spontaneous aggregation of Ex1Q49 with Thioflavin T binding assays and circular dichroism spectroscopy	28
2.1.5 Characterization of Ex1Q49 aggregate morphology by atomic force microscopy and electron microscopy	29
2.1.6 Analysis of Ex1Q49 aggregates by semi-denaturing detergent agarose gel electrophoreses	30
2.1.7 Investigating the formation of Ex1Q49 aggregation intermediates by size exclusion chromatography (SEC)	31
2.1.8 Spontaneous Ex1Q49 aggregation is a nucleation-dependent process	33
2.1.9 Analysis of polyQ-mediated Htt aggregation after proteolytic cleavage of GST-Ex1Q49 fusion protein with trypsin	34
2.1.10 Trypsin generated Δ NTEx1Q49 fragments form low molecular weight SDS-stable aggregation intermediates	37
2.2 Analysis of spontaneous Ex1Q49 aggregation with epitope specific Htt antibodies	37
2.3 Investigating the effects of small molecules on Ex1Q49 aggregation <i>in vitro</i>	40
2.3.1 The related chemical compounds orcein, O4 and resorufin influence spontaneous Ex1Q49 aggregation in cell-free assays	40
2.4 Investigating the mechanism of spontaneous Ex1Q49 aggregation using the chemical compound O4	43
2.4.1 O4 influences early events in the Ex1Q49 aggregation cascade	43
2.4.2 Characterization of O4 treated Ex1Q49 aggregates by atomic force microscopy and electron microscopy	46
2.4.3 Seeding eliminates the delay in aggregate formation induced by O4	48
2.4.4 O4 treatment alters the binding of epitope specific antibodies to aggregation-prone Ex1Q49 molecules	48
2.5 Effects of O4 treatment on Htt polyQ conformations and toxicity in cell-based assays	50

2.6	Investigating the spontaneous aggregation of an N-terminally truncated Htt-exon 1 fragment	55
2.6.1	Generation of the plasmid pGEX-6P1- Δ NHttEx1Q49 for the expression of the GST- Δ NEx1Q49 fusion protein	55
2.6.2	Production and purification of GST- Δ NEx1Q49 fusion protein	56
2.6.3	Analysis of Δ NEx1Q49 aggregation using cell-free assays	56
2.6.4	Investigating the formation of Δ NEx1Q49 aggregation intermediates by SDD-AGE, size exclusion chromatography and CD spectroscopy	59
2.6.5	O4 influences spontaneous aggregation of Δ NEx1Q49 protein	62
3.	Discussion	65
3.1	Mechanism of spontaneous polyQ-mediated Htt-exon 1 aggregation	65
3.1.1	GST Htt-exon 1 fragments form oligomers <i>in vitro</i>	65
3.1.2	Early conformational changes are critical for Ex1Q49 aggregation	66
3.1.3	The compound O4 stabilizes an early conformation in the aggregation cascade	72
3.1.4	Fitting the kinetic Ex1Q49 aggregation data to a mathematical model	73
3.2	Effect of flanking sequences on Htt aggregation	77
3.3	Structural characterization of Htt conformations and aggregates	80
3.4	Implications of O4-mediated effects on Ex1Q49 aggregation for Huntington's disease pathogenesis	81
3.5	Outlook	85
4.	Materials and Methods	86
4.1	Materials	86
4.1.1	Bacterial strains	86
4.1.2	Cell lines	86
4.1.3	Expression vectors and plasmids	86
4.1.4	Microbiological media and buffers	87
4.1.5	Media and supplements for cell culture	89
4.1.6	Antibodies	89
4.1.7	Oligonucleotides	90
4.1.8	Enzymes, proteins and markers	90
4.1.9	Kits	91
4.1.10	Chemicals and consumables	91
4.1.11	Laboratory equipment	93
4.1.12	Software	93
4.2	Methods	94
4.2.1	Molecular biology	94
4.2.2	Protein biochemistry	98
4.2.3	Analytical methods	103
4.2.4	Methods in cell biology	104
5.	Literature	108
6.	List of Abbreviations	117

List of Figures

Figure 1.1: The 4 levels of protein structure.....	2
Figure 1.2: Energy landscape for protein folding.	3
Figure 1.3: Schematic representation of the protein aggregation pathway.....	8
Figure 1.4: Cell type-specific characteristics of neuronal populations affected in HD.	12
Figure 2.1: Generation of the plasmid pGEX-6P1-HttEx1Q49 for the expression of GST-Ex1Q49 fusion protein.	22
Figure 2.2: Analysis of the proteins GST-Ex1Q49 and GST by SDS-PAGE and immunoblotting.....	23
Figure 2.3: Soluble GST-Ex1Q49 is a mainly α -helical protein.	24
Figure 2.4: Schematic representation of the filter retardation assay (FRA).	25
Figure 2.5: Proteolytic cleavage of GST-Ex1Q49 with PP induces the formation of SDS-resistant Ex1Q49 aggregates.	26
Figure 2.6: Increasing the concentration of GST-Ex1Q49 enhances the spontaneous formation of Ex1Q49 aggregates.	27
Figure 2.7: Cleavage of GST-Ex1Q49 fusion protein with PreScission protease.	28
Figure 2.8: Ex1Q49 fragments self-assemble into insoluble protein aggregates with a β -sheet-rich conformation.	29
Figure 2.9: Ex1Q49 forms large bundled fibrillar aggregates visualized by atomic force microscopy..	29
Figure 2.10: Ex1Q49 molecules assemble into aggregates with a typical fibrillar morphology.	30
Figure 2.11: Detection of high molecular weight SDS-stable Ex1Q49 aggregates by SDD-AGE analysis.....	31
Figure 2.12: Ex1Q49 molecules form transient SDS-unstable oligomers that over time assemble into large amyloid aggregates.	33
Figure 2.13: Addition of seeds to Ex1Q49 aggregation reactions leads to a reduction of the lag phase	34
Figure 2.14: Proteolytic cleavage of GST-Ex1Q49 fusion protein with trypsin.	35
Figure 2.15: Δ NTEEx1Q49 assembles into SDS-stable aggregates with a fibrillar morphology.	36
Figure 2.16: Δ NTEEx1Q49 assembles into fibrillar aggregates by a nucleation-dependent mechanism.	36
Figure 2.17: Cleavage of GST-Ex1Q49 with trypsin results in the formation of SDS-stable oligomers.	37
Figure 2.18: GST-Ex1Q49 undergoes a rapid conformational change after cleavage with PP.....	38
Figure 2.19: The monoclonal antibody MW8 specifically detects the formation of SDS-resistant aggregates observed in dot blot assays.....	39
Figure 2.20: Aggregation of GST-Ex1Q49 can be altered by addition of chemical compounds.....	41
Figure 2.21: The related compounds resorufin, O4 and orcein delay the formation of SDS-insoluble aggregates monitored by filter retardation assay.	42
Figure 2.22: Cleavage of GST-Ex1Q49 is not influenced by the addition of compounds.	42
Figure 2.23: In FRA, O4 elongates the lag phase of Ex1Q49 aggregation in a concentration-dependent manner.	43
Figure 2.24: O4 influences early events in the Δ NTEEx1Q49 aggregation cascade.	44
Figure 2.25: Investigating the effects of O4 on spontaneous Ex1Q49 aggregation by filter retardation assay and dynamic light scattering.	45
Figure 2.26: O4 treatment does not stabilize SDS-stable low molecular weight oligomers.....	45
Figure 2.27: O4 delays the formation of SDS-resistant aggregates in a time-dependent manner.	46
Figure 2.28: Ex1Q49 aggregates formed in the presence of O4 have a fibrillar morphology.	47
Figure 2.29: O4 treatment does not alter the morphology of fibrillar Ex1Q49 aggregates.	47
Figure 2.30: Addition of seeds to Ex1Q49 aggregation reactions leads to a reduction of the lag phase.	48
Figure 2.31: O4 stabilizes an early soluble 3B5H10-reactive polyQ conformation that disappears over time with the formation of SDS-stable protein aggregates.....	49
Figure 2.32: Generation of a plasmid for the expression of a YFP-Ex1Q73 fusion protein in SH-EP cells using the Gateway® technology.	50
Figure 2.33: High concentrations of O4 are toxic for SH-EP cells.	51

Figure 2.34: O4 treatment increases the amount of MW1 and 3B5H10 reactive, soluble YFP-Ex1Q73 molecules in mammalian cells.....	52
Figure 2.35: Expression levels of Ex1Q73-YFP and YFP are not changed upon treatment with O4. ...	52
Figure 2.36: The abundance of YFP-Ex1Q79 aggregates in SH-EP cells is not altered by the addition of O4.....	53
Figure 2.37: The anti-polyQ antibodies MW1 and 3B5H10 specifically recognize Htt structures that are localized at the cell membrane.....	54
Figure 2.38: Generation of the plasmid pGEX-6P1- Δ NHttEx1Q49 for the expression of GST- Δ NEx1Q49.....	55
Figure 2.39: Purification and characterization of GST- Δ NEx1Q49 fusion protein.	56
Figure 2.40: Investigating the formation of Δ NEx1Q49 aggregates by filter retardation assay and ThT assays.	57
Figure 2.41: Analysis of spontaneously formed Δ NEx1Q49 aggregates by atomic force microscopy.	58
Figure 2.42: The protein Δ NEx1Q49 converts via low molecular weight SDS-stable oligomers into fibrillar aggregates.....	58
Figure 2.43: Investigating the formation of Δ NEx1Q49 aggregates by SDD-AGE experiments.....	59
Figure 2.44: Δ NEx1Q49 forms small oligomers with a molecular size of 46 kDa in a time-dependent manner.	60
Figure 2.45: The 46 kDa fraction of Δ NEx1Q49 is immunoreactive with the 3B5H10 and GST antibodies.	61
Figure 2.46: Removal of the GST-tag from the GST- Δ NEx1Q49 fusion protein diminishes the α -helical content of the Htt-exon 1 fragments.....	62
Figure 2.47: O4 delays the formation of SDS-resistant aggregates by stabilizing a 3B5H10 reactive polyQ conformation.	63
Figure 2.48: O4 promotes the formation of spherical Δ NEx1Q49 oligomers.....	64
Figure 3.1: Potential mechanism of spontaneous Ex1Q49 aggregation after proteolytic cleavage of GST-Ex1Q49 with PP.....	70
Figure 3.2: Describing the spontaneous Ex1Q49 aggregation process by mathematical modeling.....	74
Figure 3.3: Simulation of spontaneous Ex1Q49 aggregation using an autocatalytic amyloid polymerization mechanism.....	75
Figure 3.4: Predictions for the validation of an autocatalytic mechanism of Ex1Q49 aggregation.....	76

List of Tables

Table 1.1: Summary of important protein misfolding diseases	5
Table 1.2: Table of huntingtin antibodies.	19
Table 2.1 Chemical structures and names of compounds tested in cell-free aggregation assays.	40
Table 4.1: Primary antibodies.....	89
Table 4.2: Secondary antibodies.....	89
Table 4.3: Primer.....	90

1. Introduction

1.1 Protein aggregation and conformational diseases

More than 100,000 proteins are expressed in the human organism, with diverse biological functions. They for example function as enzymes, cytoskeletal proteins, transcription factors or chaperone. To protect the cell, quality control systems exist that try to maintain proteins in their native form and to control the concentration, localization and binding interactions of individual proteins (Balch et al., 2008). The cell has to be able to respond to external signals and to maintain a stable proteome in order to adapt to new situations. The protein homeostasis is a highly sensitive equilibrium of protein expression and degradation and any disturbance of the system might lead to cell death and disease (Douglas and Dillin, 2010). Nevertheless, a growing number of human diseases are linked to protein misfolding and aggregation.

1.1.1 Protein folding and misfolding

Proteins are composed of 20 amino acids, but are diverse in composition and size. The consecutive amino acid sequence is also called the primary structure of a protein. All amino acids consist of an α -carboxyl group, an α -amino group, a hydrogen atom and a variable side chain bound to a carbon atom. The side chain gives an amino acid its individual chemical and physical properties, such as hydrophobicity, size and charge. Most amino acids are found in the conformation described above except for proline, where the side chain binds covalently to the amide nitrogen, forming a cyclic pyrrolidine ring. The polypeptide chain is formed of covalent peptide bonds between the α -carboxyl group of one residue and the α -amino group of another residue. The number of possible conformations that a protein can adopt is limited by the partial double-bonding character of the peptide bond and the size of the side chains.

Polypeptides form local ordered conformations with the most abundant and stable being α -helices, β -sheets and β -turns (Whitford, 2005). These structures are stabilized by hydrogen bonds and are characteristic for the secondary structure of a protein. A regular α -helix has 3.6 residues per turn and is stabilized by a hydrogen bond between the backbone carbonyl oxygen of one residue and the amide hydrogen of an amino acid four residues ahead in the sequence (Pauling et al., 1951). The side chains of two adjacent amino acids project outwards in opposite directions into solution. The β -strand is an extended conformation, where the side chains point out of the plain. β -strands are stabilized by hydrogen bonds with other strands forming β -sheets.

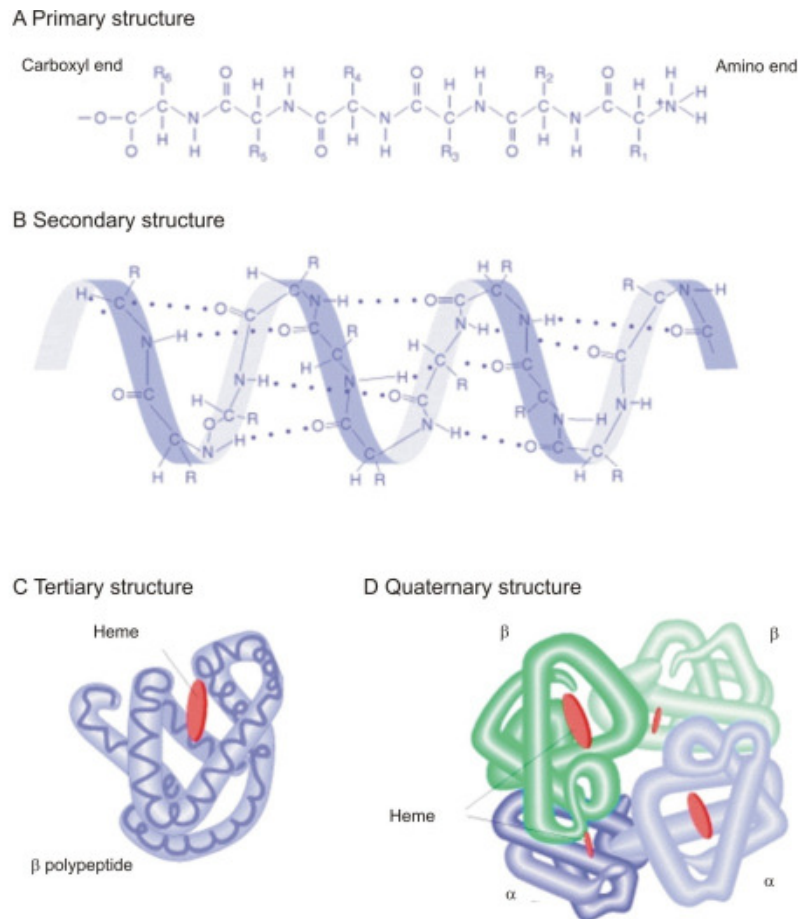


Figure 1.1: The 4 levels of protein structure. (A) Primary structure. (B) Secondary structure. The polypeptide shown in part a is drawn into an α -helix by hydrogen bonds. (C) Tertiary structure: the three-dimensional structure of myoglobin. (D) Quaternary structure: the arrangement of two α subunits and two β subunits to form the complete quaternary structure of hemoglobin. (From: An Introduction to Genetic Analysis. 7th edition. Griffiths AJF, Miller JH, Suzuki DT, et al. New York: W. H. Freeman; 2000.)

The strands can be aligned parallel or anti-parallel and can be formed between strands that are widely separated in the primary sequence. A β -turn is a four residue long loop, which is stabilized by hydrogen bonding. The element is often found in anti-parallel β -sheets, because it reverses highly volume efficiently the direction of the polypeptide chain. Regions which do not adopt a secondary structure are more flexible and are referred to as having a random coil conformation.

The tertiary structure is the three-dimensional arrangement of all atoms in a protein to an overall shape. The structure is stabilized by hydrogen bonds, ionic and hydrophobic interactions and covalent disulfide bridges. Many proteins contain two or more polypeptide chains, termed subunits. The formed multimeric species is the quaternary structure of proteins (Figure 1.1).

To become active most proteins must fold to their native structure, after synthesis at the ribosome. Anfinsen showed that Ribonuclease A refolds spontaneously after denaturation

(Anfinsen, 1973). The native structure is the most stable under physiological conditions and the information for the three-dimensional fold is encoded in the amino acid sequence. Proteins spontaneously fold within milliseconds, which is in sharp contrast to the impossibly long time calculated for a 100 residue long peptide to fold, if it samples all possible conformations. This folding problem is known as the Levinthal's paradox and led to the conclusion that large proteins must fold via partially folded intermediates (Dill and Chan, 1997). Using Nuclear Magnetic Resonance, mass spectroscopy and H/D exchange experiments these conformations could be observed (Chen et al., 2008). Computational simulations further helped to understand the process of protein folding and resulted in the formulation of different models. In the framework model a "molten globule" forms first. This state already contains most of the secondary structure elements of the native protein, although distant and tertiary contacts are missing (Ptitsyn and Rashin, 1975). In the hydrophobic collapse model condensed hydrophobic cores form prior to the formation of secondary structure (Ptitsyn, 1995). A combination of the models presented before, the nucleation condensation model, is also discussed, where a small set of interactions is sufficient to nucleate the folding process (Fersht, 2000; Fersht et al., 1992). During folding, the energy of the system decreases with the formation of native-like interactions that are on average more stable than non-native ones (Dobson and Karplus, 1999). This is illustrated in energy landscapes, where the surface represents the free energy of the system as a function of their conformational properties (Dill and Chan, 1997).

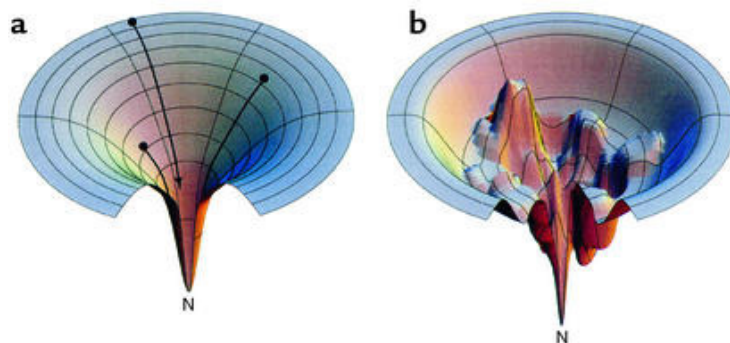


Figure 1.2: Energy landscape for protein folding. (a) Idealized funnel landscape. (b) Rugged energy landscape with kinetic traps, energy barriers and narrow throughway paths to native state (N) (From: Dill KA, Chan HS. From Levinthal to pathways to funnels. *Nat Struct Biol.* 1997;4:10–19).

The energy landscapes have the shape of a funnel (Figure 1.2). The unfolded conformations are characterized by a high conformational entropy and high free energy. Folding can occur on many different ways with distinct intermediates, which are more or less stable. As folding proceeds the number of conformations that are accessible decreases and the entropy of the system also decreases, giving a solution to the Levinthal paradox (Dinner et al., 2000; Wolynes et al., 1995).

Nevertheless the classical sequence-structure-function paradigm has to be reconsidered, with growing evidence that a large number of proteins are intrinsically unstructured proteins (IUPs) or contain intrinsically disordered regions (IDRs) (Tompa, 2002). IUPs lack a folded structure but display a highly flexible, random-coil-like conformation under physiological conditions. 35-51% of proteins in eukaryotic organisms contain at least one IDR with more than 50 residues, enriched in P, E, K, S and Q and about 10% are natively unfolded (Dunker et al., 2001). IUPs are involved in signal transduction, intracellular traffic, cell cycle and transcriptional and translational regulation. The high intramolecular flexibility enables the proteins to adopt different structures upon binding to many different partners. The high decrease in conformational entropy upon binding and folding make these highly specific interactions reversible (Tompa, 2002).

In living cells proteins are synthesized on ribosomes. Here, the genetic information encoded in the DNA is translated into the polypeptide chain. Folding can be co-translational, meaning that the folding initiates while the C-terminus of the protein is still synthesized, or occurs after termination of the protein synthesis in the cytoplasm or in the endoplasmic reticulum (ER). The environment plays an important role in the protein folding process. The protein concentration in the interior of a cell is estimated to be 300 mg/ml (Ellis and Minton, 2003). In this crowded environment the risk of aggregation and aberrant interactions is enhanced and a protective mechanism is essential for maintenance of the cellular homeostasis. The quality-control system is activated by cellular stress, such as heat stress, oxidative stress or mutations. It regulates the folding and refolding of misfolded proteins or their proteolytic degradation by up- or down-regulation of molecular chaperones, proteases and regulatory factors (Hol and Scheper, 2008). Molecular chaperones assist the protein folding by increasing the efficiency of the folding process and reducing the probability of competing reactions. Furthermore, chaperones can help to refold proteins after stress-induced denaturation. Proteins that are recognized by the quality-control system to be misfolded and can not be refolded are marked for degradation by the ubiquitin proteasome system (Whitford, 2005). They are ubiquitinated and transported to the 26S proteasome. The capacity of the quality-control system, including the up-regulation of chaperones, the ubiquitin proteasome system (UPS) and autophagy, decrease with age, and cells therefore have to cope with increasing misfolding of metastable proteins, suggesting a link to several late-onset conformational diseases (Morimoto, 2008).

1.1.2 Protein aggregation and amyloid-like inclusions

1.1.2.1 Protein aggregation and conformational diseases

Failure of the quality-control system to handle misfolded proteins is associated with a growing number of neurodegenerative diseases, such as Alzheimer's disease (AD), Parkinson's disease (PD), amyotrophic lateral sclerosis (ALS) or the group of polyglutamine diseases, including Huntington's disease (HD) or the spinocerebellar ataxias (Table 1.1). In each of these diseases a specific protein escapes the protective mechanisms of the cell and forms aggregates either intracellular or extracellular (Sunde and Blake, 1997).

Table 1.1: Summary of important protein misfolding diseases

Disease	Toxic protein	Brain region	Characteristic pathology
Alzheimer's disease (AD)	β -Amyloid (A β) Tau	Hippocampus, cerebral cortex	Extracellular plaques, intracellular tangles
Parkinson's disease (PD)	α -synuclein (α -syn)	Substantia nigra, hypothalamus	Intracellular Lewy bodies
Huntington's disease (HD)	Huntingtin (Htt)	Striatum, cerebral cortex	Intracellular inclusions
Spinocerebellar Ataxias (SCA's)	Ataxin1-3, 6-7, TBP	Cerebellar cortex, dentate nuclei, olivary nuclei	Intracellular inclusions
Dentatorubral and pallidolysian atrophy (DRPLA)	Atrophin	Dentatorubral and pallidolysian systems	Intracellular inclusions
Spinal and bulbar muscular atrophy (SBMA)	Androgen receptor	Motor neurons in the brainstem, anterior horn of the spinal cord, dorsal root ganglia	Intracellular inclusions
Familial amyotrophic lateral sclerosis (ALS)	Superoxide dismutase 1 (SOD1)	Motor cortex, brainstem	Intracellular Bunina bodies

The diseases are characterized neuropathologically by the selective loss of distinct subpopulations of neurons in the brain and synaptic abnormalities, resulting in cognitive decline and motoric dysfunction. The soluble forms of the proteins involved range from being globular to being largely unstructured polypeptides, and in the most cases they share no sequence homology. Despite the differences in the soluble conformations the aggregates have a common β -sheet rich, fibrillar structure, termed amyloids (Soto, 2003). Other cellular components, metal ions and other proteins are sometimes sequestered into aggregates, forming so called aggresomes (Johnston et al., 1998).

Some of the diseases are strictly inherited, others occur predominantly sporadic, such as AD or PD, although hereditary forms exist (Ross and Poirier, 2004). Mutations in the genes coding for the proteins involved often decrease the stability of the native state leading to partially unfolded states that are prone to aggregation (Bertoncini et al., 2005). These mutations are the cause for some of the familial cases of amyloid diseases, such as the A53T mutation in α -synuclein. Another reason for familial forms is an altered processing or degradation of the disease causing protein, leading to the accumulation of fragments of the protein in the cell (Scheuner et al., 1996). Prion diseases have been shown to be caused by an abnormal protein structure that can occur by sporadic conformational changes, mutations in the prion gene or by environmental transmission (Nguyen et al., 1995).

When tightly controlled, the formation of amyloids is not necessarily deleterious for the cell. In several organisms, even in mammalian systems, functional amyloids have been identified (Kelly and Balch, 2003).

1.1.2.2 Characteristics and structure of amyloid fibrils

Amyloids have many biochemical and biophysical characteristics in common. On binding to Congo red, amyloids show birefringence under cross-polarized light (Klunk et al., 1989) and binding to Thioflavin T shifts the fluorescence of this compound (LeVine, 1999). Amyloids have a fibrillar structure with a high β -sheet content. The fibrils are 0.1-10 μm long, straight and unbranched filamentous structures with a width of approximately 10 nm (Shirahama and Cohen, 1967). Two or more protofibrils twist around one another to form the fibril. X-ray diffraction patterns have revealed that in the core of the fibril the β -sheets are assembled in β -strands, which run perpendicular to the fibril axis (Sunde and Blake, 1997). An intensive 4.5-4.7 \AA meridian reflection corresponds to the distance between β -strands and an equatorial signal around 10 \AA represents the space between neighboring β -sheets. This structural characteristic is known as the cross- β structure (Sunde and Blake, 1997). The structure is stabilized by hydrogen bonds between amide and carbonyl groups of the polypeptide chain running nearly parallel to the long axis. Different models of β -sheet

stacking have been proposed, in which the side chains either intermesh closely forming steric zippers (Sawaya et al., 2007) or have a β -helix like structure forming “water-filled nanotubes” (Perutz et al., 2002).

Amyloid formation is an inherent or generic property of all peptide chains, with large proteins having a lower propensity to form amyloids than small proteins (Ramshini et al., 2011). The conformational antibodies WO1 and WO2 recognize the cross- β amyloid-like structures from different proteins, but not their soluble monomers, suggesting that the cross- β structure is formed by the backbone atoms (O’Nuallain and Wetzel, 2002). The differences between the amyloid-like structures derive from the respective amino acid composition of the proteins and therefore from the properties of the side chains and the stability of the native state.

1.1.2.3 Models of protein aggregation

To minimize unfavorable interactions, hydrophobic side chains and the polypeptide backbone are buried within the core of the protein in the native state of globular proteins. In order to aggregate the proteins either have to partially unfold or change their conformation as a result of proteolysis. The fact that amyloids share a common core structure suggests that the mechanism of aggregation is similar for all amyloidogenic proteins. In general the formation of aggregates is viewed as a nucleated polymerization reaction (Rochet and Lansbury, 2000).

In vitro the formation of aggregates is characterized by a sigmoidal slope with a lag phase followed by a rapid growth or elongation period. During the lag phase the aggregation-prone monomer is in equilibrium with the critical nucleus, an energetically unfavorable conformation, which can be either monomeric or oligomeric. When this nucleus is formed larger aggregated species are formed with well defined fibrillar morphology, called protofibrils. Protofibrils are short, thin fibrillar species, with high β -sheet content (Chiti and Dobson, 2006). In a further step protofibrils self-assemble into large mature amyloid fibrils, which is often accompanied by a structural reorganization of the aggregates (Harper et al., 1997) (Figure 1.3). The lag-phase can be shortened by addition of preformed aggregates, so called seeds (Scherzinger et al., 1999).

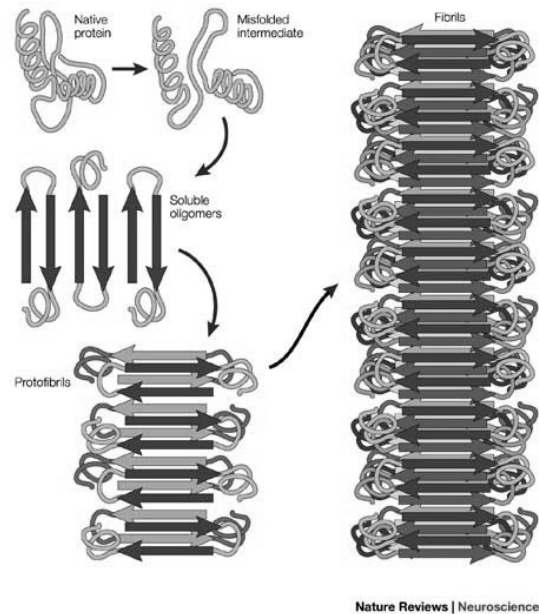


Figure 1.3: Schematic representation of the protein aggregation pathway. (Soto, 2003).

Several proteins have been shown to follow a nucleated polymerization mechanism, including A β , α -synuclein, tau, IAPP and polyglutamine proteins (Morris et al., 2008). The best studied mechanism is the aggregation of A β peptide. Above a critical concentration fibrils form after a lag phase, during which the nucleus is formed. The length of the lag-phase is concentration dependent and can be entirely bypassed by the addition of seeds (Harper and Lansbury, 1997). For A β several oligomeric and protofibrillar species have been examined using atomic force microscopy, electron microscopy, gel filtration chromatography, CD spectroscopy and silver staining of native gels (Dobson, 2003).

The spherical oligomers, observed with atomic force microscopy and electron microscopy, have a diameter of 3-6 nm. Also transiently observed are protofibrils with heights of 3-4 nm determined by atomic force microscopy, or 6-8 nm determined by electron microscopy (Glabe, 2004). These protofibrils are fibrillar and bind to Thioflavin T, but are in contrast to mature fibrils detergent soluble (Rochet and Lansbury, 2000). It has been shown using time-lapse atomic force microscopy, that fibril growth involves the addition of monomers to both protofibril ends as well as the association of immature protofibrils to thick, branched fibrils (Harper et al., 1997). Large, soluble linear aggregates or protofibrils without regular secondary structure have also been shown for polyQ peptides during the lag period, making up to about 30 % of the total peptide mass (Lee et al., 2007).

It has been shown that soluble oligomeric species from different amyloidogenic proteins share a common conformational epitope (Kayed et al., 2003). The conformational antibody A11 that was produced against a molecular mimic of soluble A β oligomers, reacts with A β ,

α -synuclein, IAPP, polyglutamine, lysozym, human insulin and the prion peptide 106-146 oligomers, but not with their monomeric proteins or fibrillar forms.

However, the molecular mechanism of the formation of amyloid fibrils is still a matter of debate because of the complexity and instability of the early intermediates. Adding up to this difficulties is the problem to distinguish between on-pathway and off-pathway intermediates. Therefore, many modeling approaches have been performed to fit the experimental data to a mathematical model and to obtain further information on structural and thermodynamic aspects of the nucleation event. In mechanisms of subsequent monomer addition one such information is the critical nucleus. Ferrone defined in 1999 the critical nucleus as the aggregate size after which the association rate exceeds the dissociation rate for the first time (Ferrone, 1999). This parameter can be calculated from the protein concentration-dependence of the rate of fibril formation. This approach was initially developed for actin and sickle cell haemoglobin assembly (Ferrone, 1999), but was also extensively applied for amyloid formation reactions. For example for polyglutamine peptides a very weak concentration-dependence was observed, suggesting a monomeric nucleus (Chen et al., 2002).

Finke and Watzky reanalyzed this data applying an "Ockham's razor"/ minimalistic 2-step model (Morris et al., 2008). In this model a slow nucleation is followed by a fast autocatalytic growth phase. They could show that the mechanism was able to fit the aggregation data of several proteins involved in neurodegeneration such as α -syn, β_2 m and polyQ (Morris et al., 2008). In addition, prion protein aggregation reactions were fitted (Watzky et al., 2008). However, an extensive study of the NM region of the yeast Sup35 prion showed that this domain aggregates via a nucleated conformational conversion mechanism (NCC). The protein first forms structurally molten, oligomeric intermediates, which slowly convert into structured oligomeric nuclei. Once structured nuclei are present elongation occurs rapidly by addition of less structured oligomers to the growing fibril-ends. In this step the fibril-ends act as templates for the conversion of unstructured oligomers into structured species (Serio et al., 2000).

In vitro aggregation can be modulated easily by changing the pH, temperature or salt concentration or by addition of metal ions. In addition, agitation has been shown to result in mechanical stress. Thus, shaking of aggregation reactions in some cases leads to fragmentation of long fibrils, producing shorter ones with more fibril-ends on which elongation might occur. In a theoretical study it has been proposed that fragmentation might lead to off-pathway aggregates and therefore slow down the formation of "inert" on-pathway fibrils (Powers and Powers, 2008). For β_2 -microglobulin, the protein responsible for aggregate formation in Haemodialysis-related amyloidoses, it has been shown that treatment of human

neuroblastoma SH-SY5Y cells with aggregates fragmented by mechanical stress reduced cell viability, while long unfragmented fibrils did not (Xue et al., 2009).

1.1.2.4 Protein aggregation and toxicity

Although the formation of fibrillar aggregates is a common hallmark of several neurodegenerative diseases, it is still unclear whether the aggregates are toxic or just the result of the pathology. Several studies have indicated that the appearance of inclusions does not correlate well with cell loss or other clinical features. In AD, the density of amyloid plaques in human post-mortem brain samples correlates weakly with the severity of the disease (Terry et al., 1991). This tendency was also found in PD, where cell loss in the substantia nigra correlates only weakly with Lewy body formation (Tompkins and Hill, 1997). Hence, it has been suggested that inclusion body formation might be even protective for the cell. In a polyglutamine model, disruption of inclusion body formation resulted in enhanced toxicity (Saudou et al., 1998). Inclusions therefore might represent the end-product of a protective mechanism of the cell to get rid of toxic intermediate species, including oligomers and pre-fibrillar aggregates.

In contrast to mature fibrils oligomeric species of A β and α -synuclein have been shown to be highly neurotoxic (Taylor et al., 2002). This toxicity might be caused by exposure of hydrophobic stretches on the protein surface, mediating aberrant interactions with other proteins, and resulting in their functional inactivation and subsequent sequestration into aggregates (Arrasate et al., 2004; Walsh et al., 1997). Several components of the quality control system have been identified to be sequestered in aggregates, probably leading to the impairment of the cytosolic stress response and further accumulation of mutated proteins in the cell (Preisinger et al., 1999; Waelter et al., 2001). A further mechanism of toxicity has been proposed for A β oligomers, but could also be applicable for other proteins involved in neurodegeneration. It has been proposed that the hydrophobic stretches interact with cellular membranes forming pores and thereby destroy the integrity of the membrane (Lashuel et al., 2002).

As a secondary effect mitochondria play an important role in the pathogenesis of neurodegenerative diseases. Mitochondrial dysfunction and oxidative stress occur early in the diseases and both contribute to ageing, suggesting a plausible cause for the late-onset of the diseases (Lin and Beal, 2006).

1.2 Chorea Huntington

Chorea Huntington or Huntington's disease (HD) is an autosomal dominant inherited, progressive neurodegenerative disorder with prevalence of about 5-7 cases per 100 000 (Walker, 2007). The average age of onset is between 30-50 years, but the range spans from childhood to the ninth decade of life. The severity of the symptoms increases with time and patients die 15-20 years after disease onset (Bates et al., 2002).

1.2.1 Clinical manifestation and neuropathology

The first symptoms in HD are a general lack of coordination and an unsteady gait along with mild personality changes and a slow impairment of intellectual functions. Involuntary, arrhythmic limb movements termed chorea, hyperkinesia and rigidity are the most common clinical motor phenotypes in the early stage of the disease (Thompson et al., 1988). The decline in motor function during the course of the disease manifests also in speech impairment, and difficulties in swallowing and chewing (Walker, 2007). These eating problems can lead to weight loss, which is commonly observed. Personality changes such as social withdrawal, depression, a reduced display of emotions, aggression, anxiety and compulsive behavior also emerge (Walker, 2007).

The cognitive impairments get worse as the disease proceeds, and mental abilities generally decline into dementia. Complications such as pneumonia and heart disease reduce life expectancy to approximately fifteen to twenty years after symptoms onset (Bates et al., 2002). Although neurological symptoms predominate, growing evidence is provided that cells from peripheral tissues of HD patients are also affected by mutant Htt expression, leading to altered glucose homeostasis and sub-cellular abnormalities in fibroblasts, lymphocytes and erythrocytes (Sassone et al., 2009).

The most striking neuropathological hallmark is the significant loss of neurons in the cerebral cortex of HD patients, apparent in the decrease of up to 40% of the total brain weight. The neurodegenerative process characteristic of HD typically starts in the striatum. Within the striatum the caudate nucleus and putamen are the first to be affected with reactive gliosis and neurons showing neuritic dystrophy. A significant loss of neurons is further observed in the cerebral cortex. At later disease stages neuronal loss can be identified in most regions of the brain (Vonsattel et al., 1985).

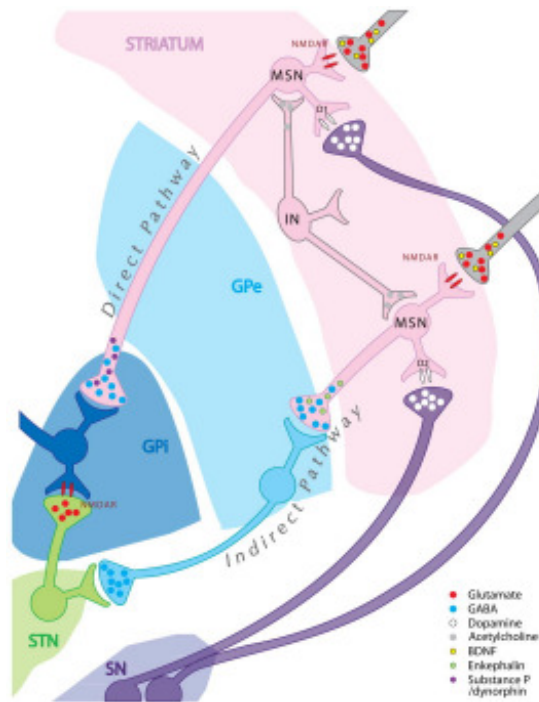


Figure 1.4: Cell type-specific characteristics of neuronal populations affected in HD. Abbreviations: MSN: medium spiny neuron; IN: interneuron; BDNF: brain-derived neurotrophic factor; D1: dopamine receptor subtype 1; D2: dopamine receptor subtype 2; NMDAR: N-methyl-D-aspartic acid receptor; GABA: γ -aminobutyric acid; GPe: external globus pallidus; GPi: internal globus pallidus; SN: substantia nigra; STN: subthalamic nucleus. (adopted from Han et al.,2010).

Of the various subtypes of projection neurons and interneurons in the striatum the medium spiny neurons (MSNs) are the first and most affected cell subtype in HD. These striatal projection neurons are morphologically characterized by a long axon, medium sized cell bodies and spiny dendrites. MSNs are partially regulated by dopaminergic inputs and the inhibitory transmitter GABA (γ -aminobutyric acid). Based on their projection targets, MSNs can be classified into two groups (Figure 1.4). MSNs in the indirect pathway are affected first in HD and the degeneration has been associated with chorea. Loss of MSNs of the direct pathway occurs late in the disease and was linked to rigidity and bradykinesia (Han et al., 2010).

Current therapies are symptomatic and aim at improving cognition or motor dysfunction. The only drug available in the US for HD is tetrabenazine. It suppresses chorea by promoting the degradation of dopamine, but does not impede the progression of the disease (Poon et al., 2010). The symptoms of rigidity can be treated with antiparkinsonian drugs and psychiatric symptoms can be controlled with antidepressant drugs (Walker, 2007). It is the aim of ongoing studies to develop treatments that delay the onset and slow the progression of HD. One such strategy would be to decrease the levels of mutant Htt by RNA interference therapies. So far, only the transplantation of fetal tissue into the caudate nucleus and the putamen has led to improvements of cognitive functions and electrophysiological tests

(Bachoud-Levi et al., 2000). However, at present this approach is limited by the availability of fetal neuronal tissue.

1.2.2 Genetics

In 1993 the IT15 gene responsible for HD was identified on the short arm of chromosome 4 (HDCRG, 1993). The gene encodes for a 3144 amino acid long protein, called huntingtin, with an abnormal expansion of a polymorphic CAG trinucleotide repeat at the 5' end of the first of 67 exons (HDCRG, 1993). In healthy individuals the CAG stretch codes for less than 35 glutamines, whereas individuals with 36-39 glutamines have an increased risk to develop HD. If the length of the polyglutamine (polyQ) stretch exceeds 40 individuals always develop symptoms during lifespan. Expansions of more than 50 repeats result in the juvenile form of the disease (Rubinsztein et al., 1996). There is an inverse correlation between the length of the CAG repeat and the disease onset. Longer repeats are correlated with an earlier age of onset (Andrew et al., 1993). Due to meiotic instability the age of onset decreases and the disease severity increases in successive generations. This phenomenon of anticipation was found in many trinucleotide-repeat diseases and is most evident when the mutation is inherited through the paternal line (Bates et al., 2002). The clinical symptoms are more severe in homozygotes, yet heterozygotes develop the disease at the same age as homozygotes with a comparable length of the CAG repeat but with less aggressive course of the disease (Squitieri et al., 2003).

1.2.3 The huntingtin protein

Wild-type huntingtin (Htt) is a 349 kDa large protein that is ubiquitously expressed in most tissues, with the highest expression levels in the two brain regions most affected in HD, namely the striatum and the cerebral cortex (Strong et al., 1993). The protein is mostly localized in the cytoplasm, but can also be found intranuclear. In neurons, where the expression is higher than in glial cells, the protein can be found in nuclei, cell bodies, dendrites and nerve terminals (DiFiglia et al., 1997). Subcellular fractionations showed that Htt is enriched in membrane-containing fractions and is associated with microtubules, the plasma membrane, endocytic and autophagic vesicles, endosomal compartments, the ER, the Golgi apparatus and mitochondria (Atwal et al., 2007; Gutekunst et al., 1999). Mutant Htt shows an altered intercellular distribution, with perinuclear accumulations and neuronal intranuclear inclusions (NIIs) (DiFiglia et al., 1997).

The full length protein contains three important motifs. Adjacent to the N-terminal polyglutamine domain that is mutated in HD, is a proline-rich region (polyP), followed by 37

HEAT (Huntingtin elongation factor 3, the PR65/A subunit of protein phosphatase 2A and the lipid kinase Tor) repeat sequences, that can be clustered into three subdomains (Andrade and Bork, 1995). HEAT repeats are sequences of 40 amino acids comprising two anti-parallel α -helices forming a hairpin. This structural motif was found to be involved in many protein-protein interactions and is enriched in proteins that play a role in cytoplasmic and nuclear transport processes, microtubule dynamics and chromosome segregation (Andrade and Bork, 1995). It is suggested that the full length Htt protein is an elongated superhelical solenoid with a diameter of $\sim 200 \text{ \AA}$ (Li et al., 2006). A crystal structure of the first exon (Ex1) of Htt protein with 17 glutamines fused N-terminally to maltose-binding protein and C-terminal to a 19 amino acids tag that was added to crystallize the protein, suggests that the polyQ region adopts multiple conformations. The N-terminal part of Ex1Q17 is α -helical followed by a mainly random-coil polyQ region. The polyP region adopts a kinked or straight polyproline helical conformation. Htt contains two nuclear export signals, one near the C-terminus (Xia et al., 2003) and one located in the first 17 amino acids is facilitated by its binding to the nuclear exporter Tpr (Cornett et al., 2005).

Four types of post-translational modification have been described for Htt. The lysines K6, K9 and K15 compete for SUMOylation and ubiquitination, modifications that could regulate the half-life and localization of Htt (Dorval and Fraser, 2007). Phosphorylation takes place at S421 by Akt or protein kinase B, at S434 by cyclin-dependent kinase 5 and at S536 (Gu et al., 2009; Warby et al., 2005). C214 is palmitoylated by Hip14 (Huntingtin interacting protein 14), regulating trafficking and function of Htt (Yanai et al., 2006).

Both wild-type and mutant Htt are cleaved by several intracellular proteases. The caspases 1, 3, 6, 7 and 8 cleave Htt at the aspartate residues D513, D552 and D586. Calpain cleaves the protein at position S536 (Graham et al., 2010; Lunkes et al., 2002; Wellington et al., 2002). Two smaller fragments, cpA and cpB were identified in cultured immortalized neurons overexpressing full length mutant Htt, in human brains and in mice. cpA is cleaved by an aspartyl protease resulting in a fragment with less than 115 amino acids that can enter the nucleus. cpB is less than 214 amino acids long and is cleaved by an unknown protease (Kegel et al., 2010). The Htt protein is highly conserved except for the polyQ and the polyP regions (Harjes and Wanker, 2003).

Htt most likely acts as a scaffolding protein interacting with numerous interaction partners. It is involved in anti-apoptotic processes, transcriptional regulation, microtubule transport, synaptic transmission and endocytosis (Harjes and Wanker, 2003). It is essential in normal brain development. In knock-out mice the loss of protein induces increased apoptosis and mouse embryos die around day 8.5 (Duyao et al., 1995; Nasir et al., 1995; Zeitlin et al., 1995).

1.2.4 Misfolding, aggregation and toxicity of mutant Htt

The extension of the polyQ tract in mutant Htt causes the protein to adopt non-native conformations resulting in the formation of insoluble protein aggregates. In the disease state putative functions of Htt in the cell might be disturbed (loss of function). In addition or alternatively new functions could arise (gain of function) through new protein-protein interactions or as a result of aggregation (Preisinger et al., 1999; Steffan et al., 2000). The altered interactome perturbs many cellular functions essential for neuronal homeostasis, such as the quality control system, transcriptional regulation, mitochondrial activity and calcium homeostasis, proapoptotic response, axonal transport or resistance to oxidative stress (Hersch and Rosas, 2001).

Differences in proteolytic cleavage of mutant Htt have been linked to altered subcellular localization (Lunkes et al., 2002). Proteolytic cleavage maps have been generated from brains of wildtype (WT) mice and HdHQ150 knock-in mice, in which mutant CAG repeats have been introduced into the endogenous mouse Htt gene. In mutant HD mice 14 N-terminal fragments were detected, with the smallest one representing an exon 1 protein fragment. Several of the larger fragments could have been generated by cleavage at known caspase or calpain recognition sites. Whereas the bigger fragments were also present in brains of WT mice, the three smallest fragments have not been detected (Landles et al., 2010), indicating that these fragments are either not produced in WT mice or that the fragments are degraded.

In HD, mutant N-terminal Htt fragments have been shown to translocate to the nucleus forming intranuclear inclusions and thereby disrupting nuclear organization and normal gene transcription (Landles and Bates, 2004). Mutant Htt disrupts the activities of several transcription factors by binding to the glutamine-rich activation domains of transcriptional regulators (Gerber et al., 1994), such as CBP (CREB (cAMP-response-element-binding protein)-binding protein) or Sp1 (Specificity protein 1). CBP, a major mediator of cell survival, interacts with mutant Htt resulting in cellular toxicity and the sequestration of CBP into insoluble Htt aggregates (Steffan et al., 2000). Interaction of mutant Htt with Sp1 disrupts the complex between Sp1 and TAF_{II}130, altering the expression of several Sp1 target genes, including the dopamine D2 receptor (Dunah et al., 2002; Qiu et al., 2006).

Furthermore, the transcriptional regulation of brain-derived neurotrophic factor (BDNF) is affected by mutant Htt (Zuccato et al., 2001). BDNF expression is important for the survival of striatal neurons and the activity of cortico-striatal synapses. Htt with a short polyQ tract binds to the BDNF-regulating REST/NRSF complex in the cytoplasm, restricting its translocation into the nucleus. Mutant Htt does not bind to the REST/NRSF complex,

allowing its translocation into the nucleus, leading to the repression of BDNF (Zuccato et al., 2001; Zuccato et al., 2003).

The disease causing step in the pathogenesis of HD is unclear. PolyQ expansion and mutant Htt cleavage lead to the formation of intranuclear and cytoplasmic inclusion bodies (IBs). *In vivo* these aggregates can be detected both presymptomatic and throughout the course of the disease. It has been shown that the density of inclusions in human brain samples correlates with the length of the polyQ stretch and that NIIs are formed prior to neurological phenotypes (Bates, 2003; Davies et al., 1997). However, the correlation between the aggregate load and the brain regions most affected in HD is little (Gutekunst et al., 1999). In a primary culture of rat striatal neurons the formation of IBs has been associated with an increased survival rate and a decrease of diffuse intracellular Htt species (Arrasate et al., 2004). Similar results have been obtained when inclusion formation was promoted with a small compound that rescued the Htt-mediated proteasomal dysfunction (Bodner et al., 2006). Down-regulation of mutant Htt expression rescued cell death in a tetracycline-regulated mouse model of HD. Pre-formed nuclear inclusions disappeared after turn-off of the expression and ameliorated behavioral phenotypes of the mice (Yamamoto et al., 2000).

Overexpression of CA150, a transcription factor and putative modifier of age of onset in HD, rescued neurodegeneration in a striatal cell model, while it increased neuritic aggregation without changing the levels of nuclear inclusions (Arango et al., 2006). Further evidence that the IBs are not toxic themselves comes from a study that shows that nuclear localization is necessary for the induction of neurotoxicity in striatal neurons. Addition of a nuclear export signal to mutant Htt fragments completely blocked inclusion formation and rescued cell survival. In this study the presence of NIIs did not correlate with Htt induced cell death, but suggests that inclusions might be a protective mechanism of the cell to inactivate or reduce the levels of intranuclear mutant Htt (Saudou et al., 1998). Several studies using fluorescent-reporter-tagged Htt fragments demonstrated that both wild-type and mutant Htt form oligomers in cells and that level of mutant Htt oligomers correlate with cytotoxicity (Lajoie and Snapp, 2010; Takahashi et al., 2008). This conformation can also be monitored with the reactivity of 3B5H10, a conformational antibody that detects expanded polyQs (Zhang et al., 2011).

Although there is increasing evidence that oligomers are the toxic species in several neurodegenerative diseases, Htt-induced toxicity could also be the result of the sequestration of other proteins into aggregates. Several glutamine-rich proteins were found to be associated with inclusions (Kazantsev et al., 1999), as well as molecular chaperones and components of the ubiquitin-proteasome system (Bence et al., 2001; Jana et al., 2001; Wyttenbach et al., 2000).

Overexpression of the Hsp70/Hsp40 chaperone system suppressed polyQ-induced toxicity in mouse and fly models, suggesting that the quality-control-system plays an important role in the prevention of cellular toxicity (Muchowski, 2002). *In vitro* the formation of amyloid-like fibrils is inhibited by the addition of chaperones in an ATP-dependent manner, leading instead to formation of amorphous, detergent-soluble aggregates (Muchowski et al., 2000). AFM studies of mutant Htt revealed that co-incubation with Hsp70 and Hsp40 decreased the formation of spherical and annular oligomers by partition mutant Htt monomers (Wacker et al., 2004). Further analysis of the oligomeric species with the anti-oligomer antibody A11 showed that the Hsp70/Hsp40 system specifically suppressed the formation of A11-reactive mutant Htt oligomers (Lotz et al., 2010).

The chaperonin TRiC binds unfolded polypeptides and facilitates their folding in an ATP-dependent reaction cycle. TRiC was found to bind to the first 17 amino acids of Htt and this interaction suppressed polyQ-mediated Htt aggregation (Tam et al., 2009).

Modulation of Htt aggregation by sequences flanking the polyQ region has been reported in several studies. In the exon 1 of Htt the first 17 amino acids adjacent to the polyQ tract adopt an α -helical structure. Compared to polyQ peptides, addition of this sequence dramatically enhances aggregation rates in yeast and *in vitro* (Duennwald et al., 2006; Thakur et al., 2009). Aggregation proceeds via the formation of spherical oligomers with the first 17 amino acids in the core (Thakur et al., 2009). Whether the first 17 amino acids are involved in the amyloid-core structure (Thakur et al., 2009) or have an α -helical structure (Sivanandam et al., 2011) and are exposed to the solvent is still unclear. However, atomistic simulations propose that in the context of an expanded polyQ tract, the first 17 amino acids adopt a β -sheet conformation rather than an α -helix (Lakhani et al., 2010). Downstream of the polyQ stretch the polyP region reduces the aggregation rate and the stability of β -sheet structures (Bhattacharyya et al., 2006). Expression of Htt-exon 1 fragments lacking the polyP region in yeast leads to the formation of numerous small foci in the cytoplasm. The formation of small aggregates is paralleled with a high toxicity in yeast, compared to cells having one or two large inclusions that are benign (Dehay and Bertolotti, 2006; Duennwald et al., 2006).

Much of what we know today about the structural changes was investigated using *in vitro* aggregation reactions. Due to the high insolubility of long polyQ tracts in solution the proteins are tagged to large fusion-proteins like glutathione S-transferase (GST) or maltose binding protein. Site-specific cleavage between the tag and the Htt protein initiates the formation of SDS-insoluble aggregates in a nucleated polymerization reaction only when the polyQ tract is in the pathogenic range (Scherzinger et al., 1997). Electron microscopy and atomic force microscopy studies have shown that the formed aggregates have a fibrillar morphology and that oligomers and protofibrils are precursors for the mature fibrils (Poirier et al., 2002).

Furthermore, the fibrils have a high β -sheet content and bind to Congo Red and Thioflavin T, suggesting that the *in vitro* aggregation is a valid model for studying Htt aggregation (Poirier et al., 2002).

Incubation of the aggregation reactions at different temperatures results in the formation of morphologically distinct amyloid conformations (Nekooki-Machida et al., 2009). Amyloids that were formed at 4°C have loop/turn structures together with mostly β -sheet. These structures are thermolabile and when added to mammalian cell culture they are toxic. In contrast, amyloids that were formed at 37°C have more extended and buried β -sheets, exhibiting only mild toxicity in cell culture (Nekooki-Machida et al., 2009).

The exact structure of polyQ molecules within the aggregates is still unknown. Based on x-ray diffraction patterns of poly-L-glutamine an anti-parallel β -sheet structure was proposed termed “polar zipper”. The neighboring β -sheets are held together by hydrogen bonds between main-chain and side-chain amides (Perutz et al., 1994). Reanalysis of the same data predicted an amyloid model where the polyQ molecules form a β -helix with 20 residues per turn, forming a water-filled nanotube. In molecules with more than one turn the structure is stabilized by hydrogen bonds along the fibril axis. A single turn would be unstable and only polyQ segments in the pathological range with more than 40 residues would favor this conformation (Perutz et al., 2002). Although Perutz’s structure is theoretically possible confirmed by molecular dynamic studies, x-ray diffraction studies of polyQ peptides of various length showed that all peptides exhibit the same structural motif with multiple reverse turns (Sharma et al., 2005).

An alternative model interpreting Perutz’s x-ray data suggest a model of antiparallel β -sheets with an intersheet distance of 8.3 Å. Analysis of x-ray patterns of fibril forming segments revealed that the fibrils contain β -sheets that run perpendicular to the fibril axis. The structure is stabilized by hydrogen bonds that are perpendicular to the fibril axis (Sikorski and Atkins, 2005). At the interface of two β -sheets the side-chains form van der Waal’s contacts between the glutamine methylene groups, in what is termed a “steric zipper” (Sawaya et al., 2007). The cross- β model is in good agreement with experimentally observed x-ray patterns (Jahn et al., 2010). Further evidence for the cross- β sheet model comes from a mutational study of a Q45 peptide that suggested an anti-parallel β -sheet structure with seven glutamines per strand, which is linked by a β -sheet turn formed of 4 residues (Sharma et al., 2005; Thakur and Wetzel, 2002). Introduction of β -sheet breaking mutations into the context of the Htt-exon 1 protein did not change the propensity of this mutated model peptides to form aggregates and induce toxicity *in vivo* as was established in human cell culture and primary cortical neurons, indicating that the formation of antiparallel β -sheets may be an important step in HD pathology (Poirier et al., 2005).

1.2.5 Anti-Htt antibodies are useful tools for the detection of Htt conformations

Identifying the toxic species and knowledge of the mechanism of aggregation is of great importance for drug development. Monoclonal antibodies can distinguish between distinct conformational epitopes formed by mutant Htt and are therefore a promising tool for the identification of potential drug targets. A broad range of antibodies spanning the whole Htt protein sequence has been developed and used to localize Htt in cell culture and brain samples, to study putative cleavage sites, to identify interaction partners in pull-down assays or to investigate aggregation intermediates.

Table 1.2: Table of huntingtin antibodies. UD: undefined

Antibody name	Antigen	Epitope		Literature
HD1	His-Ex1Q51	UD	polyclonal	Scherzinger E, 1997
CAG53b	GST-Ex1Q53	UD	polyclonal	Scherzinger E, 1997
MW1	DRPLA-19Q	polyQ	monoclonal	Ko J, 2001
MW7	HttEx1Q67 aggregates	polyP	monoclonal	Ko J, 2001
MW8	HttEx1Q67 aggregates	polyP	monoclonal	Ko J, 2001
3B5H10	polyQ	polyQ	monoclonal	Brooks E, 2004

The Htt-exon 1 with an expanded polyQ tract is sufficient to cause HD like phenotypes in transgenic mice (Mangiarini et al., 1996). Many antibodies preferentially recognize the expanded polyQs in living cells and under denaturing conditions. For one of these antibodies, MW1, it has been shown that the affinity to Htt increases with polyQ length, supporting a “linear lattice” model for polyQ, in which the number of ligand-binding sites increases with polyQ length (Bennett et al., 2002). The crystal structure of polyQ, when bound to MW1, is an extended, coil-like conformation (Li et al., 2007). The antibody 3B5H10 also binds to the expanded polyQ region. MW1 and 3B5H10 both recognize oligomers and protofibrils in R6/2 and HdH^{Q150/Q150} cortices (Sathasivam et al., 2010). When coincubated with a purified HttEx1Q53 protein in cell-free aggregation reactions 3B5H10 completely blocks fibril formation and addition of 3B5H10 to preformed aggregates resulted in complete disaggregation and the formation of globular structures (Legleiter et al., 2009). In contrast, MW1 initially increased the number of fibrils when coincubated with HttEx1Q53 and had no effect on preformed fibrils (Legleiter et al., 2009). In HT22 cells a correlation between 3B5H10 reactivity and Htt induced toxicity was found (Zhang et al., 2011). It has been proposed that 3B5H10 binds to a compact β -sheet like structure of polyQ (Peters-Libeu et al. (cited in Legleiter J et al, 2009), Arrasate M et al. (cited in Sathasivam K et al, 2010), Miller J

et al (cited in Zhang et al, 2011) and that this conformation could be toxic for mammalian cells. Two antibodies were published that bind to the polyP region in Htt. MW8 detects large, fibrillar, insoluble inclusions in primary striatal neurons and in mouse brains of R6/2 and HdH^{Q150/Q150} (Sathasivam et al., 2010). The other polyP antibody, MW7, inhibits the formation of Ex1Q53 aggregates and also disaggregates preformed fibrils similar to 3B5H10 (Legleiter et al., 2009). When MW7 is cotransfected as single-chain variable region fragment (scFv) antibody in HEK293 cells with HttEx1Q103-EGFP, it inhibits Htt aggregation and reduces cellular toxicity. In contrast, cotransfection of a MW1 single-chain variable region fragment stimulated Htt aggregation and apoptosis (Khoshnan et al., 2002).

Antibodies have been developed that are specific for amyloid fibrils (O'Nuallain and Wetzel, 2002) or oligomers (Kayed et al., 2003) of different amyloidogenic proteins, suggesting that a common motif is responsible for amyloid formation.

1.3 Aims

There is increasing evidence that formation of inclusion bodies in brains of patients with HD is the result of a protective mechanism of the cell to decrease the amount of toxic soluble conformations. However, the mechanism of aggregation is still unknown and intermediates are currently morphologically and structurally not well defined and it remains often unclear whether they form on- or off-pathway to the assembly of ordered amyloid fibrils.

It was the main aim of this study to investigate the molecular mechanism of Htt aggregation in cell-free assays. A special interest was the characterization of transient intermediates in the aggregation cascade and the influence of the different regions in a Htt-exon 1 fragment with 49 glutamines. The data was then used to establish in collaboration a mathematical model that describes the spontaneous polymerization into amyloid fibrils and allows making accurate predictions that help to understand the mechanism.

A second task was to elucidate the potential significance of the compound O4 as a drug for development of a new therapy against HD. O4 was identified in a independent study to modulate the aggregation of $A\beta_{42}$ and α -synuclein and thereby reduced toxicity in cell culture models.

2. Results

2.1 Investigating spontaneous Htt-exon 1 aggregation with time-resolved assays *in vitro*

2.1.1 Generation of pGEX-6P1-HttEx1Q49 for the expression of GST-Ex1Q49 fusion protein

For the production of GST-Ex1Q49 fusion protein the plasmid pGEX-6P1-HttEx1Q49 was constructed. First, the cDNA encoding a Htt-exon 1 protein with 49 glutamines was amplified by polymerase chain reaction (PCR) from the plasmid pHD510Q68. The primers Ex1_EcoRI_fwd and Ex1_NotI_rev were used for the amplification of a 0.34 kb DNA fragment containing the restriction sites EcoRI and NotI at the 5' and 3' ends, respectively. The fragment was cloned into the vector pGEX-6P1 using the restriction sites EcoRI and NotI. A schematic representation of the vector pGEX-6P1 is shown in Figure 2.1 A. The resulting plasmid pGEX-6P1-HttEx1Q49 was transformed into the *E. coli* strain DH10B and the correct size of the insert (0.34 kb) was confirmed by restriction enzyme digestion using EcoRI and NotI (Figure 2.1 B) as well as DNA sequencing.

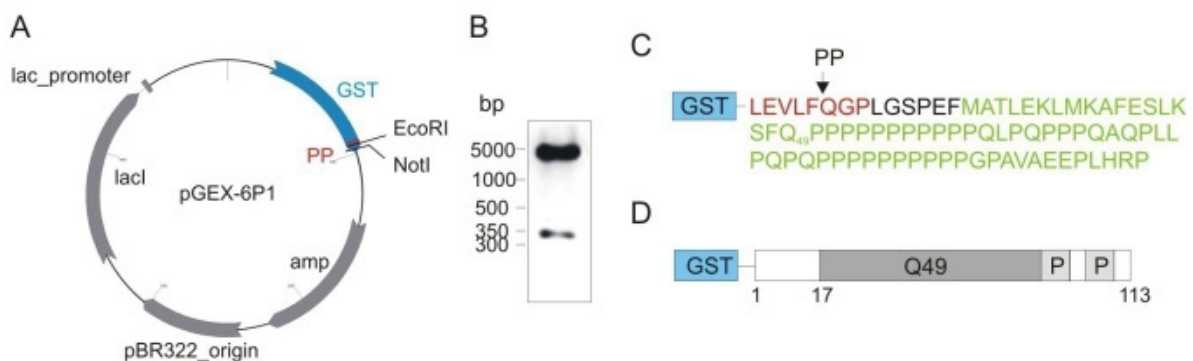


Figure 2.1: Generation of the plasmid pGEX-6P1-HttEx1Q49 for the expression of GST-Ex1Q49 fusion protein. (A) Schematic representation of the vector pGEX-6P1. (B) Restriction digestion of the plasmid pGEX6P1-HttEx1Q49 using the enzymes EcoRI and NotI; fragments were analyzed on a 1% agarose gel. The DNA insert encoding Ex1Q49 has a size of 0.34 kb. (C) Amino acid sequence of GST-Ex1Q49 fusion protein. Blue box: Schematic representation of glutathione S-transferase (GST). Red: PreScission protease (PP) cleavage site. Green: Ex1Q49 amino acid sequence. (D) Schematic representation of GST-Ex1Q49 fusion protein; GST, glutathione S-transferase; Q49, polyglutamine sequence; P, proline-rich region.

The amino acid sequence of the Htt protein fragment Ex1Q49 fused to the GST tag is shown in Figure 2.1 C. The fusion protein has a specific PreScission protease (PP) cleavage site, which is located between the GST-tag and Ex1Q49 fragment. The GST-tag at the N terminus is necessary for the expression and purification of the fusion protein. Moreover, it enhances the solubility of the Htt-exon 1 protein with a pathogenic polyglutamine stretch (Scherzinger et al., 1999). A schematic representation of the fusion protein GST-Ex1Q49 is shown in Figure 2.1 D.

2.1.2 Production and characterization of GST-Ex1Q49 fusion protein

In order to express the GST-Ex1Q49 fusion protein the plasmid pGEX-6P1-HttEx1Q49 was transformed into the *E. coli* strain BL21-RP. The expression of GST-Ex1Q49 protein was induced by addition of IPTG to the growth medium for 3 h at 37°C. Cells were harvested, lysed and the fusion protein was purified under native conditions by affinity chromatography on glutathione agarose beads. Then, 1 µg of purified fusion protein was analyzed by SDS-PAGE and Coomassie staining (Figure 2.2 A). In SDS gels GST-Ex1Q49 fusion protein has a size of 64 kDa, while the theoretical size of the protein is 40.6 kDa. This indicates that the fusion protein migrates slower than expected in SDS gels. However, this observation is in agreement with previous studies, demonstrating that fusion proteins with pathogenic polyQ tracts behave abnormally in SDS gels (Scherzinger et al., 1999). This effect is probably due to weak binding of SDS to the polyQ tract in Ex1Q49, resulting in slower migration of the fusion protein in the gels.

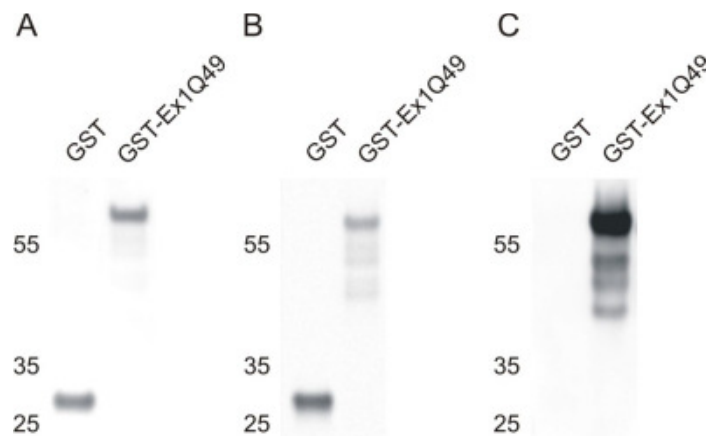


Figure 2.2: Analysis of the proteins GST-Ex1Q49 and GST by SDS-PAGE and immunoblotting Purified proteins were analyzed on a 4-16% gradient gel. (A) Coomassie staining of the purified proteins GST and GST-Ex1Q49. The polyQ containing protein runs at 64 kDa, which is higher than the expected molecular size of 40.6 kDa. GST has a molecular size of 28 kDa. Western blot analysis of proteins with anti-GST (B) and anti-Htt (HD1) antibodies (C), respectively. The anti-Htt and anti-GST antibodies both recognized the GST-Ex1Q49 fusion proteins. GST is only recognized by the anti-GST antibody, but not by the Htt specific antibody HD1.

Using this approach GST-Ex1Q49 fusion protein with high purity (90%) was produced, which is sufficient for studying spontaneous Ex1Q49 aggregation in cell-free assays. Finally, the purified fusion protein was further characterized by Western blotting using anti-GST (Figure 2.2 B) and anti-Htt specific antibodies (Figure 2.2 C). Both antibodies recognized the fusion protein and some smaller bands that probably represent degradation products. The results indicate that the produced fusion protein contains both GST and Htt-exon 1 protein.

The control protein GST was also expressed from the pGEX-6P1 vector in *E. coli* BL21-RP cells and purified by affinity chromatography as described above. When analyzed by SDS-PAGE and Coomassie staining a single band was observed with the expected molecular size of 28 kDa (Figure 2.2 A). The GST protein was only recognized by a GST antibody (Figure 2.2 B) but not by the Htt specific antibody HD1 (Figure 2.2 C).

A 3D structure of a Htt-exon 1 protein with 17 glutamines fused to the maltose-binding protein suggests that the first 17 amino acids in Htt adopt an α -helical conformation (Kim et al., 2009). In order to assess the structure of the proteins GST-Ex1Q49 and GST they were analyzed by circular dichroism spectroscopy. Spectra were measured at wavelengths from 200 to 260 nm at a protein concentration of 1 $\mu\text{g}/\mu\text{l}$. The proteins GST-Ex1Q49 and GST both showed spectra that are characteristic for α -helical proteins with negative peaks at 208 and 222 nm (Figure 2.3 A). Analysis of GST-Ex1Q49 protein with the CDNN 2.1 software showed that the protein has an α -helical content of 100%.

In comparison, for the GST protein an α -helical content of 50% and a random coil content of 22% was obtained. The remaining 28% of the protein most likely are in a β -sheet or β -turn conformation (<http://bioinformatik.biochemtech.uni-halle.de/cdnn>). To predict a secondary structure for the Ex1Q49 protein the spectrum of GST was subtracted from the spectrum of GST-Ex1Q49 (Figure 2.3 B), suggesting that Ex1Q49 in the context of the fusion protein has predominantly an α -helical conformation (100% calculated with CDNN 2.1 software).

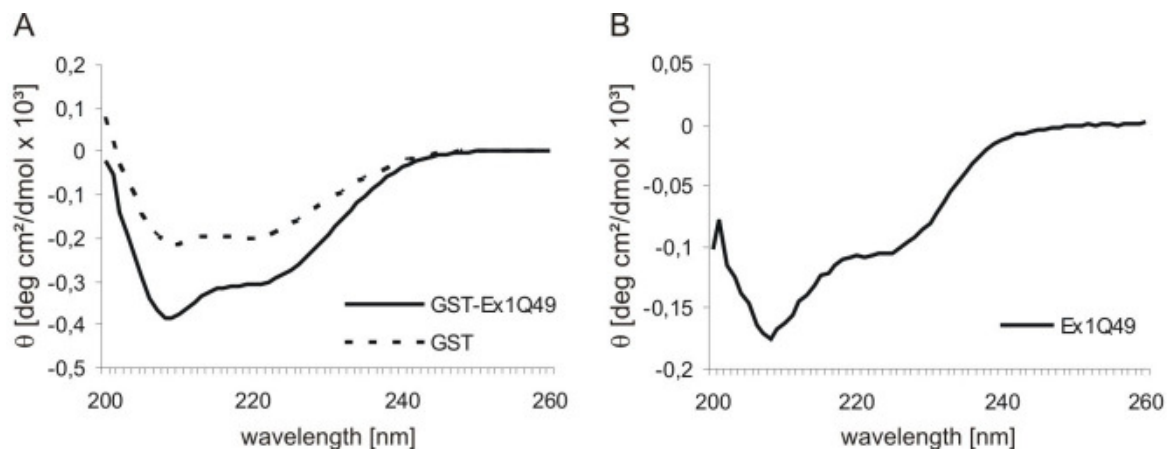


Figure 2.3: Soluble GST-Ex1Q49 is a mainly α -helical protein. (A) CD spectra of the proteins GST-Ex1Q49 and GST were measured at a concentration of 1 $\mu\text{g}/\mu\text{l}$. Both proteins showed negative peaks at 208 and 222 nm, indicating that they have a high helical content. (B) Predicted CD spectrum for Ex1Q49 after subtraction of the GST spectrum from the GST-Ex1Q49 spectrum. The predicted spectrum for Ex1Q49 has negative peaks at 208 and 222 nm, suggesting that the protein has an α -helical structure.

These results suggest that the soluble GST-Ex1Q49 fusion protein has an α -helical conformation.

2.1.3 Establishing a filter retardation assay for the detection of SDS-resistant Ex1Q49 aggregates

Previous studies have demonstrated that removal of the GST-tag from an exon 1 fusion protein with a polyQ stretch in the pathological range initiates the formation of SDS-resistant protein aggregates (Scherzinger et al., 1999). To investigate the early events in the process of polyQ-mediated Htt polymerization a time-resolved aggregation assay was established. The principle of this assay is shown in Figure 2.4.

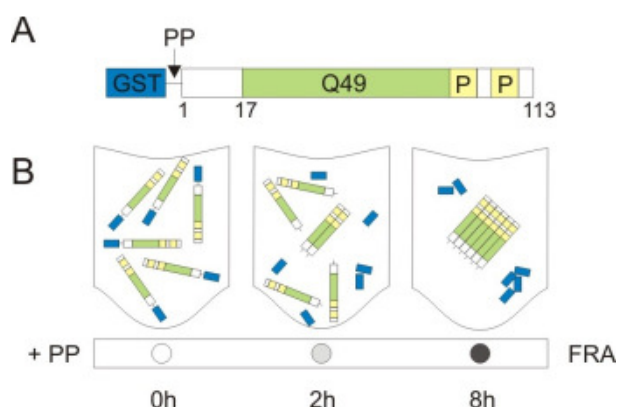


Figure 2.4: Schematic representation of the filter retardation assay (FRA). (A) Schematic representation of the GST-Ex1Q49 fusion protein. (B) Schematic description of an *in vitro* aggregation reaction in the presence of PP. The formation of SDS-resistant aggregates after cleavage of GST fusion protein with PP and the subsequent conversion of Ex1Q49 protein from the soluble to the amyloidogenic state is shown. SDS-stable protein aggregates were monitored by filter retardation assay.

GST-Ex1Q49 fusion protein was incubated at a concentration of 2 μ M in the presence or absence of PP (0.28 U per μ g of GST fusion protein) and reactions were incubated at 20°C and 300 rpm agitation for 8 h. The formation of SDS-resistant aggregates was quantified at indicated time points (Figure 2.5 A) using a filter-retardation assay (Scherzinger et al., 1999). For the filter retardation assay samples (500 ng) were removed from the aggregation reactions and frozen at -80°C. Then, samples were mixed with an equal volume of denaturing buffer (0.4% SDS and 100 mM DTT), denatured at 96°C for 5 min and filtered through a cellulose acetate membrane. SDS-resistant aggregates were finally immunodetected using an anti-Htt antibody (CAG53b).

Proteolytic cleavage of GST-Ex1Q49 fusion protein with PP induced the formation of SDS-resistant Ex1Q49 aggregates after a lag phase of 2 h, which were detectable by filter retardation assay. In contrast, such aggregates were not observed in the absence of PP, indicating that proteolytic cleavage of fusion protein was critical for the assembly of insoluble protein aggregates (Figure 2.5 A).

To study whether agitation influences the Ex1Q49 aggregation kinetics, the experiments were also repeated without shaking of aggregation reactions. Agitation at 300 rpm did not significantly enhance the formation of SDS-resistant protein aggregates *in vitro* (Figure 2.5 B), indicating that weak mechanical forces do not promote amyloid polymerization.

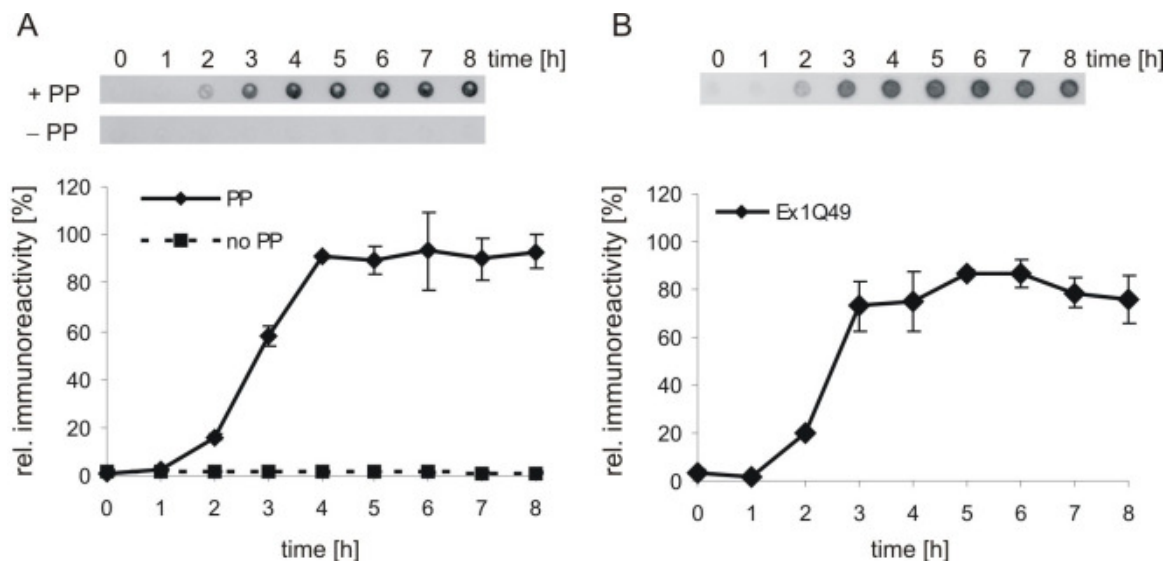


Figure 2.5: Proteolytic cleavage of GST-Ex1Q49 with PP induces the formation of SDS-resistant Ex1Q49 aggregates. GST-Ex1Q49 protein was incubated at a concentration of 2 μ M in the presence of 0.28 U PP per μ g of fusion protein. Cleavage was performed at 20°C and shaking at 300 rpm. (A) Aliquots were subjected to the filter retardation assay and immunodetected with the CAG53b antibody and the signals were quantified by densitometry using the AIDA software. In the presence of PP SDS-resistant aggregates were retained on the membrane after 2 h. No aggregates were detected in the absence of PP. (B) Reactions were incubated at 20°C without shaking. Aliquots of the reaction were analyzed by filter retardation assay and aggregates were immunodetected with CAG53b antibody. No change in the lag phase or the kinetics was observed.

To investigate whether the spontaneous aggregation of Ex1Q49 is dependent on the protein concentration, GST-Ex1Q49 fusion protein was incubated at a concentration of 20 μ M in the presence of PP and samples were analyzed over time by filter retardation assay. At a 10-fold higher concentration of GST-Ex1Q49 protein a shorter lag phase was observed (Figure 2.6 A), indicating that spontaneous polymerization of Ex1Q49 is concentration-dependent. However, an increase in the Ex1Q49 polymerization rate was observed at a concentration of 20 μ M. These results confirm previous investigations, indicating that polyQ-mediated aggregation of Htt-exon1 fragments is a concentration-dependent process (Scherzinger et al., 1999).

Dynamic light scattering (DLS) has been shown previously to be a very useful method to study the aggregation kinetics of polyQ-containing Htt fragments, allowing an estimation of particle sizes in aggregation reactions (Georgalis et al., 1998). GST-Ex1Q49 was incubated at concentrations of 5 and 20 μ M and samples were measured repeatedly every 10 ± 1 min using a Malvern Nano Zetasizer ZS. At a concentration of 5 μ M Ex1Q49 assembled after an initial lag phase of 60 min very efficiently into insoluble protein aggregates (Figure 2.6 B). After 4 h aggregate particles with a z-averaged radius of 450 nm were detectable in spontaneous aggregation reactions (Figure 2.6 B). A similar result was obtained when a 4-fold higher concentration of Ex1Q49 protein (20 μ M) was investigated by dynamic light scattering. However, assemblies were already detectable in spontaneous aggregation reactions after a lag phase of 40 min, supporting the results obtained with the filter

retardation assay that Ex1Q49 aggregation is a concentration dependent process (Figure 2.6 A).

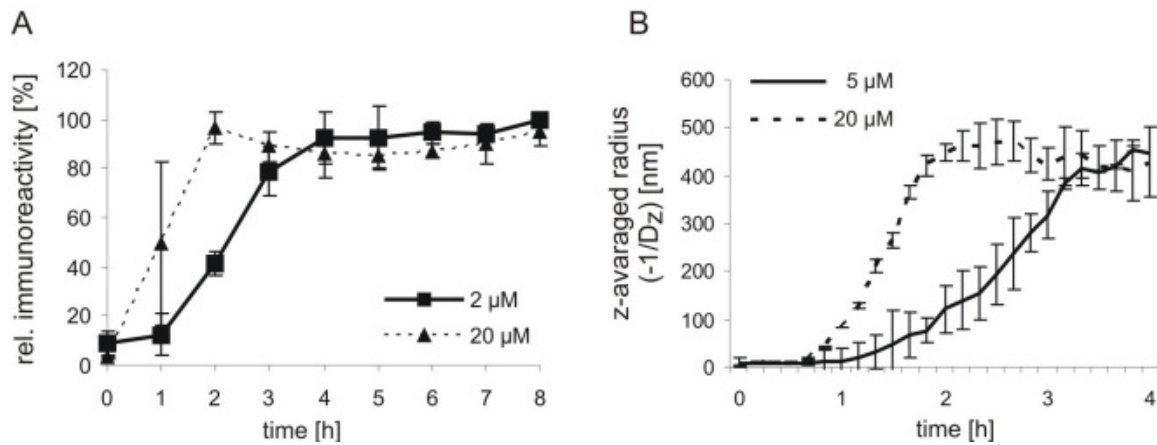


Figure 2.6: Increasing the concentration of GST-Ex1Q49 enhances the spontaneous formation of Ex1Q49 aggregates. (A) GST-Ex1Q49 was incubated at a concentration of 2 μ M or 20 μ M in the presence of PP at 20°C. Aliquots of the reactions were analyzed by filter retardation assay and immunodetection with CAG53b antibody. No lag phase was observed when reactions were incubated at a concentration of 20 μ M. (B) GST-Ex1Q49 was incubated at a concentration of 5 or 20 μ M and dynamic light scattering was measured repeatedly at 24°C every 10 \pm 1 min. Conversion of soluble Ex1Q49 into aggregates with a z-averaged radius of 450 nm can be monitored by dynamic light scattering.

Proteolytic cleavage of GST-Ex1Q49 fusion protein (2 μ M) with PP in time-resolved aggregation reactions was analyzed by SDS-PAGE and Western blotting using the anti-Htt antibody HD1 (Figure 2.7 A and B). The signals were quantified by densitometry using the AIDA software. After 3 h more than 90% of the GST-Ex1Q49 fusion protein was cleaved in spontaneous aggregation reactions (Figure 2.7 B). In parallel, after 3 h formation of SDS-resistant aggregates was detectable in SDS gels (retained in the pockets of the stacking gel) and filter retardation assays (Figure 2.5), supporting the view that proteolytic cleavage of fusion protein is a prerequisite for the assembly of insoluble protein aggregates. After proteolytic cleavage of 2-3 h no monomeric Ex1Q49 protein or SDS-stable aggregation intermediates were detectable by immunoblotting using the HD1 antibody (Figure 2.7 A), indicating that the released polyQ protein very efficiently self-assembled into high molecular weight aggregates *in vitro*.

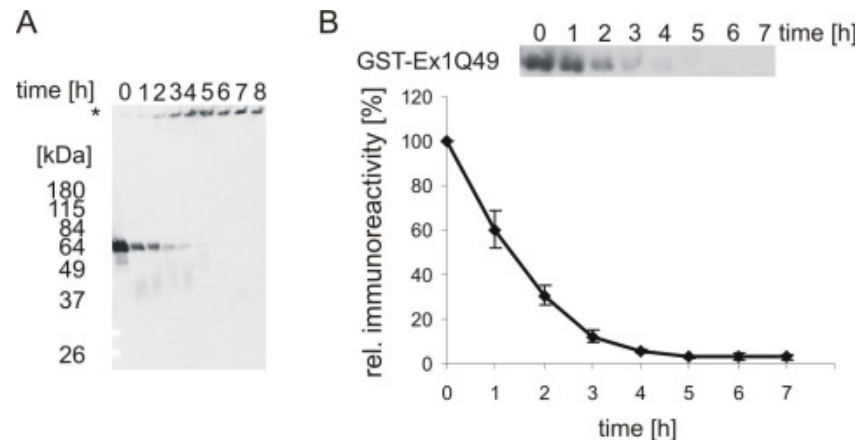


Figure 2.7: Cleavage of GST-Ex1Q49 fusion protein with PreScission protease. (A) GST-Ex1Q49 protein was incubated at a concentration of 2 μ M in the presence of 0.28 U PP per μ g of fusion protein. Cleavage was performed at 20°C and shaking at 300 rpm. Aliquots were taken from the reaction at the indicated time-points and were analyzed by SDS-PAGE on a 10% SDS-polyacrylamide gel and Western blotting using the HD1 antibody. Uncleaved GST-Ex1Q49 protein disappeared after 3 h; no monomeric Ex1Q49 was detected with the HD1 antibody in SDS gels. However, after 3 h high molecular weight species were retained in the pockets of the stacking gel, indicating that Ex1Q49 very efficiently assembles into very large aggregates. (B) The GST-Ex1Q49 band migrating at 64 kDa was quantified by densitometry using the AIDA software. The HD1 immunoreactivity was normalized to $t = 0$ h. More than 90% of the GST-Ex1Q49 fusion protein was cleaved after 3 h.

2.1.4 Investigating the spontaneous aggregation of Ex1Q49 with Thioflavin T binding assays and circular dichroism spectroscopy

While the polyQ tract in the soluble GST-Ex1Q49 fusion protein most likely has an α -helical conformation (Figure 2.3), it adopts a characteristic β -sheet structure in insoluble amyloid aggregates (Nagai et al., 2007). Previous studies have demonstrated that assembly of ordered β -sheet-rich conformations can be monitored using a Thioflavin T (ThT) binding assay. ThT is a dye that changes its fluorescence properties upon binding to β -sheet-rich structures (LeVine, 1999). The shift in fluorescence can be monitored in a plate-reader over time at an excitation wavelength of 450 nm and an emission wavelength of 485 nm.

To investigate whether Ex1Q49 fragments spontaneously assemble into β -sheet-rich structures GST-Ex1Q49 was incubated at a concentration of 1 μ M with ThT and PP and aggregation was monitored over time. As a control, buffer was also incubated in the presence of ThT and the values were subtracted from the measurements with the GST fusion protein. The ThT signal increased in PP treated aggregation reactions after a lag phase of 1 h and reached saturation after 4 h, indicating that β -sheet-rich Ex1Q49 amyloid aggregates were formed *in vitro* (Figure 2.8). In contrast, a time-dependent increase of ThT signals was not observed in the absence of PP, supporting previous results that proteolytic cleavage is critical for aggregate formation (Figure 2.8). The aggregation kinetics observed with ThT assays were very similar to the results obtained with filter retardation assays, indicating that both methods detected similar aggregate structures (compare Figure 2.5 and

Figure 2.8). Thus, the results indicate that SDS-resistant, β -sheet-rich Ex1Q49 aggregates are formed in cell-free aggregation reactions.

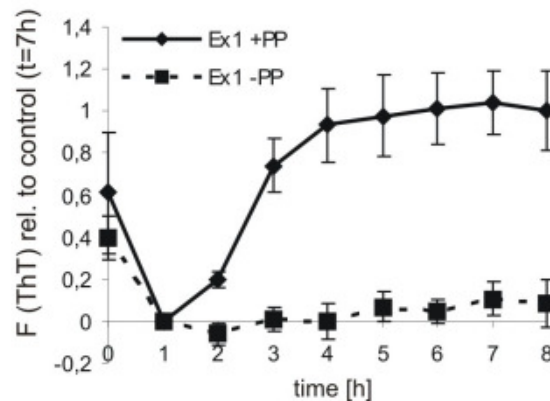


Figure 2.8: Ex1Q49 fragments self-assemble into insoluble protein aggregates with a β -sheet-rich conformation. Aggregation reactions (1 μ M GST-Ex1Q49 fusion protein) were incubated in the presence of Thioflavin T in a plate reader and ThT fluorescence was measured. The signals were normalized to the signal intensity of Ex1Q49 in the presence of PP after 7 h of incubation. After an initial drop of fluorescence intensity the signal remained constant in the absence of PP. In the presence of PP the signal increased again after 1 h reaching saturation after 4 h.

2.1.5 Characterization of Ex1Q49 aggregate morphology by atomic force microscopy and electron microscopy

In order to determine whether the observed Ex1Q49 aggregates have a fibrillar morphology they were analyzed by atomic force microscopy (AFM). Standard aggregation reactions at a concentration of 2 μ M were incubated for 0 h or 24 h and aliquots were spotted on freshly cleaved mica. The samples were imaged with a Nano Wizard® II atomic force microscope operating in tapping mode. Without addition of PP no long fibrillar aggregates were observed but rather small spherical particles with a size of 100 nm. This indicates that uncleaved GST-Ex1Q49 fusion protein forms oligomeric structures (Figure 2.9 A). In contrast, after 24 h in the presence of PP Ex1Q49 formed large bundles and heaps of fibrils (Figure 2.9 B). These fibrils had a width of 10 nm and an average length of 1-1.5 μ m, supporting previous studies that insoluble Ex1Q49 aggregates have typical amyloid structures (Scherzinger et al., 1999).

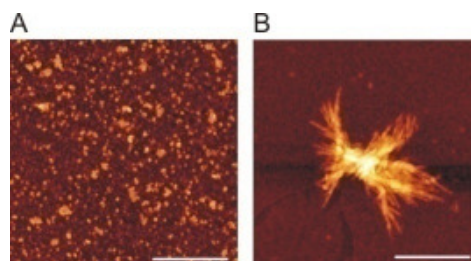


Figure 2.9: Ex1Q49 forms large bundled fibrillar aggregates visualized by atomic force microscopy. (A) Uncleaved GST-Ex1Q49 fusion protein forms small particles with a spherical morphology. (B) Ex1Q49 incubated for 24 h in the presence of PP assembles into large insoluble aggregates with a fibrillar morphology, which often appear as bundled structures. The white scale bars represent 1 μ m.

The Ex1Q49 aggregates were further analyzed by electron microscopy (EM). Aliquots of the reactions were negatively stained with uranyl acetate and imaged on formvar-carbon-coated grids under an electron microscope. In the absence of PP no aggregated fibrillar structures but rather small spherical aggregates were observed. In contrast, bundles of fibrillar aggregates of various sizes were observed after 24 h in the presence of PP (Figure 2.10 B). The Ex1Q49 fibrils had a width of 10 nm and an length of 500-1000 nm. In many cases individual fibrils were connected, suggesting that they form from the same nucleus or seed. A second phenomenon that could be observed was the formation of knot like structures in Ex1Q49 amyloid fibrils, which could be potential branching points. Branching has been suggested in studies for A β ₁₋₄₀ to be the cause for the very fast polymerization rate of amyloid fibrils (Andersen et al., 2009).

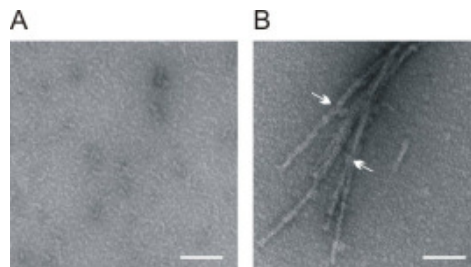


Figure 2.10: Ex1Q49 molecules assemble into aggregates with a typical fibrillar morphology. Aliquots of 2 μ M GST-Ex1Q49 fusion protein were incubated for 0 h (A) or 24 h (B) and were negatively stained with uranyl acetate and observed on formvar-carbon-coated grids with a Zeiss EM 910 electron microscope and a iTEM software. The white bars indicate 200 nm. Fibrils have a width of 10 nm and an averaged length of 500-1000 nm. Arrows indicate knot-like structures and branching points.

2.1.6 Analysis of Ex1Q49 aggregates by semi-denaturing detergent agarose gel electrophoreses

Previous studies have shown that polyQ aggregates can be analyzed by semi-denaturing detergent agarose gel electrophoresis (SDD-AGE), which allows the detection of SDS-stable oligomers and larger aggregates that are often formed as transient intermediates in amyloid polymerization reactions (Halfmann and Lindquist, 2008). Samples of standard aggregation reactions with GST-Ex1Q49 (2 μ M) were incubated with loading buffer with a final SDS concentration of 1% and separated on agarose gels containing 0.1% SDS followed by capillary blotting and immunodetection with HD1 antibody (Figure 2.11 A). Prior to cleavage GST-Ex1Q49 was detected as a single band at 400 kDa, indicating that the fusion protein is a relatively stable oligomer consisting of 10 monomers in aqueous solutions. The intensity of this band decreased and disappeared completely after 2 h upon PP cleavage. At the same time a broad band appeared at about 700 kDa that increased over time in intensity and size,

indicating the formation of large SDS-stable aggregate species (Figure 2.11 A). The time-dependent formation of SDS-resistant Ex1Q49 aggregates was also investigated by filter retardation assay. The results from this study were then compared with data from the SDD-AGE analysis (Figure 2.11 B), demonstrating that both methods detect similar types of high molecular weight SDS-insoluble Ex1Q49 aggregates. However, analysis with SDD-AGE did not allow the detection of SDS-resistant low molecular weight Ex1Q49 oligomers such as dimers, trimers or tetramers, suggesting that such structures are not SDS-stable and cannot be detected with this method (Figure 2.11 A and B).

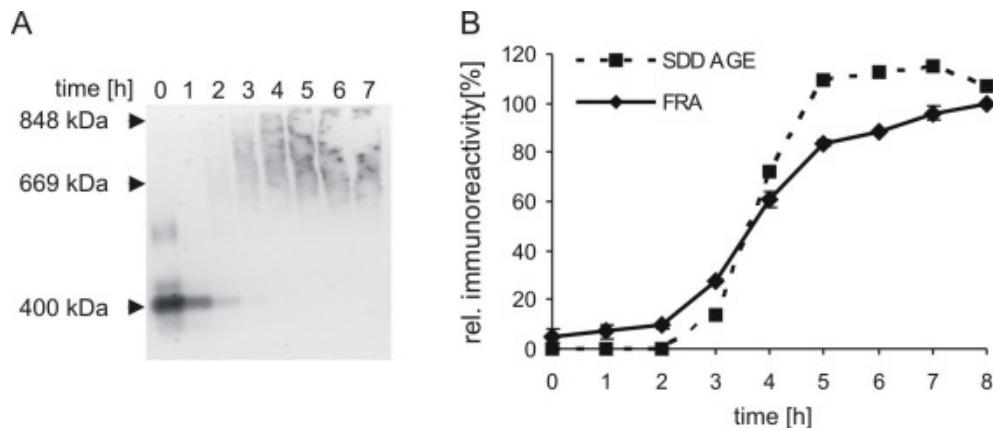


Figure 2.11: Detection of high molecular weight SDS-stable Ex1Q49 aggregates by SDD-AGE analysis. Aliquots of GST-Ex1Q49 (2 μ M) aggregation reactions with PP were subjected to SDD-AGE, transferred to PVDF membrane by capillary blotting and immunodetected with HD1 antibody. (A) Uncleaved GST-Ex1Q49 (400 kDa) disappeared completely after 3 h, while SDS-stable aggregates with a size of 700 kDa appeared over time. Sizes of high molecular weight marker are indicated. (B) Quantification of the 700 kDa band and comparison with filter retardation assay results. Areas corresponding to a molecular weight of 600-850 kDa were quantified by densitometry and the result was normalized to the signal at $t = 8$ h. The rate of formation of high molecular weight aggregate species detected by SDD-AGE is similar to the rate of formation of SDS-resistant aggregates detected by filter retardation assay.

2.1.7 Investigating the formation of Ex1Q49 aggregation intermediates by size exclusion chromatography (SEC)

Next, the formation of SDS-unstable Ex1Q49 aggregation intermediates was investigated by size exclusion chromatography. Neither in SDS-PAGE followed by Western blotting or silver staining, nor in studies with SDD-AGE low molecular weight oligomeric Ex1Q49 aggregate species were detectable (Figure 2.7 and Figure 2.11), suggesting that such structures are labile and cannot be observed under denaturing conditions.

Therefore, spontaneous Ex1Q49 aggregation reactions were analyzed under native conditions by size exclusion chromatography on a Superdex 200 10/300 GL column. To confirm that the eluted fractions indeed contain Htt protein, they were analyzed by dot blot assays using the anti-Htt antibody HD1. The signals were quantified by densitometry and were normalized to the highest intensity of uncleaved GST-Ex1Q49 fusion protein. The uncleaved GST-Ex1Q49 protein was eluted from the column with a molecular mass of

510 kDa, indicating that it is a soluble oligomer under native conditions consisting of 12 monomers (Figure 2.12 A, peak I). Next, the GST-Ex1Q49 fusion protein was analyzed after PP cleavage for 3 h at 10°C. Under these conditions the fusion protein was sufficiently cleaved by PP, however, the low temperature slowed down amyloid aggregation.

In PP treated samples the amount of full-length GST fusion protein with a size of 510 kDa (peak I, fractions 9-11) was reduced, indicating that PP treatment disassembled GST-Ex1Q49 oligomers. However, in the presence of PP multiple lower molecular weight Ex1Q49 oligomers with sizes of approximately 21 (peak VIII, fractions 27-28), 50 (peak VII, fractions 22-24), 75 (peak VI, fractions 17-19), 210 (peak V, fractions 11-13), 350 (peak IV, fractions 11-13), 590 (peak III, fractions 7-9), and 2000 kDa (peak, II fractions 3-5) were detected (Figure 2.12 B), suggesting that small SDS-unstable Ex1Q49 aggregate species are formed in spontaneous aggregation reactions.

Finally, GST-Ex1Q49 fusion protein was investigated that was pre-digested with PP for 3 h at 10°C and subsequently incubated for additional 3 h at 20°C to promote amyloid polymerization (Figure 2.12 C). However, under these conditions the amounts of SDS-unstable Ex1Q49 oligomers, which were readily detectable after 3 h at 10°C, were significantly reduced. This suggests that the SDS-unstable oligomers are transient structures that at 20°C very efficiently convert into large aggregates, which were removed from the sample by centrifugation prior to separation by size exclusion chromatography and therefore could not be detected. Interestingly, a higher molecular weight Ex1Q49 aggregate species with a size of 580 kDa was detectable after incubation for 3 h at 20°C (IX fractions 6-9), supporting the view that large protein assemblies are rapidly formed in spontaneous aggregation reactions. Thus, the size exclusion chromatography results suggest that proteolytic cleavage of GST-Ex1Q49 fusion protein resulted in the formation of small, SDS-unstable Ex1Q49 oligomers of various sizes that rapidly transformed into higher molecular weight SDS-resistant structures.

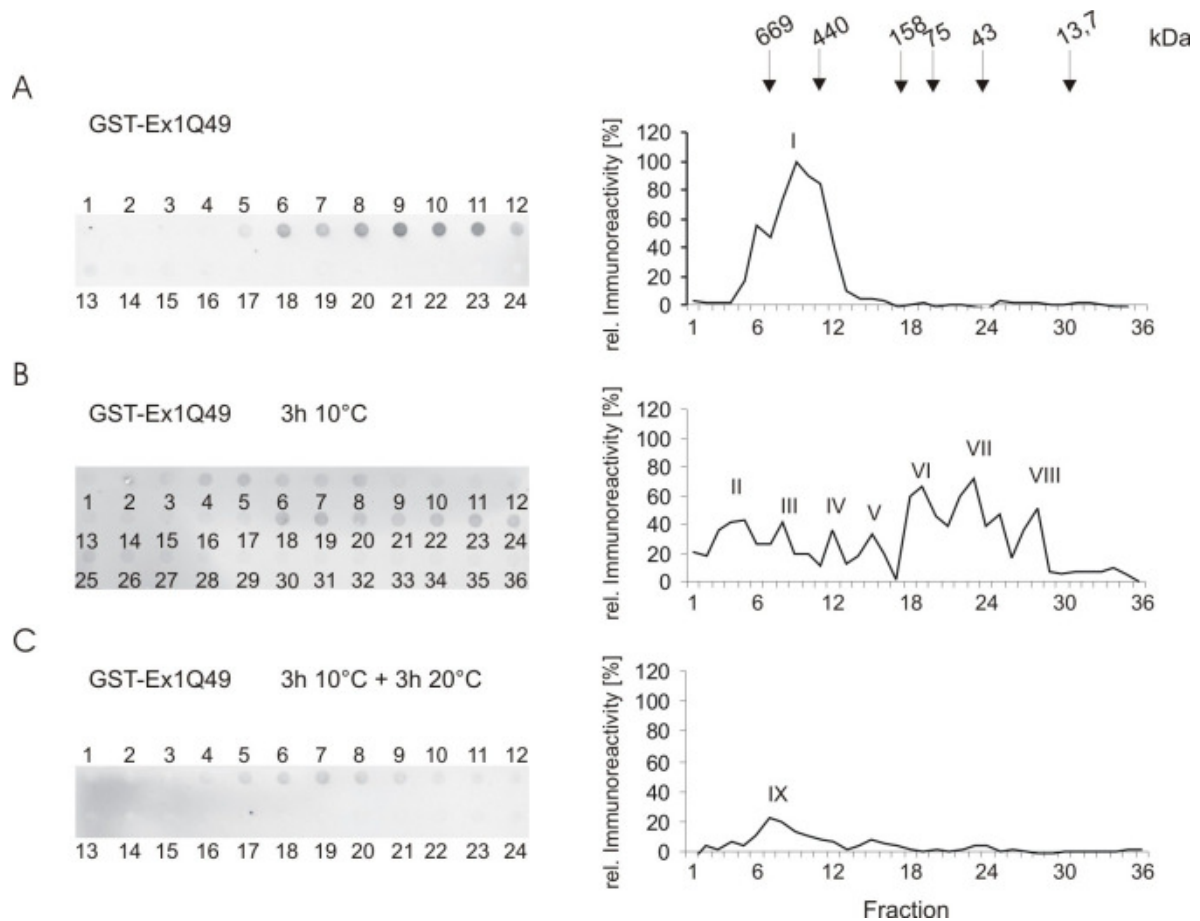


Figure 2.12: Ex1Q49 molecules form transient SDS-unstable oligomers that over time assemble into large amyloid aggregates. Size exclusion chromatography of soluble GST-Ex1Q49 fusion protein on a Superdex 200 column followed by dot blot analysis of fractions and immunodetection of Htt with the HD1 antibody. The antibody staining was quantified by densitometry and the highest signal at $t = 0$ h was set as 100% immunoreactivity. Positions of size markers are indicated in kDa. (A) Soluble GST-Ex1Q49 forms oligomers with a molecular size of 510 kDa. (B) GST-Ex1Q49 (2 μ M) was incubated for 3 h at 10°C in the presence of PP. Ex1Q49 molecules form SDS-unstable oligomers with sizes (peaks II-VIII). (C) 2 μ M GST-Ex1Q49 fusion protein was incubated for 3 h at 10°C followed by incubation for 3 h at 20°C. Samples were centrifuged at 207,000 g for 20 min prior to loading the supernatant onto the column. Most of the Ex1Q49 protein was aggregated after 3 h at 20°C and was removed from the sample prior to separation by size exclusion chromatography.

2.1.8 Spontaneous Ex1Q49 aggregation is a nucleation-dependent process

It has been shown previously that the lag phase of polyQ polymerization reactions can be shortened by the addition of preformed oligomers or small fibrillar aggregates (Scherzinger et al., 1999). As the aggregates grow on the surface of the added particles, this process has been termed seeding. In order to have a homogeneous aggregation mixture, GST-Ex1Q49 was incubated at a concentration of 1 μ M for 3 h at 10°C. Under these conditions the PP cleaved the fusion protein efficiently, while the cleaved Ex1Q49 protein did not form large aggregates. After cleavage, small Ex1Q49 aggregates that were generated by incubation of 2 μ M GST-Ex1Q49 at 20°C for 3 h in the presence of PP (seeds) were added to pre-cleaved GST-Ex1Q49 and the samples were further incubated at 20°C in order to promote amyloid polymerization. The formation of SDS-resistant aggregates was monitored by filter

retardation assay and aggregates were detected using the anti-Htt antibody CAG53b. In the presence of seeds SDS-stable aggregates were detected earlier than in their absence (Figure 2.13), supporting previous investigations that GST-Ex1Q49 amyloid polymerization has all the characteristics of a nucleation-dependent process (Ferrone, 1999).

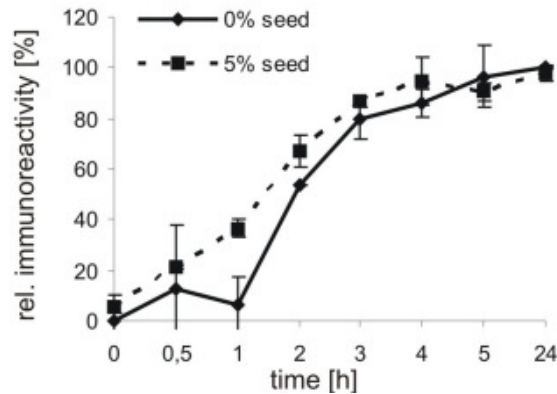


Figure 2.13: Addition of seeds to Ex1Q49 aggregation reactions leads to a reduction of the lag phase. GST-Ex1Q49 at 1 μ M was incubated at 10°C for 3 h in the presence of PP. The pre-cleaved reactions were then incubated at 20°C in the presence or absence of preformed fibrils (5%, 5 mM). Aggregates were detected by filter retardation assay using the CAG53b antibody. Signals were quantified and normalized to the highest signal of the control aggregation without seeds. Addition of seeds reduced the lag phase compared to control reactions.

2.1.9 Analysis of polyQ-mediated Htt aggregation after proteolytic cleavage of GST-Ex1Q49 fusion protein with trypsin

Next, the aggregation mechanism of Ex1Q49 was analyzed after proteolytic cleavage of the GST-Ex1Q49 fusion protein with trypsin. Removal of the GST-tag from the fusion protein by PP led to the formation of a well-defined Ex1Q49 fragment (Figure 2.4). In contrast, the enzyme trypsin has cleavage sites within the Htt-exon 1 protein (Figure 2.14 A), truncating the N- and the C-terminus of the Ex1Q49 fragment. Importantly, trypsin cleavage removes the first 16 amino acids at the N-terminus of Ex1Q49 (Figure 2.14 B), which are known to be critical for efficient polyQ-mediated aggregation of Htt fragments (Lakhani et al., 2010; Williamson et al., 2010). Thus, it is highly interesting to compare the effects of PP and trypsin cleavage on spontaneous aggregation of N-terminal Htt fragments.

Aggregation reactions were performed as described previously by Scherzinger et al. (1999) at a concentration of 10 μ M at 37°C without shaking. Analysis by SDS-PAGE and immunoblotting with the HD1 antibody revealed that GST-Ex1Q49 fusion protein was completely cleaved after an incubation of 2 h with trypsin (Figure 2.14 C and D).

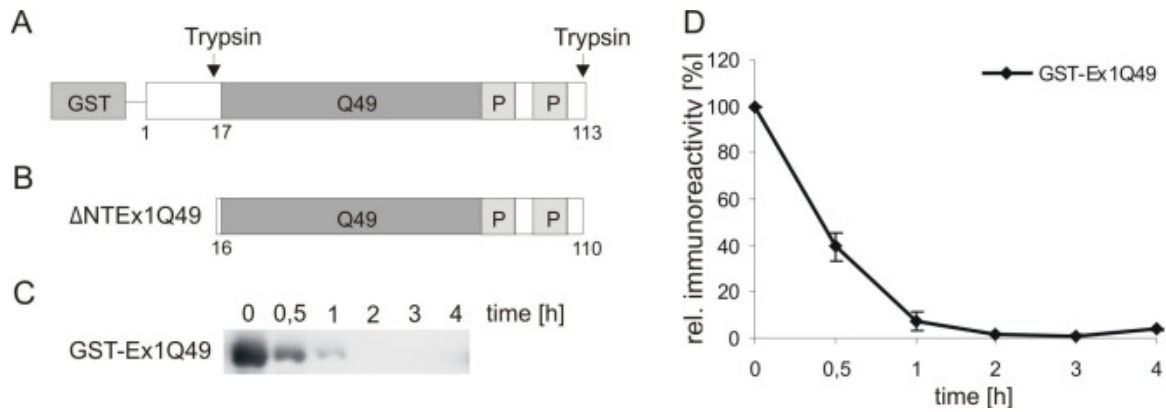


Figure 2.14: Proteolytic cleavage of GST-Ex1Q49 fusion protein with trypsin. (A) Schematic representation of trypsin cleavage sites in the GST-Ex1Q49 protein. (B) Schematic representation of Δ NTEx1Q49. (C) Analysis of trypsin cleavage of GST-Ex1Q49 protein by SDS-PAGE and Western blotting with the HD1 antibody; 10 μ M fusion protein was incubated at 37°C in the presence of 0.1 μ g trypsin per μ g of fusion protein. (D) Quantification of Western blot bands normalized to the signal at t = 0 h. More than 90% of GST fusion protein was cleaved after 1 h.

Next, the time-dependent formation of SDS-insoluble Htt aggregates in trypsin treated reactions with GST-Ex1Q49 fusion protein was analyzed by filter retardation assay. In trypsin treated reactions Δ NTEx1Q49 aggregation was reduced compared to Ex1Q49 aggregation in PP treated reactions (compare Figure 2.5 and Figure 2.14). This supports previous studies that the N-terminal 17 amino acids in Htt are critical for efficient polyQ-mediated protein aggregation (Thakur et al., 2009). Interestingly, Δ NTEx1Q49 aggregation increased very slowly over time and the stationary phase was not reached within an incubation period of 24 h at 37°C (Figure 2.15 A). In comparison, in the absence of trypsin no Δ NTEx1Q49 SDS-stable aggregates were detected within 24 h, indicating that proteolytic cleavage of the fusion protein is critical for the assembly of insoluble polyQ-containing protein aggregates.

After 24 h aliquots were removed from trypsin treated aggregation reactions and were analyzed by atomic force microscopy. Trypsin treatment of GST-Ex1Q49 fusion protein caused the formation of SDS-stable aggregates with a typical fibrillar morphology (Figure 2.15 B). These structures had lengths of 1 μ m and were similar to previously published Htt aggregates (Scherzinger et al., 1999). In contrast, small oligomeric Htt structures with a size of 100 nm were detected immediately after addition of trypsin to GST-Ex1Q49 fusion protein (t = 0 h), indicating that trypsin treatment disassembles spherical oligomers and promotes the spontaneous assembly into structures with a fibrillar morphology (Figure 2.15 B).

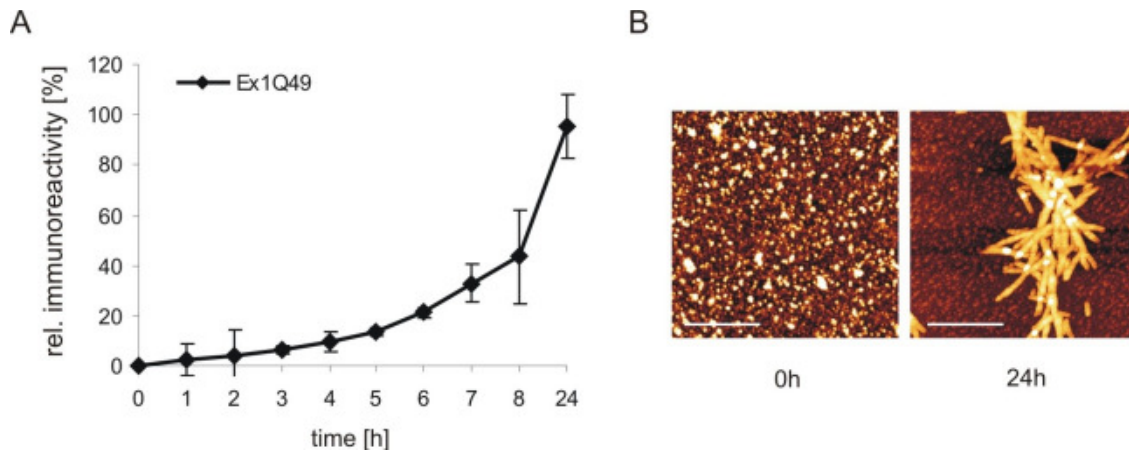


Figure 2.15: Δ NTEx1Q49 assembles into SDS-stable aggregates with a fibrillar morphology. (A) GST-Ex1Q49 fusion protein was incubated at a concentration of 10 μ M at 37°C with trypsin without shaking and formation of Δ NTEx1Q49 was analyzed by filter retardation assay using the anti-Htt antibody CAG53b. Signals were quantified and normalized to the signal at 24 h. Formation of Δ NTEx1Q49 aggregates increased slowly over time and did not reach a maximum after 24 h. (B) Aggregation reactions after 0 and 24 h were analyzed by atomic force microscopy. The indicated white bars represent 1 μ m.

To investigate whether the Δ NTEx1Q49 fragment aggregates by a nucleation-dependent mechanism seeding experiments with preformed polyQ-containing aggregates were performed. The Δ NTEx1Q49 seeds were first prepared by incubating 10 μ M GST-Ex1Q49 protein for 24 h at 37°C in the presence of trypsin. To increase the reaction surface of the generated seeds they were then sonicated 3 times for 30 sec at 4°C. Addition of 0.15% of freshly prepared seeds to an aggregation reaction (10 μ M GST-Ex1Q49 fusion protein treated with trypsin) dramatically promoted the assembly of SDS-stable Δ NTEx1Q49 protein aggregates (Figure 2.16), indicating that this fragment similar to Ex1Q49 (Figure 2.13) assembles into amyloid aggregates by a nucleation-dependent mechanism.

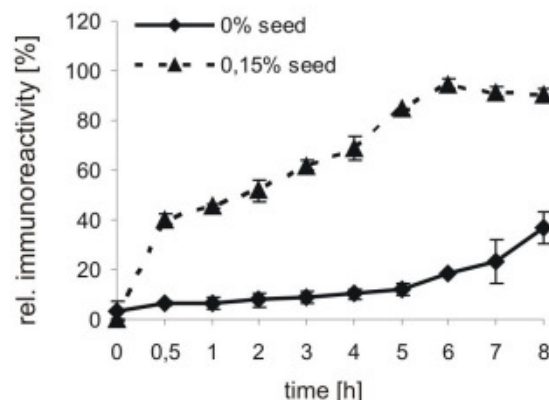


Figure 2.16: Δ NTEx1Q49 assembles into fibrillar aggregates by a nucleation-dependent mechanism. Δ NTEx1Q49 aggregation was performed with trypsin treated GST-Ex1Q49 fusion protein (10 μ M) in the presence or absence of seeds (sonicated Ex1Q49 fibrils; 0.15%, 1.5 mM). Aliquots were analyzed by filter retardation assay and immunoblotting using the anti-Htt antibody CAG53b. In the presence of seeds aggregation of Δ NTEx1Q49 was promoted.

2.1.10 Trypsin generated Δ NTE_{x1Q49} fragments form low molecular weight SDS-stable aggregation intermediates

To investigate whether the aggregation-prone Δ NTE_{x1Q49} fragments generated by trypsin digestion of GST-Ex1Q49 (10 μ M) fusion protein form SDS-stable low molecular weight oligomers, aggregation reactions were analyzed by SDD-AGE (Figure 2.17). Interestingly, SDS-stable, low molecular weight oligomers could be detected in trypsin treated GST-Ex1Q49 aggregation reactions. SDS-stable Δ NTE_{x1Q49} oligomers were readily detected after 1-3 h but disappeared after 4 h (Figure 2.17). Thus, these results indicate that amyloid polymerization is slowed down by the formation of transient SDS-stable low molecular weight Δ NTE_{x1Q49} oligomers. In comparison, Ex1Q49 fragments, which only formed SDS-unstable oligomers (Figure 2.12), very efficiently converted into β -sheet-rich amyloid aggregates (Figure 2.5).

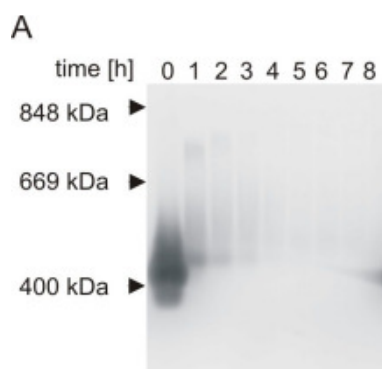


Figure 2.17: Cleavage of GST-Ex1Q49 with trypsin results in the formation of SDS-stable oligomers. 10 μ M GST-Ex1Q49 was incubated at 37°C in the presence of trypsin. Aliquots were removed from the aggregation reaction and were analyzed by SDD-AGE and immunoblotting using the antibody HD1. Trypsin cleavage of GST fusion protein caused the formation of low molecular weight SDS-stable oligomers with a molecular size of 450-650 kDa that were detectable after 1 h. After 4 h the relative amount of low molecular weight SDS-stable oligomers decreases.

2.2 Analysis of spontaneous Ex1Q49 aggregation with epitope specific Htt antibodies

Previous studies indicate that conformational changes in the polyQ sequence of N-terminal Htt fragments are a prerequisite for the formation of SDS-resistant aggregates with fibrillar morphology (Schaffar et al., 2004). To obtain further insights into the mechanism of spontaneous Ex1Q49 polymerization early misfolding events in the aggregation cascade were studied using a time-resolved dot-blot assay with epitope-specific monoclonal antibodies. For systematic studies the antibodies MW1, 3B5H10 and MW8 were applied. The antibodies MW1 and 3B5H10 recognize the polyQ tract in the soluble Ex1Q49 protein, while the antibody MW8 binds to the polyP sequence at the C-terminus of Ex1Q49 (Figure 2.18 A).

GST-Ex1Q49 fusion protein (2 μ M) was incubated in the presence of PP and at the indicated time points samples were frozen at -80°C . Then, aliquots (250 ng GST-Ex1Q49) were spotted onto nitrocellulose membranes and immunodetected with the antibodies MW1, 3B5H10 and MW8 (Figure 2.18 B and C).

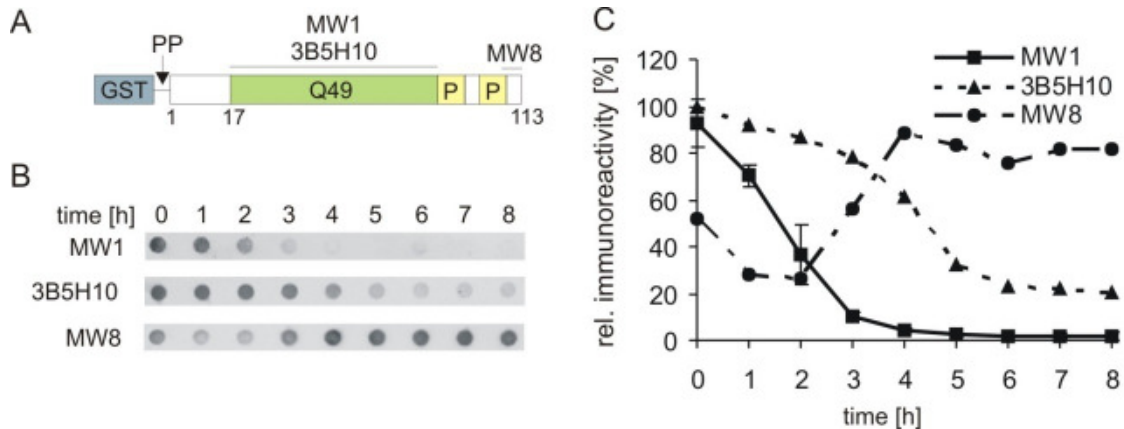


Figure 2.18: GST-Ex1Q49 undergoes a rapid conformational change after cleavage with PP. (A) Schematic representation of GST-Ex1Q49. Binding epitops of the antibodies are indicated. (B,C) 2 μ M GST-Ex1Q49 was incubated with PP for the indicated times and samples were dot blotted onto nitrocellulose membranes for immunodetection with the antibodies MW1, 3B5H10 and MW8. (B) Filter assay (C) Quantification of membranes and normalization. The signals of MW1 and 3B5H10 were normalized to the signals at $t = 0$ h, the signals of MW8 to the highest signal of the reaction. MW1 immunoreactivity disappeared rapidly after cleavage, indicating a fast conformational change in the polyQ tract. A slower decrease in immunoreactivity was observed with the 3B5H10 antibody. The polyP antibody MW8 recognized conformations at later time-points.

The signal for the MW1 antibody decreased very rapidly over time and the decrease in immunoreactivity correlated very well with the kinetic of GST-Ex1Q49 cleavage with PP (Figure 2.18 C and Figure 2.7). Thus, the data indicate that upon proteolytic cleavage of GST-Ex1Q49 with PP a very rapid conformational change in the polyQ tract occurs, which leads to a polyQ structure that cannot be recognized by the MW1 antibody.

A decrease in immunoreactivity with the polyQ-specific 3B5H10 antibody in time-resolved dot-blot assays was also observed. However, the decrease in immunoreactivity with 3B5H10 was reduced compared to the MW1 antibody, indicating that this antibody recognizes a polyQ conformation that is different from the conformation recognized by the MW1 antibody. Thus, the data suggest that the monoclonal antibodies MW1 and 3B5H10 recognize distinct polyQ conformations in Ex1Q49 molecules.

In strong contrast to the antibodies MW1 and 3B5H10 a time-dependent increase in MW8 immunoreactivity was observed (Figure 2.18 C), which was highly similar to the increase of SDS-insoluble aggregates detected by filter retardation assay (Figure 2.19 A). This suggests that the antibody MW8 preferentially recognizes insoluble Ex1Q49 aggregates that appear later in the amyloid formation cascade, while the antibodies MW1 and 3B5H10 preferentially detect early aggregate species, which disappear over time. The increase of MW8 signal in dot blot assays also correlated well with the increase of high molecular weight aggregates detected in SDD-AGE experiments (Figure 2.19 B), supporting the hypothesis that the

antibody detects large aggregates rather than monomers or small oligomers. Thus, the time-resolved studies with dot blot assays suggest that a C-terminal epitope in Ex1Q49 molecules is exposed in end-stage fibrillar aggregates.

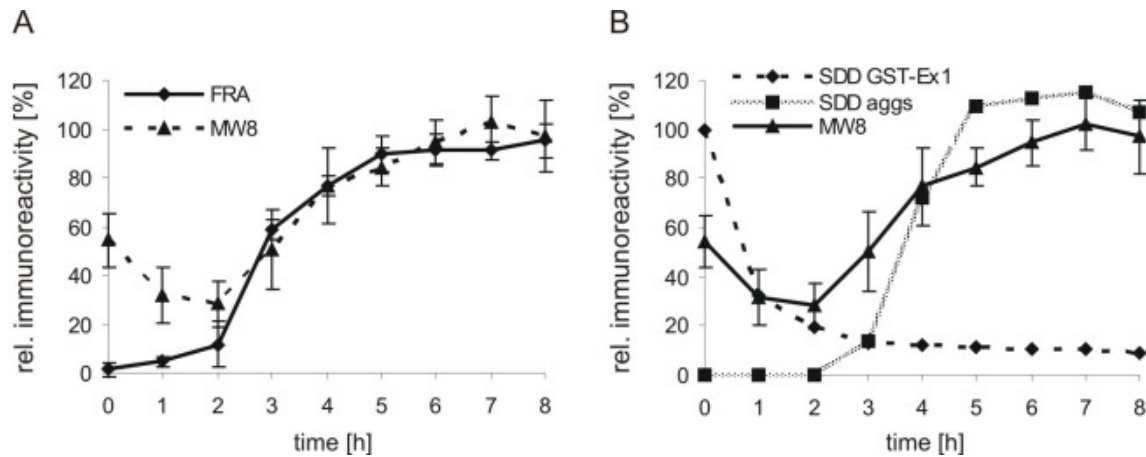


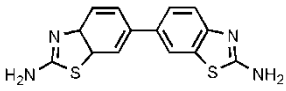
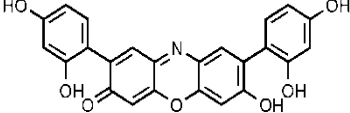
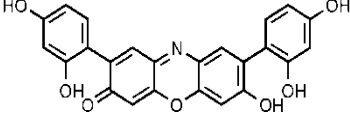
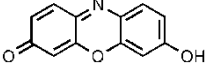
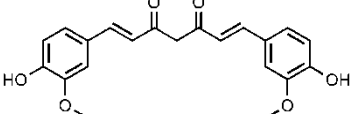
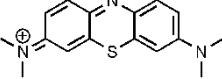
Figure 2.19: The monoclonal antibody MW8 specifically detects the formation of SDS-resistant aggregates observed in dot blot assays. (A) Comparison of results of dot blot assays with the MW8 antibody with results from filter retardation assays with the CAG53b antibody. With both assays the formation of SDS-resistant Ex1Q49 aggregates over time are monitored. (B) Comparison of results of dot blot assays with MW8 antibody and results with SDD-AGE. The time-dependent formation of insoluble Ex1Q49 aggregate species (700 kDa) in SDD-AGE experiments was monitored with the HD1 antibody. Monitoring high molecular weight Ex1Q49 aggregates with SDD-AGE and dot blot assays with MW8 antibody give similar results. All signals were normalized to the highest signal of the aggregation.

2.3 Investigating the effects of small molecules on Ex1Q49 aggregation *in vitro*

2.3.1 The related chemical compounds orcein, O4 and resorufin influence spontaneous Ex1Q49 aggregation in cell-free assays

Previous studies have demonstrated that chemical compounds can be successfully utilized as tools to study the molecular mechanisms of amyloid fibrillogenesis (Ehrnhoefer et al., 2008). Therefore, well-known modulators of amyloidogenesis (Table 2.1) were tested whether they can influence spontaneous Ex1Q49 aggregation in the established time-resolved aggregation assays. The compounds were solubilized in DMSO at a concentration of 20 mM and were diluted in water to a final concentration of 0.2 mM. Controls were treated with DMSO diluted 1:100 in water.

Table 2.1 Chemical structures and names of compounds tested in cell-free aggregation assays.

Structure	Name	Short name	Literature
	PGL-034 6-(2-amino-1,3-benzothiazol-6-yl)3H-1lambda,4,3-benzothiazol-2-amine	PGL034	(Heiser et al., 2002)
	Orcein	Orc	(Heiser et al., 2002)
	O4 2,8-bis-(2,4-dihydroxy-phenyl)-7-hydroxy-phenoxazin-3-one	O4	Bieschke J, 2011
	Resorufin 7-Hydroxy-3H-phenoxazin-3-one	Res	
	Curcumin (E,E)-1,7-bis(4-Hydroxy-3-methoxyphenyl)-1,6-heptadiene-3,5-dione	Curc	(Dikshit et al., 2006) (Yang et al., 2005)
	Methylen blue 3,7-bis(Dimethylamino)phenazathionium chloride	MB	(Oz et al., 2009)

The compounds curcumin, methylen blue, PGL-034, orcein, O4 and resorufin (see Table 2.1) were incubated at different molar ratios (1:3, 1:1 and 5:1) with GST-Ex1Q49 fusion protein (2 μ M) and PP; the formation of SDS-stable protein aggregates was monitored by filter retardation assay (Figure 2.20 and Figure 2.21).

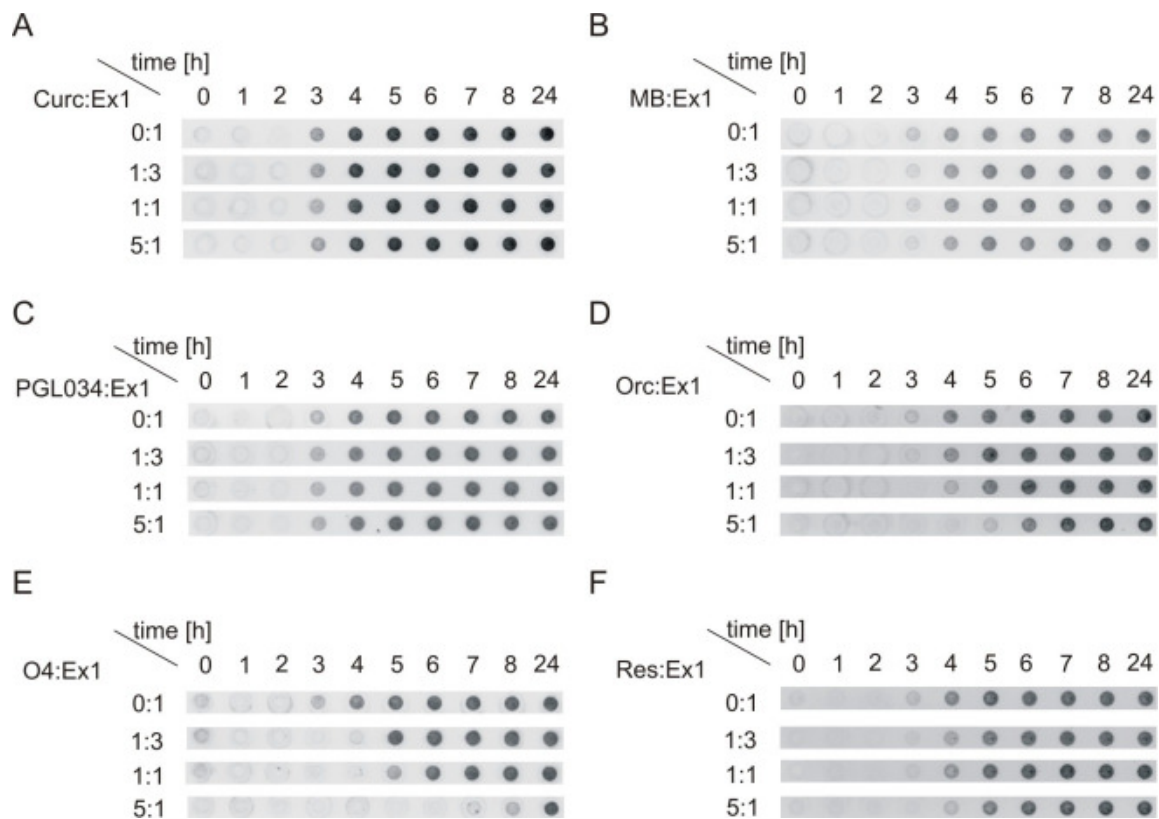


Figure 2.20: Aggregation of GST-Ex1Q49 can be altered by addition of chemical compounds. Aggregation reactions of 2 μ M GST-Ex1Q49 were incubated in the absence or in the presence of three different concentrations of compound. Aliquots were taken at the indicated time-points and analyzed by filter retardation assay. While the compounds curcumin (A), methylene blue (B) and PGL-034 had no effect, the compounds orcein (D), O4 (E) and resorufin (F) reduced the formation of SDS-resistant aggregates.

The compounds curcumin, methylene blue and PGL-034 did not influence spontaneous Ex1Q49 aggregation in cell free assays, while the compounds orcein, O4 and resorufin showed a concentration-dependent effect on amyloid polymerization. The strongest effect on Ex1Q49 aggregation was detected with the compound O4, which at an equimolar concentration (1:1) significantly delayed Ex1Q49 aggregation for about 2 h (Figure 2.21 B).

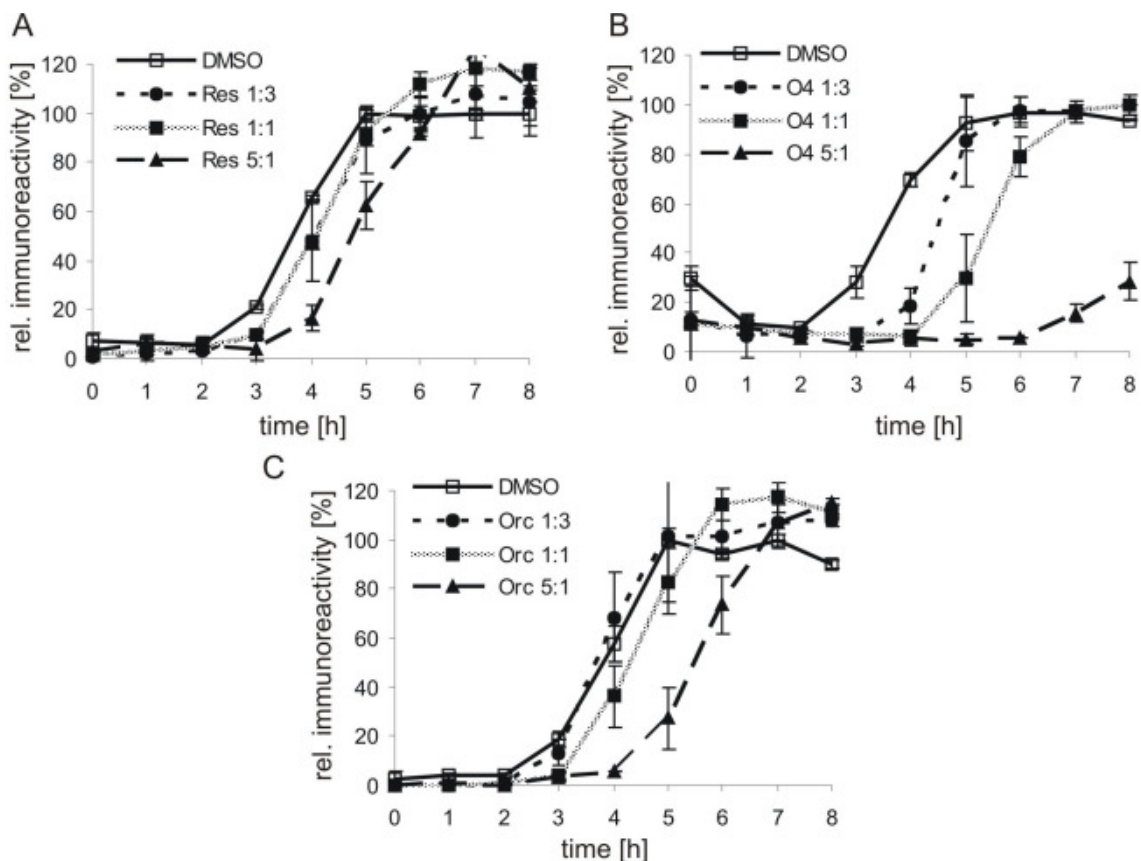


Figure 2.21: The related compounds resorufin, O4 and orcein delay the formation of SDS-insoluble aggregates monitored by filter retardation assay. Filters shown in Figure 1.20 were quantified by densitometry using AIDA software. The signals were normalized to the signal at $t = 8$ h in the absence of compound. The drugs resorufin (A), O4 (B) and orcein (C) delayed the formation of SDS-resistant aggregates in a concentration-dependent manner.

In order to study whether the chemical compounds orcein, resorufin and O4 influence PP-mediated cleavage of the GST-Ex1Q49 fusion protein, aliquots of aggregation reactions were analyzed by SDS-PAGE and Western blotting using the HD1 antibody. These compounds did not significantly influence cleavage of GST-Ex1Q49 protein with PP (Figure 2.22), indicating that their effects on Ex1Q49 aggregation were not caused by inhibiting PP cleavage.

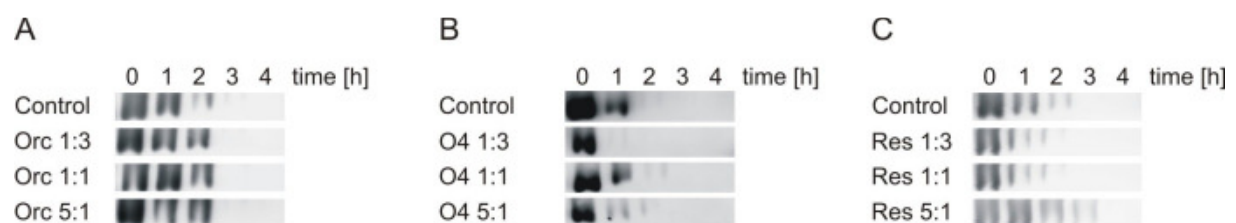


Figure 2.22: Cleavage of GST-Ex1Q49 is not influenced by the addition of compounds. GST-Ex1Q49 aggregation ($2 \mu\text{M}$) was performed in the presence or absence of different concentrations of compounds. Cleavage was controlled by SDS-PAGE and Western blotting with HD1 antibody. (A) Orcein (B) O4 and (C) resorufin.

From the tested compounds O4 had the strongest effect on spontaneous Ex1Q49 SDS-resistant aggregate formation. Thus, O4 was selected for application in further experiments as molecular tool to study the mechanism of spontaneous Ex1Q49 amyloid polymerization *in vitro*.

2.4 Investigating the mechanism of spontaneous Ex1Q49 aggregation using the chemical compound O4

2.4.1 O4 influences early events in the Ex1Q49 aggregation cascade

To analyze the effects of O4 on Htt-exon 1 aggregation time-resolved *in vitro* aggregation assays were performed using different concentrations of the chemical compound. 2 μM of GST-Ex1Q49 fusion protein was co-incubated with PP and 1, 2, or 4 μM O4. Aliquots of aggregation reactions were taken at different time-points and were analyzed by filter retardation assay (Figure 2.23 A). O4 delayed the formation of SDS-resistant aggregates in a concentration dependent manner, indicating that very early events in the aggregation cascade such as the assembly of oligomers were altered by the chemical compound. In contrast, the compound did not significantly alter the exponential growth phase of amyloid fibrils, which is a relatively late event in the amyloid formation cascade (Figure 2.23 B).

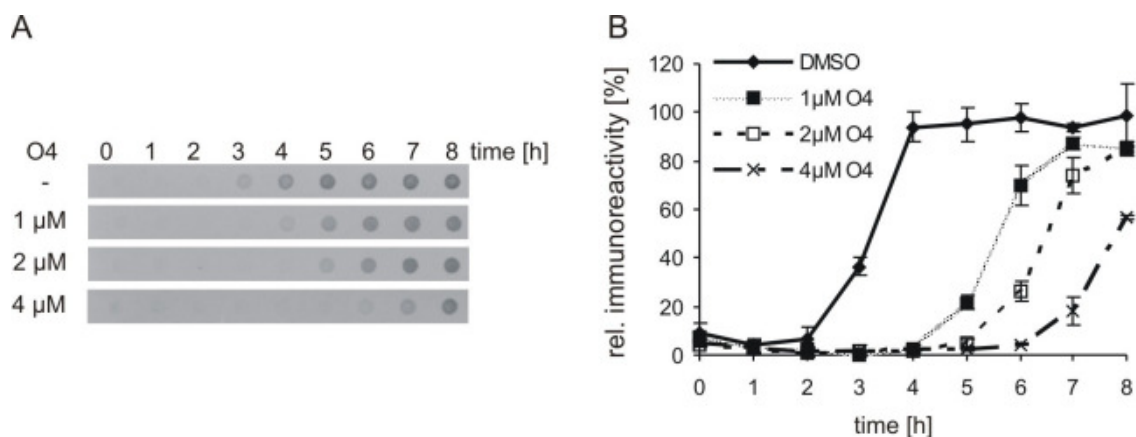


Figure 2.23: In FRA, O4 elongates the lag phase of Ex1Q49 aggregation in a concentration-dependent manner. 2 μM GST-Ex1Q49 was incubated with PP in the presence or absence of 1, 2 or 4 μM of O4. (A) Aliquots were analyzed by filter retardation assay and aggregates were immunodetected with CAG53b antibody. (B) Aggregates on filter membranes were quantified by densitometry and signals were normalized to the signal at $t = 8$ h in the absence of compound. The elongation of the lag phase was concentration-dependent, whereas the chemical compound did not influence the rate of fibril growth.

Next, the influence of the chemical compound O4 on spontaneous $\Delta\text{NTE}1\text{Q49}$ aggregation was analyzed. 10 μM GST-Ex1Q49 fusion protein was incubated with O4 (10 μM) and trypsin

at 37°C and time-dependent formation of SDS-stable protein aggregates was analyzed by filter retardation assay and immunodetection using the CAG53b antibody (Figure 2.24 A). In the absence of O4 a time-dependent increase of Δ NTE Δ Ex1Q49 aggregates was observed (Figure 2.24 A), while in the presence of O4 SDS-resistant aggregates were undetectable after an incubation period of 8 h. However, after a 24 h incubation period with O4 SDS-resistant aggregates were detectable by filter retardation assay (data not shown). This confirms the results obtained with PP that O4 altered early events in the aggregation cascade but did not influence fibril growth.

Finally, the spontaneous formation of Δ NTE Δ Ex1Q49 aggregates in the presence and absence of O4 was analyzed by dot blot assays using the MW8 antibody (Figure 2.24 B). In the absence of O4 the MW8 immunoreactivity increased slowly after proteolytic cleavage of GST-Ex1Q49 fusion protein, while an increase of MW8 immunoreactivity was not detected in the presence of O4. These results support the data obtained with the filter retardation assay that O4 targets early events in the Δ NTE Δ Ex1Q49 aggregation cascade. (Figure 2.24 A).

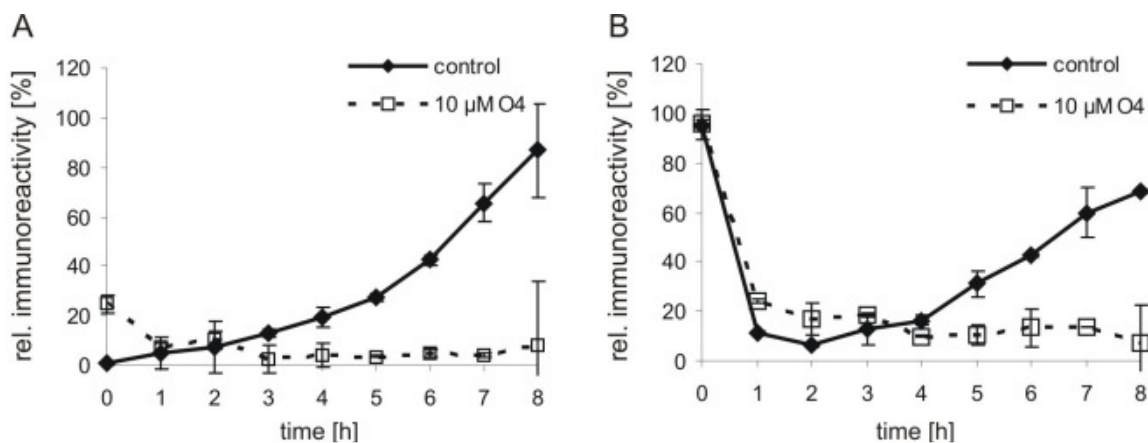


Figure 2.24: O4 influences early events in the Δ NTE Δ Ex1Q49 aggregation cascade. 10 μ M GST-Ex1Q49 was incubated at 37°C with trypsin and an equimolar concentration of the chemical compound O4. (A) filter retardation assay immunodetected with CAG53b antibody. O4 treatment inhibits the formation of SDS-resistant aggregates. (B) Time-resolved dot blot assay immunodetected with the MW8 antibody. The formation of MW8 immunoreactive aggregate species was inhibited by O4.

Next, 20 μ M GST-Ex1Q49 fusion protein was used to study the effect of O4 on spontaneous Ex1Q49 aggregation. Fusion protein was cleaved with PP in the presence or absence of O4 (20 μ M) and aliquots of aggregation reactions were then analyzed by filter retardation assay using the anti-Htt antibody CAG53b. O4 treatment elongated the lag phase of Ex1Q49 aggregation at both high (20 μ M) and low (2 μ M) concentrations of GST fusion protein (Figure 2.25 A). Furthermore, this result was confirmed by dynamic light scattering (Figure 2.25 B) indicating that O4 at an equimolar concentration (20 μ M) slowed down the assembly of higher molecular weight aggregate species for about 30 min.

Taken together these studies indicate that the compound O4 is a potent modulator of Ex1Q49 aggregation in different cell free assays.

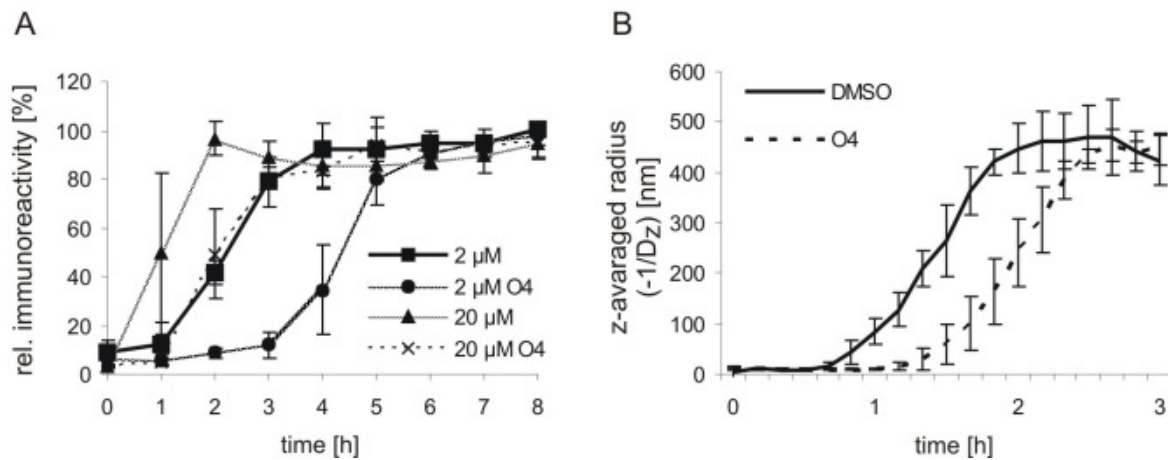


Figure 2.25: Investigating the effects of O4 on spontaneous Ex1Q49 aggregation by filter retardation assay and dynamic light scattering. (A) GST-Ex1Q49 (2 or 20 μM) was incubated with PP in the presence or absence of an equimolar concentration of O4. Aliquots of reactions were analyzed by filter retardation assay using the CAG53b antibody. The signals were quantified by densitometry and normalized to the 8 h control signal at 20 μM . O4 delayed the formation of SDS-resistant aggregates at both concentrations. (B) 20 μM GST-Ex1Q49 fusion protein was incubated with PP at RT in the presence or absence of an equimolar concentration of O4; formation of Ex1Q49 aggregates was monitored by dynamic light scattering (measured every 10 min \pm 1 min). In the presence of O4 the formation of larger particles with an average size of 450 kDa was delayed.

To investigate whether O4 treatment causes the stabilization of aggregation intermediates time-resolved aggregation reactions were analyzed by SDD-AGE. Upon PP cleavage uncleaved GST-Ex1Q49 fusion protein with a size of 400 kDa disappeared after 2 h, while after 3 h SDS-stable, high molecular weight Ex1Q49 protein aggregates with an average size of 700 kDa were detectable. A similar result was also observed in the presence of O4. However, in this case the formation of large aggregates was delayed for 1 h. Thus, these data show that O4 treatment did not stabilize the formation of SDS-stable aggregation intermediates with a size of 400-650 kDa in spontaneous aggregation reactions (Figure 2.26).

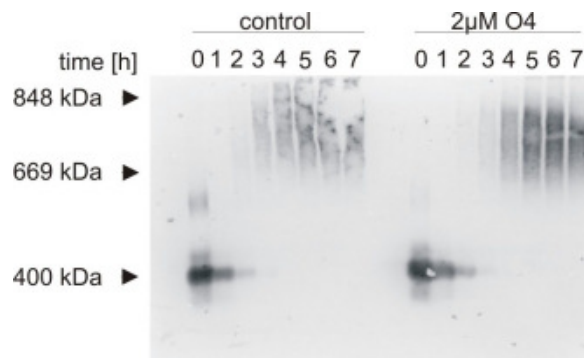


Figure 2.26: O4 treatment does not stabilize SDS-stable low molecular weight oligomers. Aliquots of aggregation reactions (2 μM GST-Ex1Q49 protein incubated with PP) in the presence or absence of O4 were analyzed by SDD-AGE followed by immunodetection with HD1 antibody. No low molecular weight Ex1Q49 oligomers were observed in the presence of O4. However, O4 treatment delayed the formation of large 700 kDa aggregate species.

Several lines of evidence indicate that SDS-stable Ex1Q49 aggregate species are formed by a nucleation-dependent mechanism (Chen et al., 2002; Ferrone, 1999). As O4 has an effect on the lag phase, but not on exponential fibril growth (Figure 2.23), it seems reasonable to speculate that addition of the compound to reactions at later time-points does not influence spontaneous aggregate formation. To test this hypothesis, O4 was added to aggregation assays at different time points (Figure 2.27 A and B). Addition of O4 after 2 or 3 h did not influence Ex1Q49 aggregation, while addition of the compound after 30 min significantly delayed the onset of spontaneous amyloid polymerization. This strongly supports the hypothesis that the compound perturbs a very early event in the amyloid formation cascade.

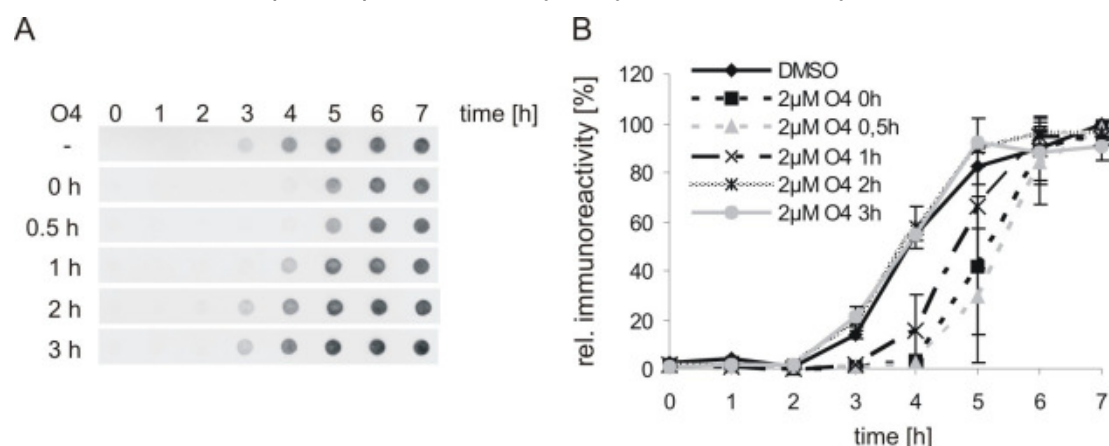


Figure 2.27: O4 delays the formation of SDS-resistant aggregates in a time-dependent manner. 2 μM GST-Ex1Q49 fusion protein was incubated with PP and the compound O4 was added to the aggregation reactions at the indicated time-points. (A) Aliquots of the reactions were analyzed by filter retardation assay using the CAG53b antibody. (B) The filter were quantified and normalized to the 7 h time-point of the control. Addition of O4 after 30 min delayed the onset of aggregation, while addition of the compound after 2 h had no effect.

2.4.2 Characterization of O4 treated Ex1Q49 aggregates by atomic force microscopy and electron microscopy

The effect of O4 on the morphology of Ex1Q49 aggregates was analyzed by atomic force microscopy. Aliquots of aggregation reactions (2 μM GST-Ex1Q49 fusion protein with PP) were incubated with an equimolar concentration of O4 and imaged after 24 h by atomic force microscopy. Both in the presence and absence of O4 large bundles of fibrillar Ex1Q49 aggregates were detected after 24 h (Figure 2.28 C-F), indicating that compound treatment did not alter the morphology of amyloid structures. However, in the presence of O4 the population of aggregates was more diverse than in the absence of the compound, indicating that the compound caused the stabilization of oligomeric and small fibrillar structures. The oligomers formed in the presence of O4 had an averaged diameter of 100 nm. In the absence of PP no fibrillar aggregates were formed and spherical GST-Ex1Q49 oligomers

with a diameter of 100 nm (Figure 2.28 A and B) were detected, confirming the results obtained with SDD-AGE (Figure 2.26).

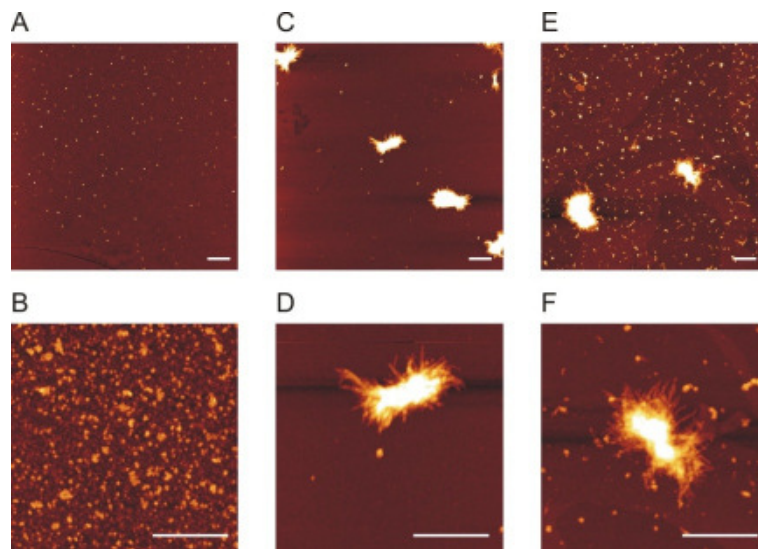


Figure 2.28: Ex1Q49 aggregates formed in the presence of O4 have a fibrillar morphology. Aggregates incubated for 24 h in the presence or absence of O4 were analyzed by atomic force microscopy. White scale bars indicate 1 μ m. (A,B) No aggregates were observed in the absence of PP. (C,D) In the absence of O4 large bundles of fibrillar aggregates were observed, while in the presence of O4 (E,F) spherical oligomers were detected in addition to fibrillar aggregates.

In addition, the insoluble Ex1Q49 aggregates formed in the presence of O4 for 24 h were imaged by electron microscopy (Figure 2.29). Similar to the results obtained by atomic force microscopy with electron microscopy large bundles with multiple associated fibrils were observed, indicating that the compound delayed the onset of amyloidogenesis but did not significantly influence the formation of large fibrillar structures and their morphology.

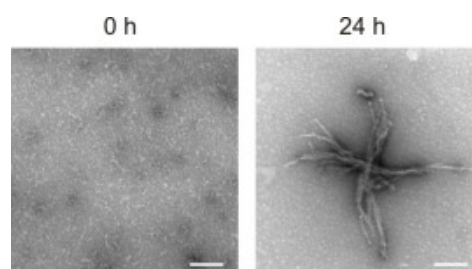


Figure 2.29: O4 treatment does not alter the morphology of fibrillar Ex1Q49 aggregates. GST-Ex1Q49 fusion protein (2 μ M) was incubated with PP in the presence of an equimolar concentration of O4. Aliquots were negatively stained with uranyl acetate and observed on formvar-carbon-coated grids with a Zeiss EM 910. The white bars indicate 200 nm. Fibrils have a width of 10 nm and a length of 0.5-1 μ m.

2.4.3 Seeding eliminates the delay in aggregate formation induced by O4

It has been shown previously that addition of seeds to Ex1Q49 aggregation reactions reduced the lag phase of SDS-stable aggregate formation (Figure 2.13). To investigate whether the effect of O4 is still present in the presence of preformed seeds 1 μ M GST-Ex1Q49 was incubated with PP at 10°C for 3 h in the presence or absence of O4. After addition of 5% seeds the samples were further incubated at 20°C and the formation of SDS-stable aggregates was monitored by filter retardation assay and immunodetection with the anti-Htt antibody CAG53b. In the presence of O4, aggregation was delayed for 2 h compared to the control (Figure 2.30). Addition of seeds almost completely eliminated the effect of O4 and aggregation proceeded comparable to control aggregation reactions. The results further indicate that O4 targets an early event in the aggregation cascade.

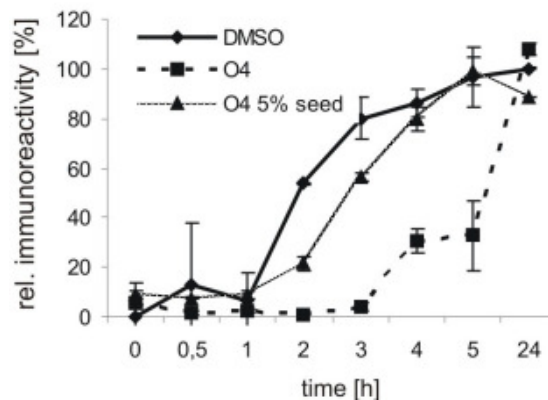


Figure 2.30: Addition of seeds to Ex1Q49 aggregation reactions leads to a reduction of the lag phase. GST-Ex1Q49 at 1 μ M was incubated at 10°C for 3 h in the presence of PP. The pre-cleaved reactions were then incubated at 20°C in the presence or absence of preformed fibrils (5%, 5 mM). Aggregates were detected by filter retardation assay using the CAG53b antibody. Signals were quantified and normalized to the highest signal of the control without seeds. Addition of seeds reduced the lag phase compared to control reactions in the presence and absence of equimolar concentrations of O4.

2.4.4 O4 treatment alters the binding of epitope specific antibodies to aggregation-prone Ex1Q49 molecules

Next, the accessibility of epitopes in Ex1Q49 aggregates was analyzed in the presence and absence of O4 using dot blot assays and the conformational antibodies MW1, MW8 and 3B5H10 (Figure 2.31 A). In the absence of O4 the MW1 antibody efficiently recognized the GST-Ex1Q49 fusion protein. Upon cleavage of the fusion protein with PP the polyQ sequence in the Ex1Q49 protein rapidly changed its conformation, which could be detected with the MW1 antibody. This conformational conversion was not influenced by the addition of O4 to aggregation reactions (Figure 2.31 B), suggesting that the compound does not target the α -helical polyQ structure that is present in the GST-Ex1Q49 fusion protein. However, O4

treatment altered the immunoreactivity of the 3B5H10 antibody, which also recognizes the polyQ sequence in the Ex1Q49 protein (Figure 2.31 C). In the presence of O4 the epitope recognized by the 3B5H10 antibody was longer accessible for the antibody, indicating that the compound stabilizes a polyQ conformation that is critical for the delay of aggregation onset (Figure 2.18 C). This view is also supported by the results, which were obtained with the MW8 antibody (Figure 2.31 D). O4 treatment significantly delayed the increase of the MW8 immunoreactivity in aggregation reactions, indicating that the compound-mediated stabilization of the 3B5H10-reactive polyQ conformation is a cause for the delay in MW8 immunoreactivity increase. Thus, dot blot assays with O4 treated and untreated aggregation reactions allow the detection of underlying relationships in spontaneous aggregation reactions.

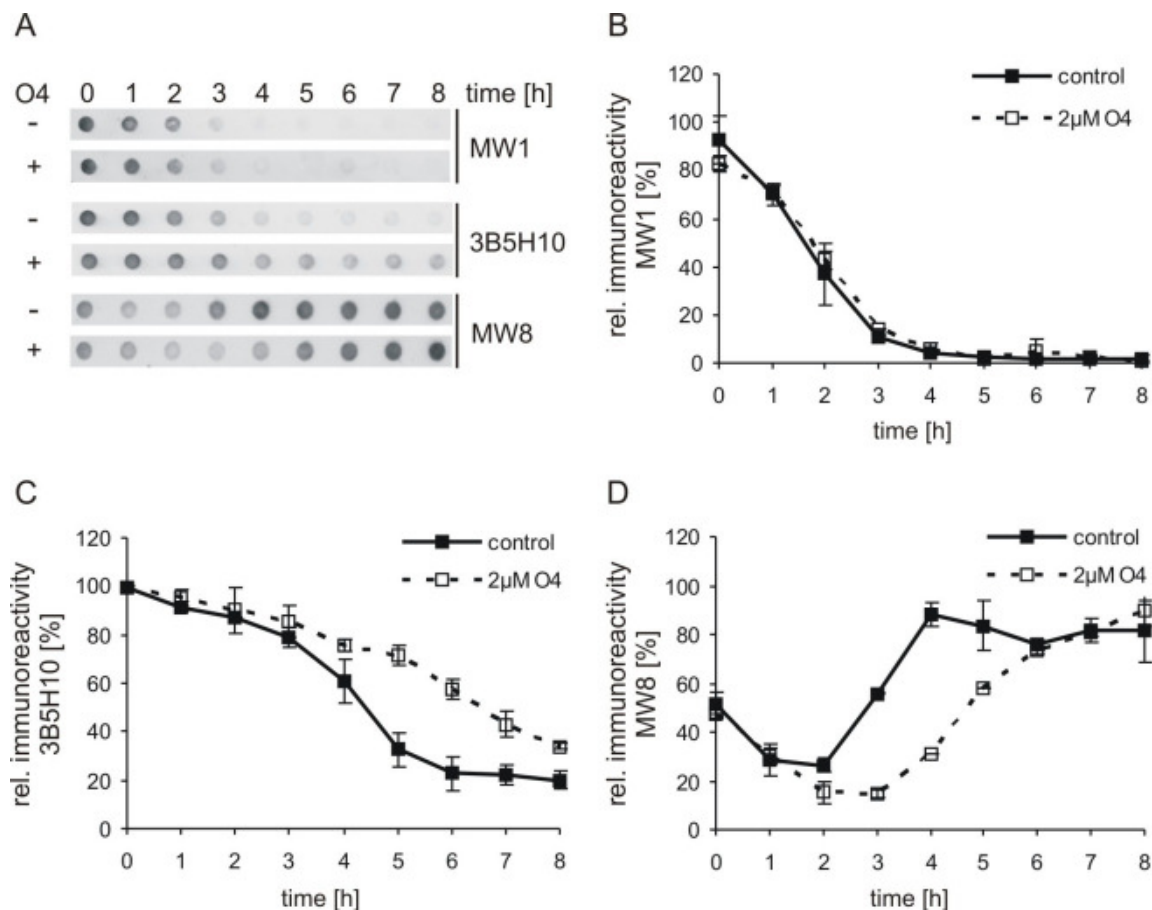


Figure 2.31: O4 stabilizes an early soluble 3B5H10-reactive polyQ conformation that disappears over time with the formation of SDS-stable protein aggregates. 2 μ M GST-Ex1Q49 fusion protein was incubated with PP for the indicated times and samples were dot blotted on nitrocellulose membrane for immunodetection with the antibodies MW1, 3B5H10 and MW8 (A). (B) Quantification of MW1 signal and normalization to the signal at $t = 0$ h of the control. O4 treatment does not influence the rapid disappearance of MW1 immunoreactivity upon cleavage with PP. (C) The signals of 3B5H10 were quantified and normalized to the signal at $t = 0$ h of the control. O4 treatment caused a stabilization of the polyQ conformation that was recognized by the 3B5H10 antibody. (D) The quantified signals of MW8 were normalized to the signal at $t = 8$ h of the control. A delay in Ex1Q49 aggregate formation monitored by an increase in MW8 immunoreactivity was detected upon O4 treatment.

2.5 Effects of O4 treatment on Htt polyQ conformations and toxicity in cell-based assays

Next, the effect of O4 on the stability of the 3B5H10-reactive polyQ conformation in a Htt-exon 1 fragment was analyzed in the human neuroblastoma SH-EP cell line. It has been shown previously that the 3B5H10 antibody staining correlates with Htt induced toxicity in mammalian cells (Legleiter et al., 2010; Zhang et al., 2011), suggesting that the 3B5H10 antibody recognizes a potentially toxic Htt conformation. Therefore, increased 3B5H10 immunoreactivity of Htt is potentially toxic for mammalian cells. Having established that O4 stabilizes a soluble conformation *in vitro* that can be recognized by the 3B5H10 antibody suggests that this compound might also increase the immunoreactivity of a soluble YFP-HttEx1Q73 fusion protein in mammalian cells.

For the production of the YFP-HttEx1Q73 protein in SH-EP cells, a Gateway compatible entry clone was generated by amplification of a fragment encoding the Ex1Q73 sequence from the plasmid FLmixQ73p with a stop codon at the C-terminus. The primers attB_Ex1_fwd and attB_Ex1_rev contained the attB cloning sites for recombination into the pDONR™221 plasmid. The reaction was catalyzed by the BP CLONASE mix, generating the entry clone pDONR-Ex1Q73s. The fragment encoding the Htt protein was transferred from entry clone into a new expression vector by recombination with the pdEYFP-attR plasmid. The obtained plasmid pdEYFP-Ex1Q73 expresses a YFP-Ex1Q73 fusion protein, which could be readily detected by immunofluorescence microscopy in mammalian cells (Figure 2.32 A-D).

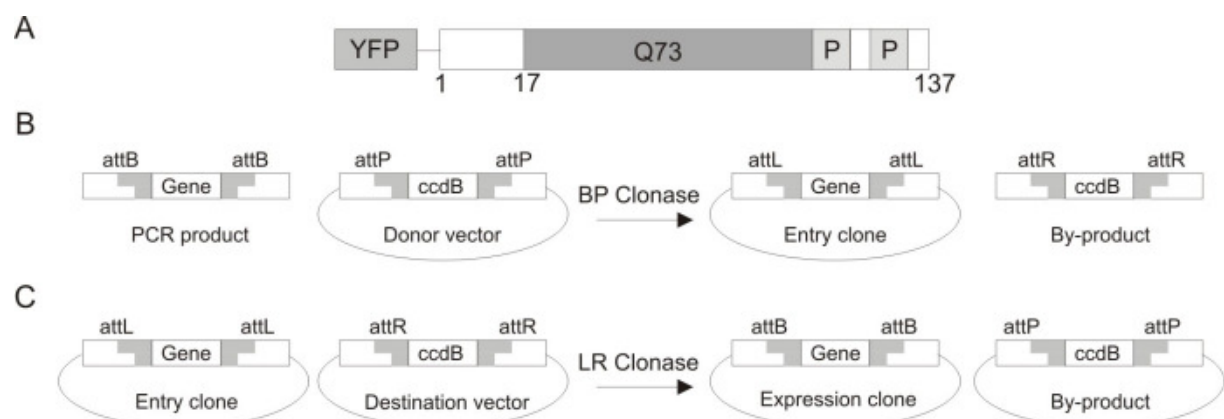


Figure 2.32: Generation of a plasmid for the expression of a YFP-Ex1Q73 fusion protein in SH-EP cells using the Gateway® technology. (A) Schematic representation of the YFP-Ex1Q73 fusion protein. (B) Schematic representation of a Gateway BP reaction. (C) Schematic representation of a Gateway LR reaction. (B and C adopted from Invitrogen).

The human neuroblastoma cell line SH-EP was transiently transfected with pdEYFP-Ex1Q73 expressing YFP-Ex1Q73. After 6 h the medium was exchanged with medium containing either the solvent DMSO or different concentrations of O4. After 48 h a MTT assay was

performed to evaluate the cellular viability. This assay monitors the ability of cells to metabolize MTT to formazan which can be quantified by measuring the absorbance at 570 nm. The addition of 20 μ M O4 to SH-EP cells did not change the viability of cells significantly, whereas the addition of 40 μ M of the compound reduced cell viability, indicating that at this concentration O4 per se is toxic for mammalian cells (Figure 2.33). Interestingly, expression of YFP-Ex1Q73 did not significantly influence the viability of SH-EP cells compared to untransfected controls, indicating that the pathogenic Htt protein under these conditions is not toxic for this cell model.

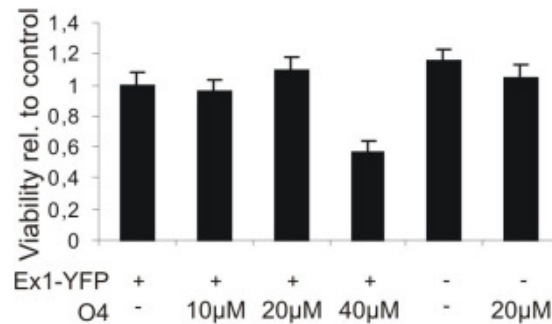


Figure 2.33: High concentrations of O4 are toxic for SH-EP cells. SH-EP cells were transiently transfected with pdEYFP-Ex1Q73 using the Lipofectamine 2000 (Invitrogen). Medium was exchanged after 6 h with medium containing different amounts of O4 and cell survival was evaluated by MTT assay after 2 days. In the absence of the Htt protein the addition of O4 to the growth medium slightly improved cell survival at a concentration of 20 μ M O4. 40 μ M of compound were toxic for the cells.

To investigate whether O4 stabilizes polyQ-exposing conformations in Htt, cells were transfected with the plasmid pdEYFP-Ex1Q73 or the empty vector expressing YFP. 6 h after transfection the medium was exchanged with medium containing either 20 μ M O4 or DMSO as a control. Cells were incubated for 48 h, fixed and immunolabeled with MW1, 3B5H10 or MW8 antibody. The YFP fluorescence intensity of individual cells was analyzed using an automated high-throughput fluorescence microscope. To determine the soluble Htt protein in cells the fluorescence intensity of aggregated Htt was subtracted from the total YFP signal. Soluble YFP intensity was plotted against MW1, MW8 and 3B5H10 intensity. None of the antibodies detected YFP in control cells and the signals were also unchanged by the addition of O4 (data not shown). In cells expressing YFP-Ex1Q73 the addition of O4 significantly increased the immunoreactivity of the antibodies MW1 and 3B5H10 (Figure 2.34 A and B), suggesting that the compound stabilizes the polyQ epitope in the soluble YFP-Ex1Q73 fusion protein. In comparison, no such effect was observed with the MW8 antibody (Figure 2.34 C), which recognizes insoluble Htt aggregates. These results indicate that O4 in cell-free as well as in cell-based assays can influence the conformation of polyQ tracts.

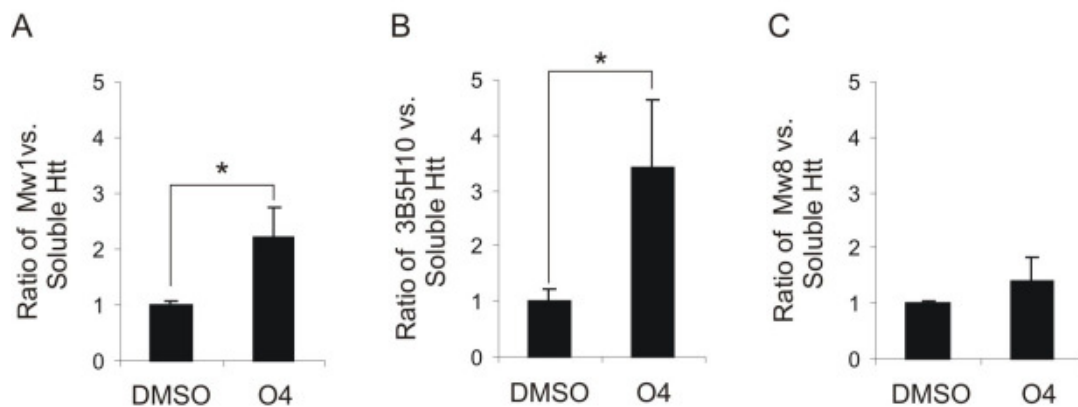


Figure 2.34: O4 treatment increases the amount of MW1 and 3B5H10 reactive, soluble YFP-Ex1Q73 molecules in mammalian cells. SH-EP cells were transiently transfected with pdYFP-Ex1Q73. 20 μ M O4 or DMSO were added to the growth medium after 6 h and cells were fixed after 2 days and immunolabeled with (A) MW1, (B) 3B5H10 or (C) MW8. Cells expressing YFP-Ex1Q73 were analyzed with an automated high-throughput fluorescence microscope. Soluble Ex1Q73-YFP was estimated by subtracting the intensity of insoluble YFP-Ex1Q73 aggregates from the total signal. Soluble YFP intensity for individual cells was quantified and plotted against the immunoreactivity of the antibodies MW1, 3B5H10 and MW8. In the presence of O4 the ratios of MW1 and 3B5H10 compared to soluble Htt increased significantly ($p < 0.01$, $n = 3$). O4 had no effect on the ratio of MW8 to soluble Htt.

In parallel, the expression of the proteins YFP and YFP-Ex1Q79 was analyzed by SDS-PAGE and Western blotting using a YFP antibody (Figure 2.35). The YFP-Ex1Q73 fusion protein had a size of 70 kDa, running higher as the calculated molecular weight of 40 kDa. In comparison for YFP the expected size of 26 kDa was detected. No change in the YFP and YFP-Ex1Q79 protein levels was observed when the cells were treated with 20 μ M O4. Therefore, the increase in polyQ-exposing conformations was not caused by an increase in the amount of soluble Htt fusion protein.

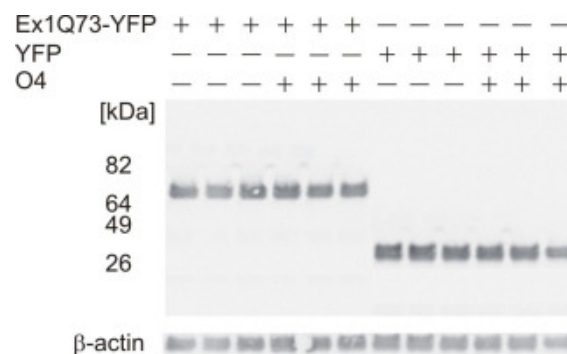


Figure 2.35: Expression levels of Ex1Q73-YFP and YFP are not changed upon treatment with O4. SH-EP cells were transiently transfected with pdEYFP-Ex1Q73 or pdEYFP. 20 μ M O4 or equivalent volumes of DMSO were added to the growth medium and expression was evaluated by SDS-PAGE and Western blotting using the HD1 antibody. The addition of O4 to the growth medium had no effect on the protein levels in SH-EP cells. As a control β -actin expression was analyzed by immunodetection with the AC-15 β -actin antibody.

One reason for the O4-mediated increase in MW1 and 3B5H10 immunoreactivity in YFP-Ex1Q79 expressing SH-EP cells could be that the compound slowed down protein aggregation. Therefore, the formation of SDS-resistant aggregates was analyzed in lysates of

O4 treated SH-EP cells expressing YFP-Ex1Q73 or YFP after 48 h using the filter retardation assay and the Htt antibody CAG53b. No SDS-resistant aggregates were observed in cells expressing YFP. In contrast, in cells expressing YFP-Ex1Q73 SDS-resistant aggregates were detectable. However, a significant decrease in insoluble Htt aggregates upon O4 treatment was not detectable by filter retardation assay (Figure 2.36). This indicates that the compound influences the abundance of soluble MW1 and 3B5H10 reactive Htt molecules in cells but not the abundance of SDS-stable protein aggregates.

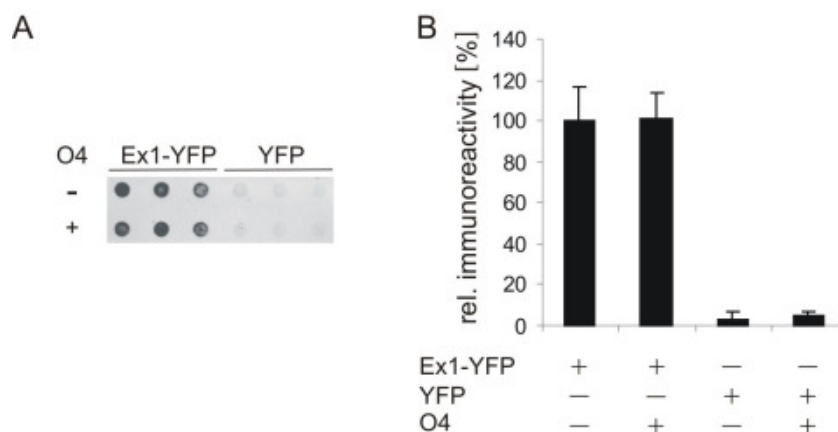


Figure 2.36: The abundance of YFP-Ex1Q79 aggregates in SH-EP cells is not altered by the addition of O4. SH-EP cells were transiently transfected with the pdYFP-Ex1Q73 or pdYFP-attR plasmid and treated with 20 μ M of O4 or the solvent DMSO. (A) After two days of expression cell lysates were prepared and subjected to the filter retardation assay. Aggregates were detected using the CAG53b antibody. (B) Quantification of membranes normalized to the control. O4 had no effect on insoluble Ex1Q73-YFP protein aggregates formed in SH-EP cells.

Finally, experiments were performed to investigate whether the polyQ-binding antibodies MW1 and 3B5H10 recognize a specific subpopulation of Htt conformations in Htt expressing mammalian cells. SH-EP cells were grown on cover slips and were transiently transfected with pdEYFP-Ex1Q73. After 24 h cells were fixed and immunolabeled with MW1 and 3B5H10 and a mouse Cy5 secondary antibody. Cells were imaged using a Leica SP2 confocal microscope (Figure 2.37). Ex1Q73-YFP showed a diffuse cytoplasmic distribution in cells with enrichment in the perinuclear region and at the plasma membrane. The conformations recognized by MW1 and 3B5H10 were localized specifically at the plasma membranes, indicating that the antibodies recognize highly distinct cellular Htt structures.

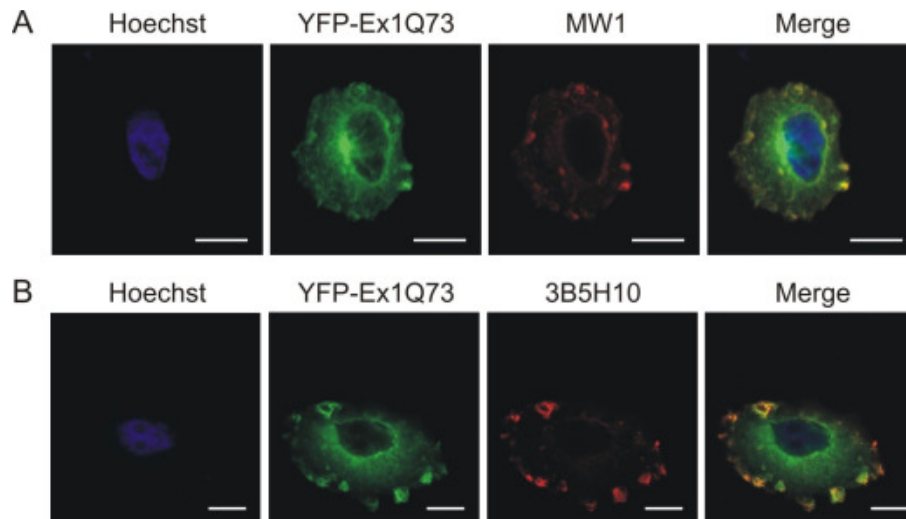


Figure 2.37: The anti-polyQ antibodies MW1 and 3B5H10 specifically recognize Htt structures that are localized at the cell membrane. Scale bars represent 10 μm . SH-EP cells were transiently transfected with pEYFP-Ex1Q73. Ex1Q73-YFP was expressed for 24 h and cells were fixed and immunolabeled with (A) MW1 and (B) 3B5H10 antibody.

2.6 Investigating the spontaneous aggregation of an N-terminally truncated Htt-exon 1 fragment

Previous studies have shown that polyQ-mediated aggregation of N-terminal fragments is dramatically influenced by polyQ-flanking amino acid sequences (Lakhani et al., 2010; Williamson et al., 2010). It was suggested that the N-terminal 17 amino acids in Htt function as an enhancer of polyQ-mediated protein aggregation (Duennwald et al., 2006; Thakur et al., 2009), while the polyP region located downstream of the polyQ tract suppresses spontaneous aggregation (Bhattacharyya et al., 2006). The results obtained with the Δ NEx1Q49 fragment, which is released by proteolytic cleavage of GST-Ex1Q49 with trypsin, support the view that the N-terminal amino acids in Htt promote amyloid polymerization (Figure 2.15).

2.6.1 Generation of the plasmid pGEX-6P1- Δ NHttEx1Q49 for the expression of the GST- Δ NEx1Q49 fusion protein

To investigate whether the N-terminus in Htt is indeed an enhancer of spontaneous Ex1Q49 aggregation a plasmid was generated that allows the expression of a GST-Htt-exon 1 fusion protein without the first 15 amino acids of Htt. The cDNA fragment encoding the Δ NEx1Q49 protein was amplified by polymerase chain reaction from a pGEX-6P1-HttEx1Q49 plasmid using the primers delta1-17_fwd_EcoRI and Ex1_NotI_rev. The obtained fragment with a size of 0.31 kb was then subcloned into the expression vector pGEX-6P1 using the restriction sites EcoRI and NotI. The resulting plasmid pGEX-6P1- Δ NHttEx1Q49 was transformed into *E. coli* strain DH10B and the correct insertion of the cDNA fragment was analyzed by the same enzymes, confirming the expected size of the fragment (Figure 2.38 A). The plasmid insert was further characterized by sequence analysis. The protein sequence of the GST fusion protein is shown in Figure 2.38 B and a schematic representation of the protein is given in Figure 2.38 C.

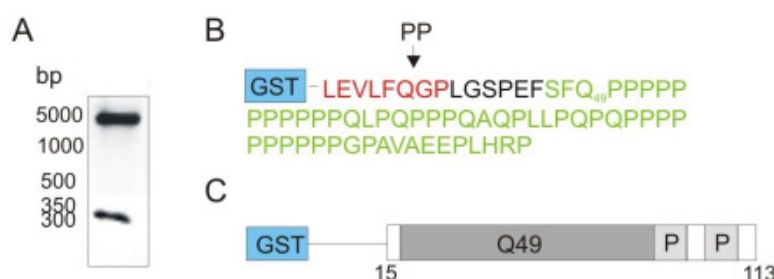


Figure 2.38: Generation of the plasmid pGEX-6P1- Δ NHttEx1Q49 for the expression of GST- Δ NEx1Q49. (A) Restriction digestion of pGEX-6P1- Δ NHttEx1Q49 using the restriction enzymes EcoRI and NotI. Fragments were analyzed on a 1% agarose gel. The DNA insert had a size of 0.31 kb. (B) Amino acid sequence of GST- Δ NEx1Q49 fusion protein. Blue box: Schematic representation of glutathione S-transferase (GST). Red: PP recognition site. Green: amino acids of the Δ NEx1Q49 protein. (C) Schematic representation of the GST- Δ NEx1Q49 fusion protein.

2.6.2 Production and purification of GST-ΔNEx1Q49 fusion protein

The plasmid pGEX6P1-ΔNHttEx1Q49 was transformed into *E. coli* strain BL21-RP and expression of the GST-ΔNEx1Q49 fusion protein was induced by addition of 1 mM IPTG to the growth medium of liquid cultures (3 h at 37°C). Cells were harvested and recombinant protein was purified under native conditions by affinity chromatography on glutathione agarose. 1 μg of the purified protein was analyzed by SDS-PAGE and Coomassie staining (Figure 2.39 A), indicating that the GST-Htt fusion protein has a size of 60 kDa. The protein was further characterized by Western blotting with a GST (Figure 2.39 B) and an anti-Htt antibody (Figure 2.39 C). Both antibodies recognized the fusion protein and some degradation products, indicating that the fusion protein GST-ΔNEx1Q49 is suitable for aggregation studies in cell-free assays.

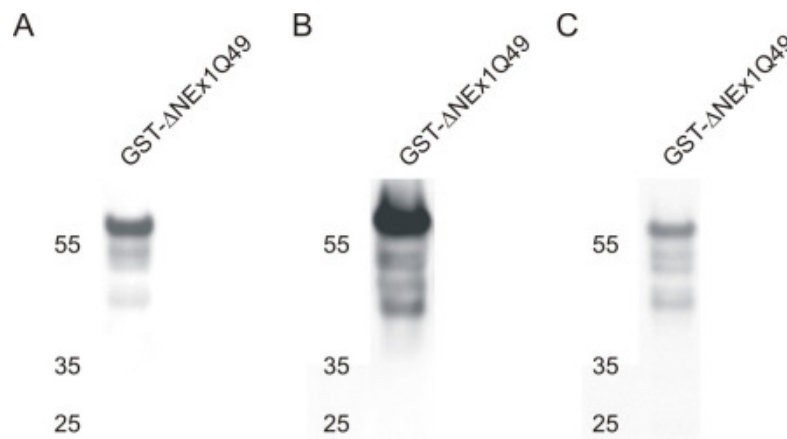


Figure 2.39: Purification and characterization of GST-ΔNEx1Q49 fusion protein. Purified GST fusion protein was analyzed on a 4-16% gradient gel. (A) Coomassie staining of GST-ΔNEx1Q49 fusion protein. The polyQ containing protein runs at a higher molecular size than expected. (B) Western blot analysis with an anti-GST antibody and the anti-Htt antibody HD1 (C). The HD1 and GST antibodies both recognized the full-length GST-ΔNEx1Q49 fusion protein.

2.6.3 Analysis of ΔNEx1Q49 aggregation using cell-free assays

Previous studies have shown that flanking sequences of polyQ tracts influence the aggregation kinetics of N-terminal Htt fragments (Duennwald et al., 2006; Thakur et al., 2009). To study the spontaneous aggregation of the ΔNEx1Q49 fragment, GST-ΔNEx1Q49 fusion protein (10 μM) was incubated with PP and formation of SDS-stable protein aggregates was quantified over time with the filter retardation assay using the anti-Htt antibody CAG53b. Insoluble ΔNEx1Q49 aggregates were formed after a lag-phase of 8 h (Figure 2.40 A and B), indicating that the truncated protein aggregates much slower than the Ex1Q49 protein *in vitro* (Figure 2.5). Thus, the studies with the ΔNEx1Q49 fragment

confirmed the results with the Δ NTE x 1Q49 fragment, which was released from GST-Ex1Q49 by trypsin digestion (Figure 2.15).

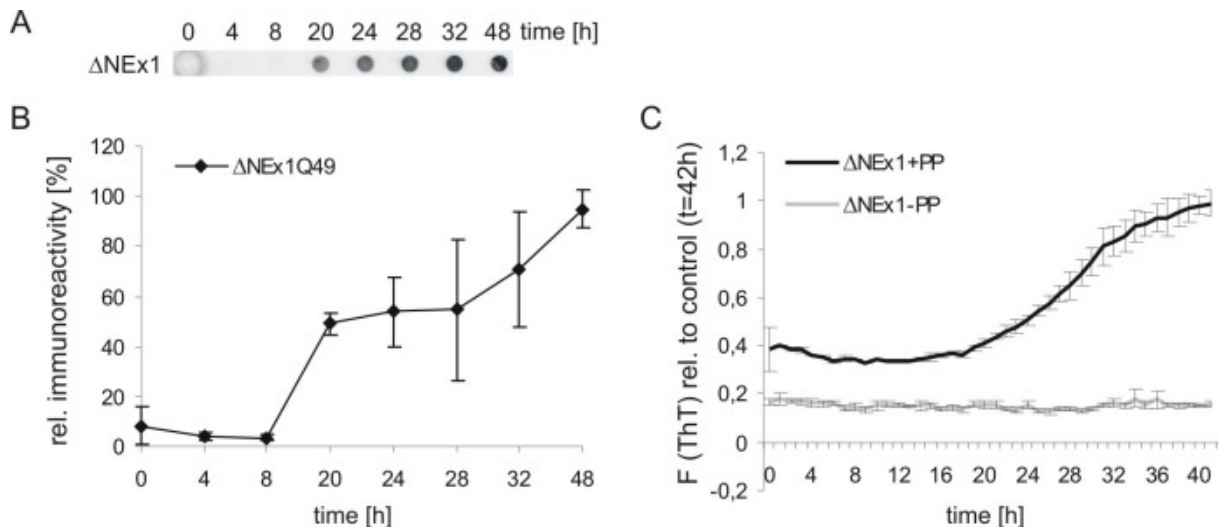


Figure 2.40: Investigating the formation of Δ NEx1Q49 aggregates by filter retardation assay and ThT assays. (A,B) Detection of SDS-resistant Δ NEx1Q49 aggregates by filter retardation assay using the CAG53b antibody. Δ NEx1Q49 forms SDS-resistant aggregates after 8 h and aggregation increases further over time. (C) Analysis of Δ NEx1Q49 aggregation using a ThT assay. ThT kinetics for 10 μ M Δ NEx1Q49 incubated continuously in the presence or absence of PP at 24 $^{\circ}$ C. ThT signals were normalized to the final signal of the reaction in the presence of PP.

The formation of Δ NEx1Q49 aggregates was also investigated using a Thioflavin T (ThT) fluorescence assay. GST- Δ NEx1Q49 fusion protein (10 μ M) was incubated with ThT in the presence or absence of PP and formation of aggregates was monitored over time at a wavelength of 485 nm (Figure 2.40 B). ThT fluorescence increased after a lag phase of 16 h and reached saturation after 38 h, essentially confirming the results with the filter retardation assay (Figure 2.40 A). These results indicate that the generated insoluble Δ NEx1Q49 aggregates have a β -sheet-rich structure.

To investigate whether the insoluble Δ NEx1Q49 aggregates have a fibrillar morphology the aggregates were also analyzed by atomic force microscopy. In the absence of PP, oligomers formed of GST- Δ NEx1Q49 fusion proteins with a diameter of 100 nm were detected (Figure 2.41 A). In strong contrast, bundles of fibrillar Δ NEx1Q49 aggregates were observed after an incubation of GST fusion protein for 48 h with PP (Figure 2.41 B), supporting the results observed with the ThT assay that ordered, β -sheet-rich aggregates are spontaneously formed (Figure 2.40).

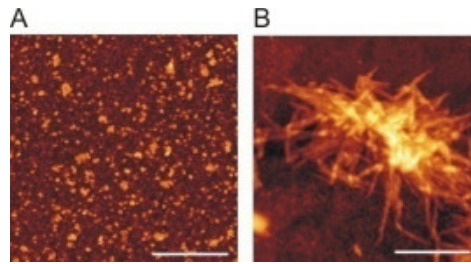


Figure 2.41: Analysis of spontaneously formed Δ NEx1Q49 aggregates by atomic force microscopy. 10 μ M GST- Δ NEx1Q49 fusion protein was incubated for 48 h in the presence of PP and aliquots were spotted on freshly cleaved mica. Aggregates were imaged in tapping mode using a Zeiss Nano Wizard II atomic force microscope. (A) In the absence of PP GST- Δ NEx1Q49 protein forms oligomers with a diameter of 100 nm. (B) Δ NEx1Q49 forms fibrillar aggregates after proteolytic cleavage with PP for 48 h.

To investigate whether the Δ NEx1Q49 protein forms SDS-stable oligomers, aggregation reactions (10 μ M GST- Δ NEx1Q49 protein incubated with PP) were analyzed by SDS-PAGE and immunoblotting using an anti-Htt antibody. Interestingly, cleavage of GST fusion protein with PP resulted in the formation of a 180 kDa SDS-stable oligomer, which disappeared after 24 h, when large SDS-resistant aggregates were formed and could be detected in the pockets of the gel (Figure 2.42 A). A quantitative analysis of GST- Δ NEx1Q49 cleavage finally also showed that more than 90% of the fusion protein was cleaved after 1 h in the presence of PP (Figure 2.42 B). Thus, Δ NEx1Q49 protein converts via SDS-stable oligomers into insoluble β -sheet-rich aggregates with a fibrillar morphology.

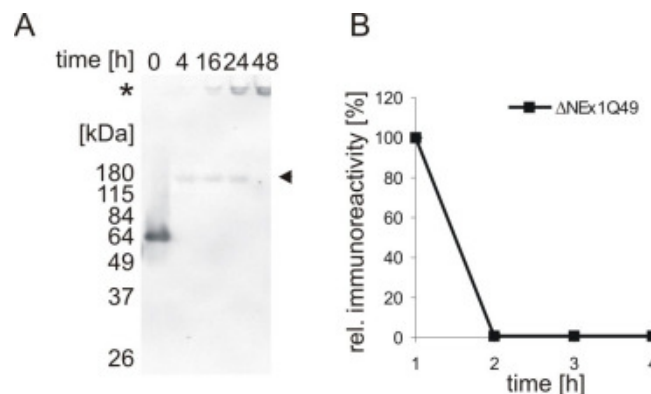


Figure 2.42: The protein Δ NEx1Q49 converts via low molecular weight SDS-stable oligomers into fibrillar aggregates. (A) GST- Δ NEx1Q49 fusion protein (10 μ M) was incubated with PP and formation of aggregates was analyzed by SDS-PAGE and Western blotting using the HD1 antibody. After 4 h no uncleaved GST- Δ NEx1Q49 protein was detected. Instead a band at 180 kDa appeared that disappeared again when aggregation proceeded and aggregates were detected in the stacking gel. (B) Aliquots of the aggregation reaction were analyzed by SDS-PAGE and Western blotting using the HD1 antibody. Uncleaved GST- Δ NEx1Q49 fusion protein with a size of 64 kDa was quantified and signals were normalized to $t = 0$ h. 95% of the fusion protein was cleaved after 1 h.

2.6.4 Investigating the formation of Δ NEx1Q49 aggregation intermediates by semi-denaturing detergent agarose gel electrophoreses, size exclusion chromatography and CD spectroscopy

Having established that Δ NEx1Q49 forms SDS-stable oligomers with a size of 180 kDa (Figure 2.42 A), spontaneous aggregation reactions of PP treated GST- Δ NEx1Q49 fusion protein (10 μ M) were also analyzed by SDD-AGE. GST- Δ NEx1Q49 fusion protein was cleaved completely after 4 h and large Δ NEx1Q49 aggregates with a size of 700 kDa were detected after 24 h (Figure 2.43), indicating that low molecular weight SDS-stable oligomers cannot be detected with SDD-AGE but with SDS-PAGE (Figure 2.42 A).

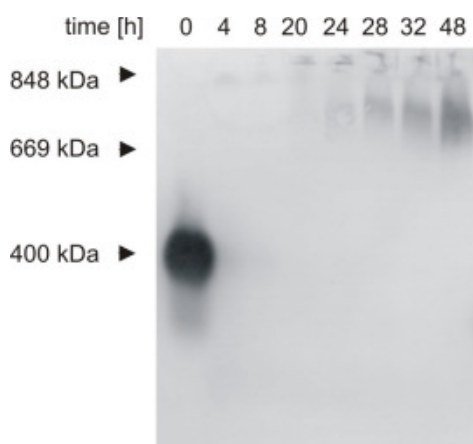


Figure 2.43: Investigating the formation of Δ NEx1Q49 aggregates by SDD-AGE experiments. Aliquots were taken from 10 μ M GST- Δ NEx1Q49 aggregation reactions and separated on SDD agarose gels, transferred by capillary blotting to a PVDF membrane and immunodetected with HD1 antibody. GST- Δ NEx1Q49 had a size of 400 kDa and disappeared completely after 4 h. Δ NEx1Q49 formed high molecular weight species of 700 kDa that increased over time after 24 h of incubation.

To exclude the possibility that SDD-AGE is too insensitive to resolve small amounts of Δ NEx1Q49 intermediates, aliquots of aggregation reactions were also analyzed by size exclusion chromatography. 10 μ M of GST- Δ NEx1Q49 protein were incubated for 0, 4 or 48 h in the presence of PP. Then, samples were centrifuged for 20 min at 208,000 g to remove aggregates and were separated on a size exclusion column. The eluted fractions were finally analyzed by dot blotting using the HD1 antibody. For the uncleaved GST-fusion protein two peaks with sizes of 240 and 700 kDa were obtained (Figure 2.44 A). The 240 kDa peak (fraction I) was further analyzed by SDS-PAGE and Western blotting with HD1 and GST antibodies. After denaturation of the sample, a band of 64 kDa was detected by immunoblotting (Figure 2.44 B), confirming earlier results that GST- Δ NEx1Q49 protein has a size of about 60 kDa in SDS gels (Figure 2.42). These results suggest that the GST- Δ NEx1Q49 fusion protein forms oligomers under native conditions that dissociate under denaturing conditions into monomers. As expected, no monomeric GST migrating at 28 kDa was detected prior to proteolytic cleavage (Figure 2.44 B lower panel).

After incubation of samples with PP for 4 h the intensity of the peaks at 240 and 700 kDa were diminished (Figure 2.44 A). However, a new peak (II) with a size of 46 kDa appeared, containing potential Δ NEx1Q49 oligomers. The fractions of peak II were pooled, concentrated by TCA precipitation and analyzed by immunoblotting using anti-Htt and anti-GST antibodies. After denaturation the 46 kDa species eluted from the column was resolved as a 180 kDa oligomer in SDS gels (Figure 2.44 C), indicating that indeed SDS-stable oligomers are formed in spontaneous Δ NEx1Q49 aggregation reactions. The oligomeric species was further analyzed by dot blot assays with the polyQ-specific antibody 3B5H10. This antibody recognized the 46 kDa species but no aggregated species (Figure 2.45 A), indicating that the antibody recognizes soluble Δ NEx1Q49 oligomers, which are intermediate in the aggregation cascade. After an incubation of 48 h the amount of aggregated species with a molecular size of 700 kDa was increased and the amount of 46 kDa species was decreased, supporting the view that the 46 kDa species are aggregation intermediates. Analysis by SDS-PAGE and immunoblotting revealed that only a very faint 180 kDa band could be observed after 48 h (Figure 2.44 D).

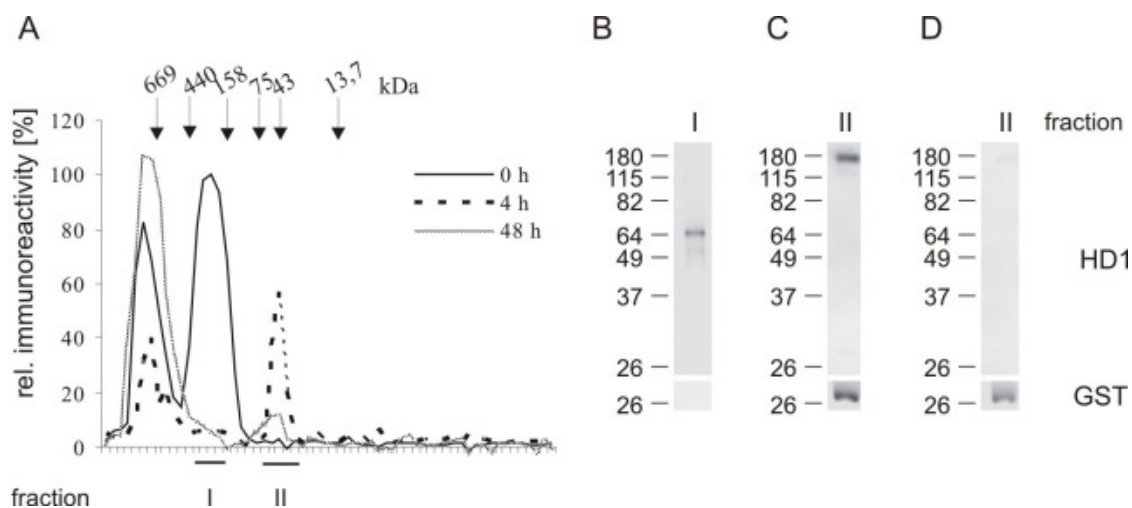


Figure 2.44: Δ NEx1Q49 forms small oligomers with a molecular size of 46 kDa in a time-dependent manner. Size exclusion chromatography of PP treated and untreated GST- Δ NEx1Q49 fusion protein. Aliquots were incubated for 0, 4 or 48 h at 20°C, centrifuged for 20 min at 207,000 g and separated on a Superdex 200 column. (A) Fractions were dot blotted, immunodetected with HD1 antibody and quantified by densitometry. Signals were normalized to the highest signal at 0 h, corresponding to the GST- Δ NEx1Q49 peak. Molecular markers are indicated in kDa. GST- Δ NEx1Q49 was eluted as oligomers with a molecular size of 240 kDa and larger aggregates with a molecular size of 700 kDa. After 4 h the peak of the uncleaved fusion protein (I) almost completely disappeared and a weaker peak at 700 kDa was observed. However, an oligomer with a size of 46 kDa appeared. After 48 h the majority of Δ NEx1Q49 was present in the 700 kDa fraction. (B-D) Indicated fractions were pooled and analyzed by SDS-PAGE and Western blotting using HD1 and GST antibodies. (B) The 240 kDa fraction was dissociated into GST- Δ NEx1Q49 monomers running at a molecular size of 64 kDa. No monomeric GST running at 27 kDa was detected. (C) The 46 kDa species was resolved to a 180 kDa species in the SDS gel at 4 h (B) and 48 h (D). Cleaved GST was found in the same fraction running at 27 kDa after denaturing (lower panels).

GST was recovered from the column as an oligomeric species with a molecular size of 54 kDa (Figure 2.45 B), representing approximately a dimer. After denaturation the protein migrated in SDS gels with a size of 27 kDa (fraction II). Thus, the data suggest that both GST

dimers and Δ NEx1Q49 oligomers elute together from the column in peak II. The possibility that GST is associated with Δ NEx1Q49 protein could not be excluded but while the amount of oligomeric Δ NEx1Q49 was decreased after 48 h the amount of oligomeric GST was not, suggesting that the two proteins form homomeric complexes (Figure 2.44 B and C lower panels). Deletion of the first 15 amino acids adjacent to the polyQ tract stabilized a transient Δ NEx1Q49 oligomer with a molecular size of 46 kDa.

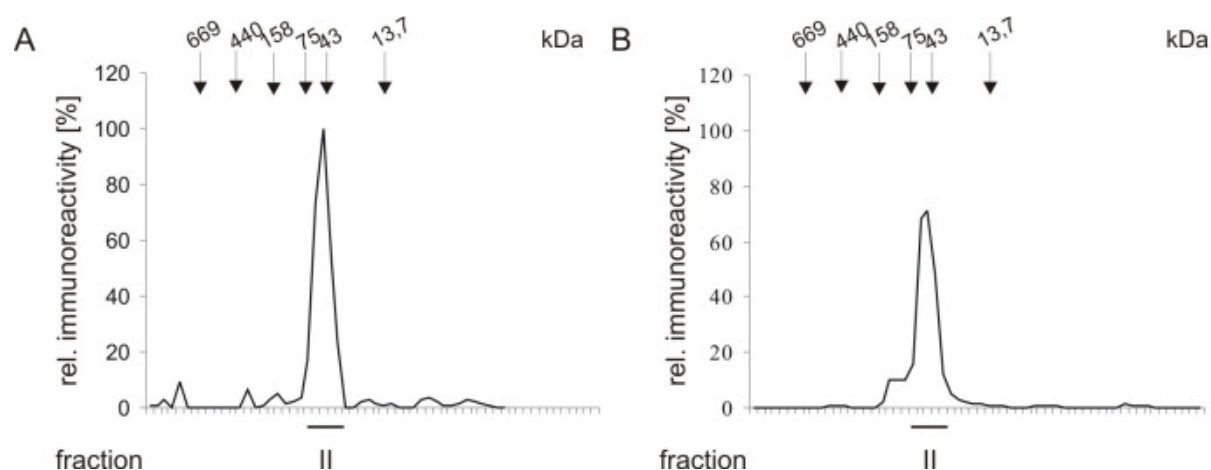


Figure 2.45: The 46 kDa fraction of Δ NEx1Q49 is immunoreactive with the 3B5H10 and GST antibodies. The fractions from SEC experiments of Δ NEx1Q49 incubated for 4 h at 20 °C and separated on a Superdex 200 column were analyzed by dot blot assays and immunodetection with 3B5H10 and GST antibodies. Molecular markers are indicated in kDa. (A) The 3B5H10 signals were quantified and normalized to the highest signal. The antibody 3B5H10 recognized the 46 kDa oligomers. (B) Dot blot assays with GST antibody. The signal was normalized to the GST signal prior to cleavage. After cleavage of the fusion protein, released GST molecules form dimers with a molecular size of 54 kDa.

To study whether the formation of Δ NEx1Q49 aggregates is accompanied by a change in secondary structure PP treated and untreated fusion protein were investigated by CD spectroscopy (Figure 2.46). Spectra were measured between 200 and 260 nm at a protein concentration of 1 μ g per μ l. Prior to cleavage for the GST- Δ NEx1Q49 fusion protein a CD spectrum characteristic for an α -helical protein with negative peaks at 208 and 222 nm was obtained. Using the CCDN 2.1 software the helical content was calculated to be 100%. Then, the GST-tag was removed from the fusion protein by PP cleavage (at 20 °C for 1 h) and the remaining uncleaved GST-fusion protein, GST and the PP were removed from the mixture by binding to glutathion sepharose for 30 min and filtering through a 50 kDa filter. After removal of the GST-tag and of the PP, the helical content of the remaining protein decreased to 70%, while 22% of the protein was calculated to have β -sheets and 8% were predicted to have a random coil conformation using the CCDN 2.1 software. This data suggests that initially α -helical Δ NEx1Q49 protein undergoes a conformational change upon removal of the GST-tag, leading to β -sheet-rich protein complexes.

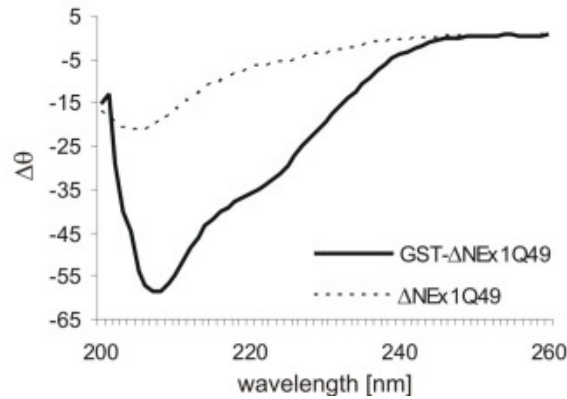


Figure 2.46: Removal of the GST-tag from the GST-ΔNEx1Q49 fusion protein diminishes the α -helical content of the Htt-exon 1 fragments. Fragments were incubated at 20°C for 1 h in the presence of PP. To remove GST and the PP (which is also a GST tagged protein) from the reaction the samples were incubated with glutathione sepharose 4B for 30 min at 4°C and the glutathione sepharose was removed by centrifugation through a 50 kDa filter. The signal for ΔNEx1Q49 was reduced due to removal of the aggregates by filtering.

2.6.5 O4 influences spontaneous aggregation of ΔNEx1Q49 protein

In order to investigate the mechanism of O4-induced perturbation of Htt-exon1 aggregation, the formation of SDS-insoluble ΔNEx1Q49 aggregates was analyzed by filter retardation assay in O4 treated and untreated samples. Cleavage of GST-ΔNEx1Q49 fusion protein with PP was controlled by SDS-PAGE and Western blotting using the HD1 antibody. Both in the presence and absence of O4 the fusion protein was cleaved completely after 1 h (Figure 2.47 A). Next, the effect of O4 on the formation of SDS-resistant aggregates was monitored by filter retardation assay. In the presence of O4, ΔNEx1Q49 aggregate formation was delayed, indicating that the compound perturbs early events in the aggregation cascade (Figure 2.47 B). This result was also confirmed with time-resolved dot blot assays using the conformational antibody MW8 (Figure 2.47 C). Dot blot assays with the antibodies MW1 (Figure 2.47 D) and 3B5H10 (Figure 2.47 E) recognizing the polyQ tract in ΔNEx1Q49 were also performed. The results indicate that O4 treatment did not influence the time-dependent decrease in MW1 immunoreactivity but altered the decrease in 3B5H10 immunoreactivity. Thus, the data are similar to the results obtained with the Ex1Q49 protein (Figure 2.18), indicating that O4 treatment stabilizes a soluble polyQ conformation, which is recognized by the monoclonal antibody 3B5H10, leading to a decrease in the polymerization of SDS-resistant, β -sheet-rich amyloid aggregates.

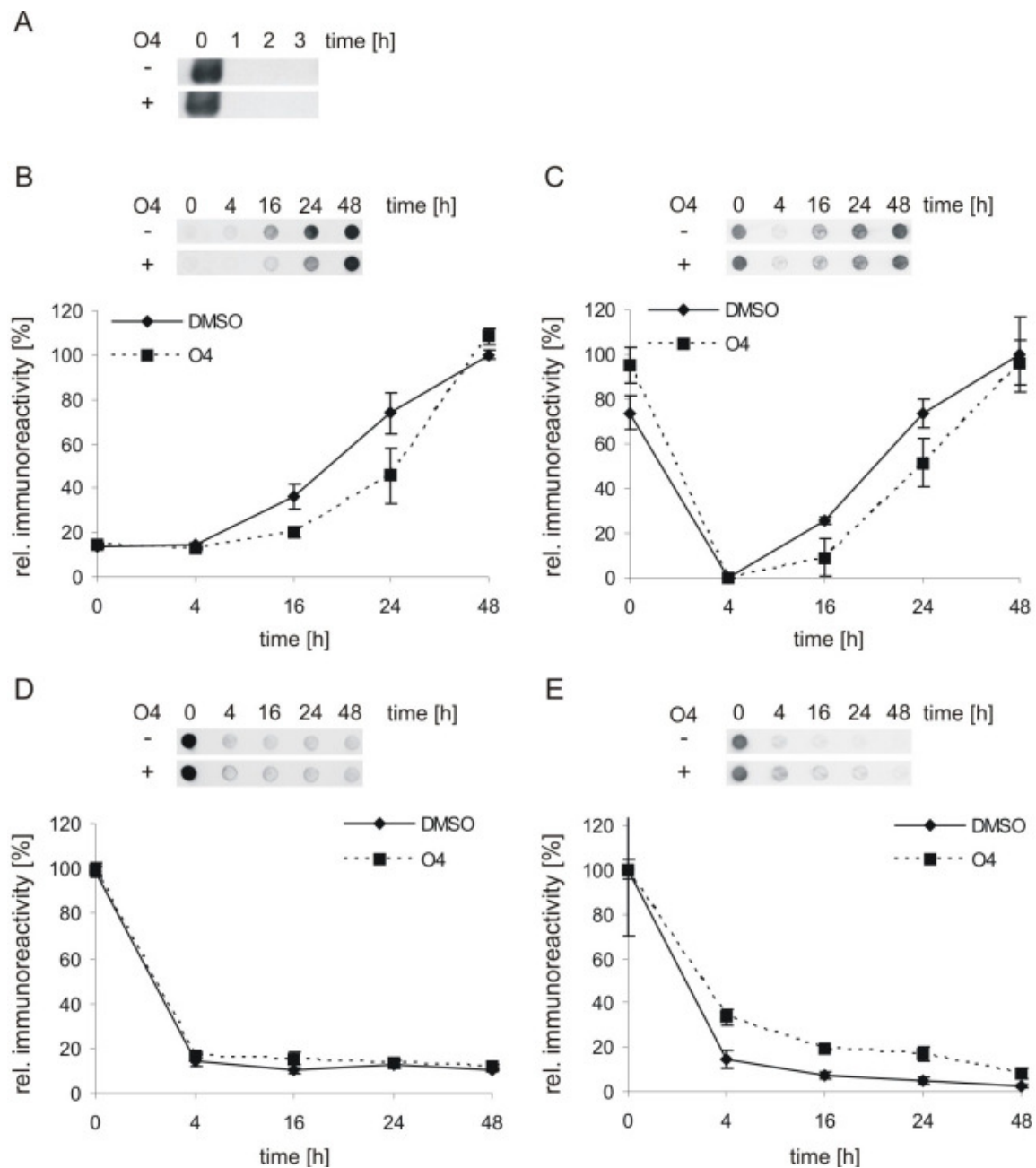


Figure 2.47: O4 delays the formation of SDS-resistant aggregates by stabilizing a 3B5H10 reactive polyQ conformation. 10 μ M GST- Δ NEx1Q49 fusion protein was incubated with PP at 20°C in the presence or absence of an equimolar concentration of O4. (A) Cleavage control by SDS-PAGE and Western blotting with HD1. O4 had no effect on GST- Δ NEx1Q49 cleavage. (B) Analysis of SDS-stable Δ NEx1Q49 aggregates by filter retardation assay using the CAG53b antibody. O4 delayed the formation of SDS-resistant aggregates. (C) Dot blot assays of Δ NEx1Q49 aggregation reactions with the MW8, (D) MW1 and (E) 3B5H10 antibodies. O4 had no effect on the polyQ conformation detected with the MW1 antibody but influenced the immunoreactivity of the MW8 and 3B5H10 antibodies.

To further analyze the effect of O4 on the morphology of fibrillar Δ NEx1Q49 aggregates, aliquots of aggregation reactions taken after 24 and 48 h were analyzed by atomic force microscopy. In the absence of O4 fibrillar aggregates were observed after 24 h and their size and number increased after 48 h. In the presence of the chemical compound no fibrillar aggregates but oligomeric structures were observed after 24 h. After 48 h some bundled fibrillar aggregates were detected together with oligomeric Δ NEx1Q49 species, indicating that the compound slowed down fibrillogenesis and stabilized the assembly of spherical oligomeric particles (Figure 2.48).

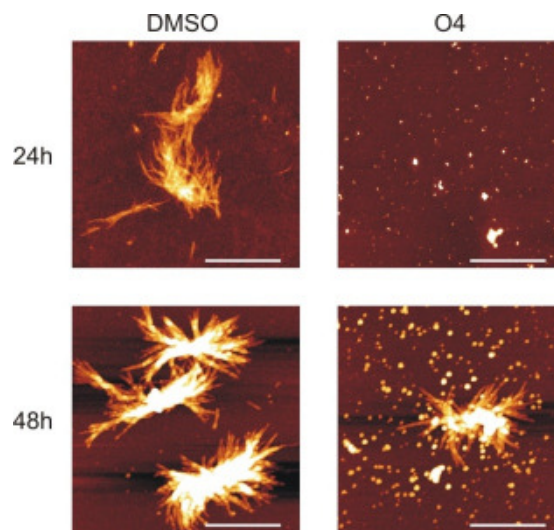


Figure 2.48: O4 promotes the formation of spherical Δ NEx1Q49 oligomers. 10 μ M GST- Δ NEx1Q49 was incubated with PP and equimolar concentrations of O4 for 24 or 48 h or with the solvent DMSO. In the absence of O4 Δ NEx1Q49 formed large bundled aggregates after 24 h that increased in size and number after 48 h. In the presence of O4 no fibrillar aggregates but oligomers were observed after 24 h. After 48 h bundled fibrillar aggregates as well as large numbers of spherical oligomers were observed.

The atomic force microscopy data confirm results from the filter retardation assay that the N-terminal 15 amino acids in Htt function as an enhancer of polyQ-mediated aggregation and that deletion of this region slows down spontaneous aggregation. The data further indicates that the reduced aggregation rate promotes the formation of oligomeric species that are recognized by the polyQ-specific antibody 3B5H10 confirming results from size exclusion chromatography and dot blot assays. Taken together, this data indicates that the spontaneous aggregation of Δ NEx1Q49 is similar to Ex1Q49 aggregation in cell free assays.

3. Discussion

The formation of insoluble amyloidogenic protein aggregates is a characteristic hallmark of various neurodegenerative diseases such as Huntington's disease or Alzheimer's disease. Elongation of the polyQ tract in the N-terminal region of Htt leads to the accumulation of aggregates in the brains of patients, and progressive protein deposition is accompanied by neuronal dysfunction and death (Sunde and Blake, 1997). However, the formation of aggregates and the occurrence of cell death do not always correlate well, suggesting that amyloidogenic aggregates are not the cause for neuronal cell death in neurodegenerative diseases (Terry et al., 1991). Increasing evidence indicates that small, soluble aggregates that are potential intermediates in the amyloid formation cascade, play an important role in disease pathogenesis (Saudou et al., 1998). However, the molecular mechanism by which long polyQ tracts spontaneously convert from a soluble into an aggregated state is largely unclear. A better understanding of the amyloid formation process is also highly important for the development of new therapeutic strategies for HD. Currently, all medications are symptomatic treatments and no drugs are able to efficiently slow down disease progression (Walker, 2007). Patients are generally diagnosed at a relatively late stage of the disease, when symptoms become evident and neuronal loss is already advanced. Therefore, elucidating the disease mechanism could help to identify new targets for therapeutic drugs that interfere with early processes in the disease pathology.

In this study, the mechanism of spontaneous polyQ-mediated Htt protein aggregation was systematically analyzed *in vitro* using an N-terminal Htt-exon 1 fragment with a pathogenic polyQ tract of 49 glutamines (Ex1Q49). Furthermore, the effects on aggregation of sequences flanking the polyQ tract in Ex1Q49 were analyzed.

3.1 Mechanism of spontaneous polyQ-mediated Htt-exon 1 aggregation

3.1.1 GST Htt-exon 1 fragments form oligomers *in vitro*

The Htt protein is a 3144 amino acid long protein (HDCRG, 1993). Several studies have shown that the expression of an N-terminal Htt-exon 1 fragment with a pathogenic polyQ tract is sufficient to cause neuronal deficits and degeneration in HD mice and fly models (Ehrnhoefer et al., 2009; Marsh et al., 2003). Moreover, it has been shown that in mice expressing full-length Htt, short N-terminal fragments are generated by proteolytic cleavage with a size similar to the exon 1 fragment (Landles et al., 2010). Htt-exon 1 fragments with pathogenic polyQ tracts have also been shown previously, to spontaneously convert into

β -sheet-rich amyloidogenic aggregates in cell-free assays (Poirier et al., 2002; Scherzinger et al., 1999). It has been demonstrated that fusion of Htt-exon 1 with a pathological polyQ tract to GST increases its solubility and inhibits the spontaneous formation of aggregates (Scherzinger et al., 1997). Removal of the GST-tag by proteolytic cleavage on the other hand initiates the formation of SDS-stable aggregates. Therefore, in this study, a Htt-exon 1 fragment with 49 glutamines fused to GST with a specific PP cleavage site has been used. The protein was purified from *E. coli* extracts under native conditions and analyzed by SDS-PAGE and immunoblotting. Interestingly, it was found that this GST fusion protein under denaturing conditions has a higher molecular weight than predicted based on their amino acid sequence. This phenomenon, which has been well-known for proteins with long polyQ tracts, is maybe due to the weak binding of SDS to the polyQ tract in Ex1Q49, resulting in slower migration of the fusion protein through gels. Analysis of the GST-fusion protein with monoclonal antibodies against GST and different Htt epitopes, suggests that the protein has an open conformation. GST-Ex1Q49 was recognized by antibodies detecting GST, the polyQ tract (MW1, 3B5H10), the proline-rich region (MW8) and the first 17 amino acids in Htt (not shown).

Under native conditions, the GST-Ex1Q49 fusion protein formed oligomers of various sizes. In size exclusion chromatography as well as in SDD-AGE experiments GST-Ex1Q49 oligomers with sizes of 510 and 400 kDa respectively were detected, suggesting that structures containing 10 or 12 monomers are formed *in vitro*. The differences in size are probably due to the different experimental conditions and the sensitivity of the oligomer detection assays. The fusion protein forms a 510 kDa oligomer under native conditions, in size exclusion chromatography experiments (Figure 2.12). This oligomer already starts to fall apart upon the addition of small amounts of SDS in SDD-AGE, indicating that smaller oligomers may be formed. It is not clear whether the Ex1Q49 Htt fragment or the N-terminal GST-tag facilitates the oligomerization of GST-Ex1Q49. However, it is possible that in addition to Ex1Q49, GST might also be critical for the spontaneous formation of GST-Ex1Q49 oligomers, because it is known to form homodimers under physiological conditions (Fabrini et al., 2009).

3.1.2 Early conformational changes are critical for Ex1Q49 aggregation

The release of the GST-tag from the fusion protein allows the analysis of Ex1Q49 aggregation under highly controlled conditions. The PreScission Protease (PP) specifically cleaves the fusion protein between the GST tag and the Ex1Q49 fragment, allowing the analysis of the spontaneous aggregation of a well defined Htt fragment with 113 N-terminal

highly aggregation-prone amino acids (Figure 2.1). In contrast, when GST-Ex1Q49 is cleaved with trypsin, the first 15 amino acids of the Htt-exon 1 fragment are removed as well as one amino acid at the C-terminus of the protein (Figure 2.14). As PP cleavage of GST-Ex1Q49 results in the release of the complete exon 1 fragment, the influence of the polyQ flanking sequences (e.g., the N terminal 17 amino acids) on spontaneous aggregation can be analyzed when the fusion protein is treated with trypsin, producing a shorter fragment. A further advantage of the PP is the possibility to separate cleavage and aggregation by lowering the temperature. The protease is most reactive at 4°C (Dian C, 2002), while spontaneous Ex1Q49 aggregation is very inefficient. However, a subsequent increase in temperature up to 20°C promotes Ex1Q49 aggregation. This approach allows the accumulation of potential Ex1Q49 aggregation intermediates that are otherwise undetectable in fast aggregation reactions (Figure 2.12).

Upon cleavage of GST-Ex1Q49 the released Ex1Q49 fragment undergoes a conformational rearrangement that can be monitored by a time-dependent reduction in MW1 antibody reactivity. Interestingly, the loss of signal occurs with the same kinetics as the cleavage of GST-Ex1Q49 with PP. This conformational change has been observed before by FRET experiments (Schaffar et al., 2004). In parallel, the accessibility of the proline-rich region detected with the monoclonal antibody MW8 decreases very fast, suggesting that the Htt-exon 1 fragment forms a compact structure after cleavage of the fusion protein, in which the proline-rich region is hidden (Figure 2.18). Further analysis of the very early steps in the aggregation cascade with the monoclonal polyQ-binding antibody 3B5H10 revealed a slower decrease in immunoreactivity than with the MW1 antibody, suggesting that this antibody detects a different polyQ conformation. The antibody 3B5H10 has been shown previously to bind to a compact β -sheet-rich polyQ conformation (Poirier et al., 2002), indicating that the polyQ tract converts from an α -helical into a β -sheet conformation upon PP cleavage.

According to the aggregation model proposed by Perutz et al. (2002) it seems reasonable to speculate that polyQ domains with more than 40 glutamines can undergo a structural rearrangement converting from a random conformation to a β -sheet-rich structure. These polyQ structures are stabilized by hydrogen bonds between main chain and side chain amides, forming a “polar zipper” (Perutz et al., 2002). This model is in agreement with the results obtained with the epitope-specific antibodies in this study, suggesting that the Ex1Q49 fragment undergoes a fast conformational rearrangement after proteolytic cleavage. However, data in this study indicate that Htt in the fusion protein has an α -helical structure, which converts upon PP cleavage into a β -sheet. In cells, proteolytic cleavage of full-length Htt could induce a similar conformational change and increased processing of Htt in ageing cells could, therefore, be a possible explanation for the late onset of symptoms in HD.

The formation of high molecular weight aggregates with a fibrillar morphology proceeds rapidly when the concentration of aggregation-prone monomers exceeds the critical concentration and a nucleus is formed (Ferrone, 1999).

Here, the results revealed that after 2 h, when more than 70% of the fusion protein was cleaved, Ex1Q49 already started to form SDS-resistant aggregates (Figure 2.7). These aggregates were retained on a cellulose acetate membrane with a pore size of 0.2 μm and were readily detected with a CAG53b antibody. Spontaneous Ex1Q49 aggregation was complete after 4 h, indicating that the polyQ-mediated polymerization process is very fast. However, no aggregates were observed in the absence of PP or when Htt-exon 1 with a non-pathological polyQ tract of 25 glutamines was incubated in the presence of PP (data not shown). In an earlier study, it has been shown that GST exon 1 fusion proteins only form SDS-stable aggregates, when the polyQ tract has more than 37 glutamines (Busch et al., 2003; Chen et al., 2002; Scherzinger et al., 1999).

The formation of Ex1Q49 aggregates was comprehensively monitored in this study by dynamic light scattering, Thioflavin T assays, time-resolved SDD-AGE and dot blot assays with the polyP binding antibody MW8. The formation of high molecular weight aggregates could be monitored using all the above mentioned techniques and the lag phase and the aggregation rate of Ex1Q49 were comparable. This suggests that all methods detect similar Ex1Q49 aggregate species. Here, the formation of SDS-resistant aggregates could be directly linked to the formation of β -sheet-rich structures, by binding to Thioflavin T, a dye which is known to bind to β -sheet-rich amyloid structures. Finally, the results from dot blot assays developed with the MW8 antibody suggest that in Ex1Q49 aggregates, the proline-rich region is exposed, whereas the polyQ tract is hidden, as analyzed by dot blot assays immunodetected with MW1 and 3B5H10, showing a decrease in reactivity as aggregation proceeds.

The data indicating that GST-Ex1Q49 undergoes a conformational rearrangement upon proteolytic cleavage and that this switch can be monitored with the MW1 antibody are not in full agreement with the results published by Lotz et al. (2010). In their study GST-Ex1Q53 was incubated at a concentration three times higher than used here. The reactions were also incubated at a higher temperature of 37°C and a faster shaking at 800 rpm. Although the protein was cleaved after 3 h and fibril formation reached saturation after 5 h the immunoreactivity of the MW1 antibody decreased slowly and was still detectable after 5 h. In that study, size exclusion chromatography experiments revealed that under these conditions the antibody recognizes oligomers with a broad size distribution from 230-530 kDa. The higher Brownian motion at the higher incubation temperature of 37°C may influence the equilibrium between the compact polyQ structure recognized by 3B5H10 and the more open

conformation recognized by the polyQ antibody MW1. Surprisingly, this seems to have no effect on nucleus formation, as the formation of SDS-resistant aggregates follows a similar time-course with comparable lag phases. This suggests that the incubation at the lower temperature of 20°C has the advantage that the initial steps in the aggregation cascade can be distinguished by the two polyQ antibodies.

Based on the time-resolved Ex1Q49 aggregation data, a working model was generated, describing the different steps in the aggregation process. Prior to cleavage GST-Ex1Q49 exists as an oligomer of approximately 500 kDa. The Ex1Q49 protein in this oligomer has an open α -helical conformation and all epitopes recognized by the antibodies MW1, 3B5H10 and MW8 are accessible. Upon removal of the GST-tag the epitopes recognized by the MW1 and 3B5H10 antibodies disappear. Similarly, the epitope recognized by the MW8 antibody becomes less detectable during the first 2 h of PP cleavage. In the soluble Ex1Q49 protein, the polyQ tract is exposed whereas the proline-rich region is buried in the protein.

When Ex1Q49 assembles into insoluble aggregates, however, the accessibility of the polyQ tract disappears while the proline-rich region gets exposed. This suggests that the polyQ tracts are not exposed on the surface of insoluble Ex1Q49 aggregates. The resulting insoluble Ex1Q49 aggregates have a β -sheet-rich fibrillar conformation. This aggregation model is in agreement with the results published by Tam et.al. 2009, who studied the influence of the first 17 amino acids on spontaneous Htt-exon 1 aggregation. They showed that N-terminal Htt fragments with long polyQ tracts undergo a conformational change, leading to an amyloidogenic nucleus. This conformation is stabilized by interactions between the first 17 amino acids of two Htt molecules and by intramolecular interactions between the first 17 amino acids and the polyQ tract. Once this nucleus has been formed, aggregation proceeds rapidly.

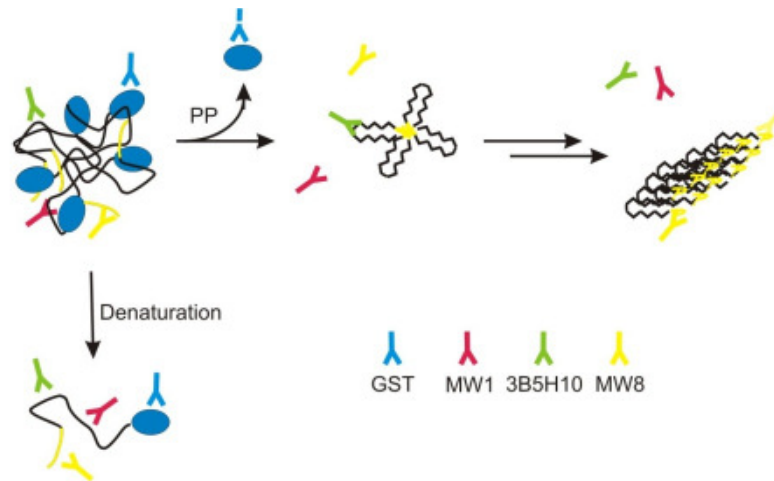


Figure 3.1: Potential mechanism of spontaneous Ex1Q49 aggregation after proteolytic cleavage of GST-Ex1Q49 with PP. GST-tagged Ex1Q49 forms oligomers that dissociate upon denaturation. Both native and denatured GST-Ex1Q49 can be recognized by all 4 antibodies. Upon the addition of PP, Ex1Q49 undergoes a fast conformational change, leading to the loss of MW1 and MW8 reactivity. However, the soluble Ex1Q49 oligomers formed by PP cleavage are detectable by the anti-polyQ antibody 3B5H10. When Ex1Q49 forms insoluble aggregates, the 3B5H10 is undetectable, suggesting that the polyQ tract has been integrated into the aggregates and is not accessible for the antibody. The mature aggregates can be recognized by the polyP antibody MW8, indicating that this epitope is exposed on the surface of aggregates. The blue circle represents GST. Yellow stretch proline-rich region.

The ability to detect well-defined aggregation intermediates with conformation-specific antibodies is of high importance for the understanding of the mechanism by which fibrillar Ex1Q49 aggregates are formed. To further analyze the biochemical properties of aggregation intermediates, cleavage was performed at 10°C allowing the PP to efficiently remove the GST-tag under conditions where spontaneous Ex1Q49 aggregation is slow. Under these conditions, the GST fusion protein was cleaved to about 90% after 3 h of incubation and no SDS-stable aggregates were detectable by the filter retardation assay. When the samples were subjected to size exclusion chromatography, a broad range of low molecular weight Ex1Q49 oligomers was detected, which disappeared when samples were incubated for longer periods of time at 20°C. This indicates that transient, SDS-unstable Ex1Q49 oligomers are spontaneously formed that convert over time into insoluble amyloid structures.

However, no low molecular weight Ex1Q49 oligomers were detected in SDD-AGE experiments. The broad distribution of low molecular weight Ex1Q49 oligomers in size exclusion chromatography experiments might explain why no oligomers were detected with SDD-AGE as the sensitivity might be too low to detect oligomers. If the critical nucleus for the Ex1Q49 aggregation is small and aggregation follows a nucleated polymerization mechanism, intermediates will assemble into aggregates very rapidly. Thus, it is not

unexpected that small Ex1Q49 oligomers are highly difficult to detect in the spontaneous aggregation reactions.

Previous kinetic studies have demonstrated that the size of the “critical nucleus” for simple polyQ peptides such as Q47 is 1 (Chen et al., 2002), indicating that amyloidogenic fibrils are formed spontaneously without passing through a stable oligomeric intermediate. However, polyQ tracts with flanking sequences have been shown to follow a more complex aggregation mechanism, involving the assembly of transient oligomers that appear prior to the formation of β -sheet-rich amyloid fibrils (Thakur et al., 2009). Spherical Htt oligomers have also been detected in the brains of HD transgenic mice (Sathasivam et al., 2010), supporting the view that Htt oligomers are indeed formed *in vivo*.

It has previously been shown that the Ex1Q49 aggregation is a nucleation dependent process (Ferrone et al., 2002). This process is characterized by a lag-phase during which a nucleus is formed, followed by a fast fibril growth phase often termed the elongation phase. The aggregation rate is highly concentration-dependent and aggregates form when a critical concentration of monomers is reached (Ferrone et al., 2002). The lag phase can be shortened by the addition of seeds (preformed fibrils), which function as templates for fibril growth. For efficient seeding, preformed aggregates must have an appropriate surface structure that allows for the addition of monomers or oligomers. It has previously been shown that the seeding of amyloid structures is only efficient, if the fibrils used as seeds are closely related to the potentially aggregating monomers (Krebs et al., 2004). When seeding was performed at 20 °C the formation of SDS-resistant aggregates in the presence of seeds was unchanged compared to controls without seeds (data not shown). Under these conditions, the limiting step could potentially be the proteolytic cleavage. Therefore, the addition of seeds can not further enhance fibril formation. When the GST-Ex1Q49 fusion protein was cleaved at 10 °C prior to aggregation, however, the addition of freshly synthesized Ex1Q49 aggregates that were produced in an independent experiment for 3 h at 20 °C, seeding of amyloid aggregates was most effective (Figure 2.13), indicating that small Ex1Q49 aggregates or oligomers but not mature fibrils are the most potent inducers of amyloid polymerization. In various studies, the seeding of polyQ amyloid structures is generally performed with aggregates that were incubated for 24 h and sonicated to increase their reactive surface (Scherzinger et al., 1999). Here, preformed Ex1Q49 aggregates were used as seeds that were generated by incubating GST-EX1Q49 fusion protein for 3 h with PP. At this time-point Ex1Q49 aggregates have already been formed but are still short and have a high fibril-ends to length ratio. Thus, the results of this study indicate that small aggregates, which are formed early in the aggregation cascade, are functional seeds that promote Ex1Q49 fibril polymerization in cell-free assays.

3.1.3 The compound O4 stabilizes an early conformation in the aggregation cascade

To obtain further information on the mechanism of fibril formation the aggregation process was disturbed using chemical compounds. 6 compounds were chosen based on available literature information about well-known modulators of amyloidogenesis (Bieschke, 2011; Dikshit et al., 2006; Heiser et al., 2002; Oz et al., 2009; Yang et al., 2005). All compounds have conjugated π -systems and several donor- or acceptor-groups, which are critical for the activity of aggregation modulators (Desai et al., 2006; Zhang et al., 2005). The compounds were tested in time-resolved aggregation assays, whether they can affect spontaneous Ex1Q49 polymerization (Figure 2.20). The compound O4 was found to have the strongest effect on Ex1Q49 aggregation (Figure 2.21). Weaker effects were obtained with the two structurally related compounds orcein and resorufin. Interestingly, the compound O4 delayed the onset of Ex1Q49 aggregate formation in a concentration dependent manner. However, the aggregation rate of Ex1Q49 fibril formation was not changed by O4, suggesting that it influences early events in the amyloid formation cascade such as the formation of oligomers or nuclei. To test this hypothesis, O4 was added to the Ex1Q49 aggregation reaction at later time-points and assembly of SDS-resistant aggregates was analyzed by filter retardation assay. Strikingly, addition of O4 30 min after the initiation of Ex1Q49 aggregation with PP delayed the onset of fibril formation, while addition of the compound after 2 h had only a very weak effect. These results support the hypothesis that that O4 targets very early events in the aggregation cascade and slows down the conversion of soluble, aggregation-prone Ex1Q49 molecules into seeding-competent β -sheet-rich structures.

In order to investigate whether O4 affects the size of spontaneously formed amyloid aggregates DLS and SDD-AGE experiments were performed. With both methods O4 delayed the onset of aggregate formation. However, the size of formed aggregates was not significantly changed upon O4 treatment. Interestingly, in the presence of O4 no low molecular weight aggregation intermediates were stabilized that could be detected with DLS or SDD-AGE. Hence, the data suggest that O4 targets Ex1Q49 monomers or very small oligomers that appear very early in the aggregation cascade and that are not abundant or stable enough for detection.

Having established that O4 does not stabilize larger oligomeric Ex1Q49 aggregation intermediates, time-resolved dot blot assays using the monoclonal antibodies MW1, 3B5H10 and MW8 were performed, in order to analyze whether the effect of O4 on Ex1Q49 aggregation is accompanied by conformational changes in the Htt protein. Addition of O4 had no effect on the decrease in MW1 immunoreactivity in Ex1Q49 aggregation reactions, suggesting that the compound does influence the conversion of the polyQ tract from an

α -helical into a more compact, aggregation-prone structure. However, the conformations recognized by the 3B5H10 and MW8 antibodies were influenced by O4 treatment. The immunoreactivity of 3B5H10 decreased much slower in the presence of the compound, indicating that the polyQ conformation recognized by this antibody is stabilized. In addition, O4 also delayed the increase of MW8 immunoreactivity, which indicates the appearance of SDS-resistant Ex1Q49 aggregates (Figure 2.31). Thus, these studies with O4 strongly suggest that the formation of the polyQ conformation, which is recognized by 3B5H10 antibody, is prerequisite for the efficient polymerization of Ex1Q49 amyloid aggregates.

Previous studies of the polyQ-mediated Htt aggregation cascade have never provided such a deep insight into the aggregation mechanism. The compound EGCG, which is found in green tea, has been shown to influence the decrease in MW1 immunoreactivity in Ex1Q51 aggregation reactions (Ehrnhoefer et al., 2006). However, the consequences of this effect on spontaneous amyloid polymerization have not been studied in detail. Similarly, it has been demonstrated that the dye Congo Red inhibits polyQ-mediated Htt aggregation (Poirier et al., 2002), but the mechanism of action is largely unclear. Evidence has been provided that Congo Red binds to Htt aggregates at a late stage and thereby prevents further aggregation (Poirier). However, these results were not substantiated with time-resolved aggregation assays and experiments with conformation-specific antibodies. In this study for the first time the effect of a compound on Htt aggregation could be correlated with a conformational change in an early aggregation intermediate (Figure 2.31).

The mechanistic studies with conformational antibodies suggest that the polyQ conformation recognized by 3B5H10 is a critical precursor of insoluble amyloid fibrils. This is in agreement with data provided by Legleiter et al. (2009) showing that addition of the antibody 3B5H10 to aggregation reactions completely blocks spontaneous Htt polymerization. If the polyQ conformation recognized by the 3B5H10 antibody would be off-pathway one would assume that fibrillogenesis can occur in the presence of the 3B5H10 antibody.

3.1.4 Fitting the kinetic Ex1Q49 aggregation data to a mathematical model

Although numerous efforts are currently ongoing to elucidate the molecular mechanism of amyloid formation structural information about transiently forming aggregation intermediates are mostly not available. Amyloidogenesis in many aspects resembles a simple nucleation polymerization reaction, which has been successfully applied to describe actin assembly (Ferrone et al., 2002). Based on these kinetic studies the so-called “critical nucleus” can be calculated from aggregation reactions at different protein concentrations. For simple extended polyQ peptides a critical nucleus of $n = 1$ has been calculated, suggesting that the nucleus is a monomer and polyQ fibrils are formed without the stabilization of oligomeric

intermediates (Chen et al., 2002). Studies with more complex polyQ peptides containing the N-terminal flanking sequences of Htt-exon 1 have shown that longer polyQ peptides most likely have a more complicated aggregation mechanism, involving the formation of oligomeric intermediates before β -sheet-rich amyloids are formed (Thakur et al., 2009). However, the previously published studies addressing the mechanism of polyQ aggregation have several limitations and do not allow a molecular characterization of aggregate species that are formed during the nucleation phase.

The data presented here were used for computational modeling of the Ex1Q49 aggregation process, including the time-dependent formation of SDS-stable aggregates monitored by filter retardation assay as well as the conformational changes observed in dot blot assays with conformation-specific antibodies. A mathematical model has been generated in cooperation with mathematicians in the group of Dr. Jana Wolf (Mathematical modeling of cellular processes, Max Delbrueck Center for Molecular Medicine, Berlin). Three conformational states were distinguished based on the antibody binding data (Figure 3.2).

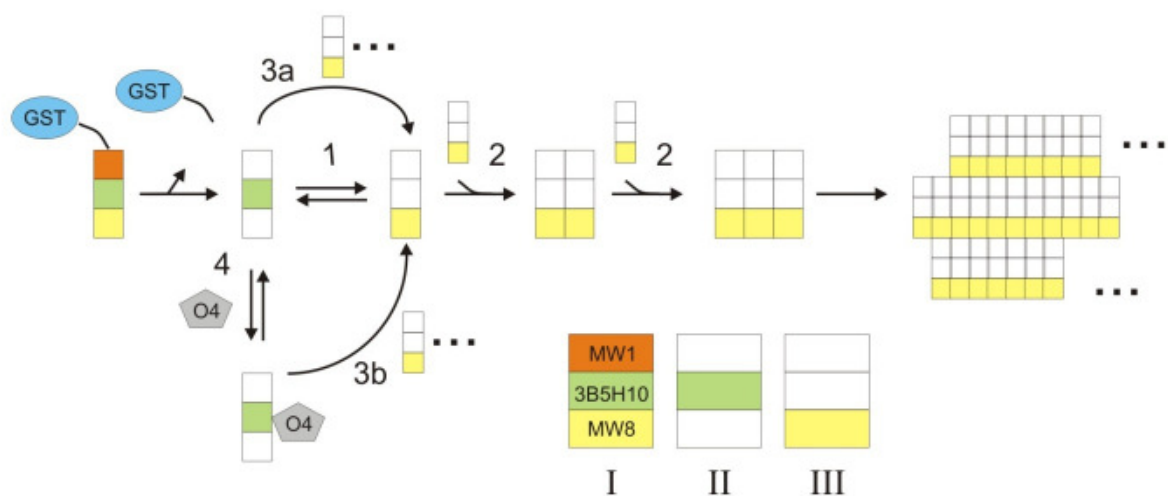


Figure 3.2: Describing the spontaneous Ex1Q49 aggregation process by mathematical modeling. Three conformational states (I, II and III) can be distinguished that are differently recognized by the antibodies MW1, MW8, and 3B5H10. After removal of the GST-tag Ex1Q49 can switch from conformation II to III (reaction 1). Only in conformation III monomers can aggregate and form fibrils (reaction 2). These structures can then function as templates for the formation of new seeds by inducing the switch to conformation III (reaction 3a). The drug O4 binds reversibly to conformation II (reaction 4) and thereby impairs the switch to conformation III. When aggregates have formed the conversion to conformation III is catalyzed and aggregation proceeds (reaction 3b).

Prior to cleavage, state I (GST-Ex1Q49 fusion protein with an α -helical conformation) is recognized by all three monoclonal antibodies (MW1, 3B5H10 and MW8). After removal of the GST-tag the Ex1Q49 protein undergoes a rapid conformational change to state II, which is only recognized by the polyQ-binding antibody 3B5H10. This probably monomeric conformation is in equilibrium with the amyloidogenic conformation III, which is only

recognized by the MW8 antibody (reaction 1). In this state Ex1Q49 can readily aggregate by binding to existing fibril-ends (reaction 2). The model includes an autocatalytic step (reaction 3a), which promotes the conversion of 3B5H10 reactive molecules into non-reactive molecules that assemble into new fibrils. Stabilization of the 3B5H10 conformation with the compound O4 delays the onset of amyloid formation, suggesting that this conformation is a prerequisite for Htt amyloid polymerization. In this model the conversion of Ex1Q49 molecules into the 3B5H10 conformation (II) and the switch of this conformation into conformation III can only occur via catalysis by other filaments (reaction 3b).

The generated mathematical model using an autocatalytic mechanism reliably reproduces the process of Ex1Q49 aggregation monitored by filter retardation assay data as well as the results obtained with dot blot assays using the monoclonal antibodies MW1, 3B5H10 and MW8 (Figure 3.3 A). The simulations indicate that the assumption of a critical nucleus of one is sufficient to reproduce the data, but larger nuclei (e.g. $n = 2$ and 3) give equally good fits. The model also encompasses the effect of O4 to elongate the lag phase by 2 h, while the rate of aggregation and the final aggregation level remain unchanged (Figure 3.3 B). In the model the delay in SDS-stable aggregate formation is caused by a reduced tendency of Ex1Q49 to switch from state II to state III (reaction 1). However, when enough aggregates are present, the catalytic conversion dominates and promotes Htt polymerization with the same aggregation rate as in the absence of compound.

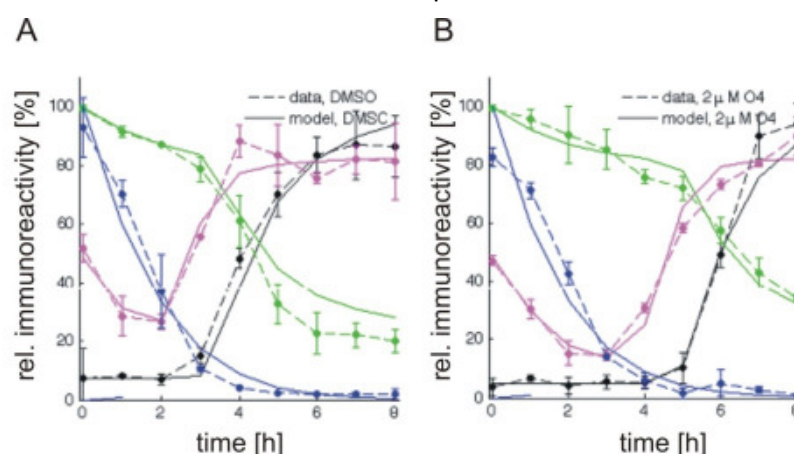


Figure 3.3: Simulation of spontaneous Ex1Q49 aggregation using an autocatalytic amyloid polymerization mechanism. Simulations and data of aggregation reactions of GST-Ex1Q49 at $2 \mu\text{M}$ in the presence of DMSO (A) and $2 \mu\text{M}$ O4 (B). Model simulations (solid lines) and experimental data (dashed lines) of filter retardation assay (black), MW1 (blue), MW8 (magenta) and 3B5H10 (green) immunoreactivity.

An autocatalytic step in the aggregation process is necessary to model the effect of O4 on the lag phase (delay for 2 h) while the rate of amyloid polymerization remains unchanged. Previous studies with other amyloidogenic proteins such as $\text{A}\beta$ or α -synuclein also found that an autocatalytic step is important for efficient amyloid formation (Bernacki and Murphy, 2009;

Morris et al., 2009). For four other aggregation mechanisms (slow initiation model, monomer partitioning model and sequential growth model) that were previously associated with amyloid formation, the effect of a perturbation on the aggregation kinetics was investigated. For all models the filter retardation assay data was modeled by varying the rate constant. None of the other models has been capable of reproducing the effect of O4. Only the autocatalytic model showed a large increase in the delay of SDS-stable aggregate formation with only little changes in the aggregation rate and no changes in the maximal value of the signal.

Two predictions were proposed from the mathematical model to validate the autocatalytic model. First, addition of O4 at later time-points will have no effect and second, the addition of seeds can induce the conformational conversion of monomers even when monomers are bound to O4.

To test the first prediction, aggregation reactions of 2 μM GST-Ex1Q49 in the presence of PP were performed and O4 was added at later time-points. The results presented in Figure 2.27 are in good agreement with the predictions (Figure 3.4 A), indicating that addition of O4 after 2 h of aggregation has no effect.

In order to test the second prediction, seeding experiments in the presence of O4 were performed (Figure 2.30). The experimental results indicate that addition of seeds to Ex1Q49 aggregation reactions abolished the effect of the compound. The results are in good agreement with the mathematical predictions (Figure 3.4 B).

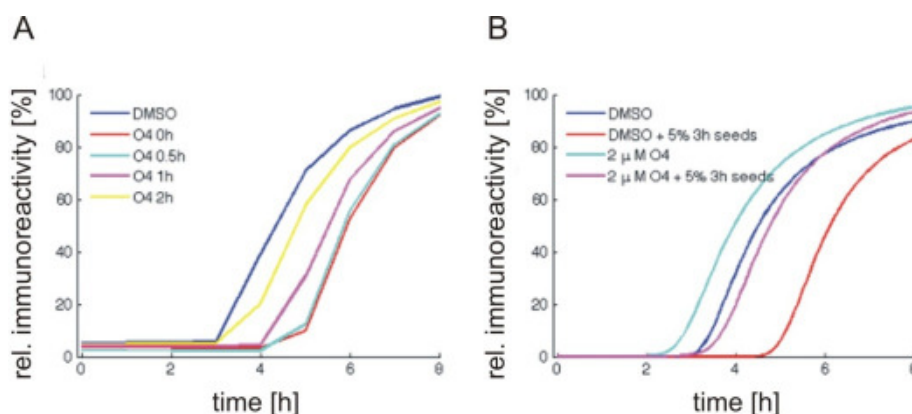


Figure 3.4: Predictions for the validation of an autocatalytic mechanism of Ex1Q49 aggregation. (A) Simulation of the effect of O4 addition to 2 μM Ex1Q49 aggregation reactions at later time-points in the presence of PP. Simulations were performed for addition of O4 at $t = 0$ h (red), $t = 0.5$ h (cyan), $t = 1$ h (magenta), $t = 2$ h (yellow) and in the absence of O4 (blue). (B) Simulation of SDS-stable aggregate formation in seeded aggregation reactions of 1 μM Ex1Q49 with 5% seeds (3 h, 2 μM GST-Ex1Q49, 20°C in the presence of PP). In control reactions (blue) the addition of seeds (cyan) mildly promote Ex1Q49 aggregation. The effect of O4 (red) is almost completely abolished in the presence of seeds (magenta) and the dynamics approaches the control case (blue).

The experimental results very nicely confirm the mathematical assumption that β -sheet-rich Ex1Q49 amyloid fibrils are spontaneously formed by an autocatalytic process in the absence of stable, oligomeric intermediates.

3.2 Effect of flanking sequences on Htt aggregation

The flanking sequences of polyQ tracts have been shown to dramatically influence aggregation of N-terminal Htt fragments (Duennwald et al., 2006; Thakur et al., 2009). Today nine neurodegenerative polyQ diseases are known to be caused by CAG repeat expansions in genes that normally produce proteins with short polyQ tracts (Sunde and Blake, 1997). While the wildtype and the mutated proteins with expanded polyQ tracts both are broadly expressed, the diseases affect only specific brain regions and the clinical features differ between the diseases (Soto, 2003). This suggests that the flanking sequences of pathogenic polyQ might be critical for the disease-specific phenotypes in patients.

The expanded polyQ tract adopts a β -sheet-rich conformation in fibrillar protein aggregates that is stabilized by hydrogen bonds (Perutz et al., 2002; Poirier et al., 2002). It has been shown that the polyQ tract alone is sufficient to induce the formation of fibrillar amyloids in a slow nucleated polymerization reaction (Chen et al., 2002). Studies on the flanking sequences of the extended polyQ tract in the Htt-exon 1 protein have identified the N-terminal region as an endogenous intrinsic enhancer of aggregation (Tam et al., 2009). Blocking of the hydrophobic surface of the helical structure formed by the first 17 N-terminal amino acids has a dominant negative effect on spontaneous amyloid formation (Tam et al., 2009), supporting the view that this region in Htt functions as an enhancer of amyloid polymerization. In strong contrast, the proline-rich region located down-stream of the polyQ tract reduces the aggregation rate of N-terminal Htt fragments (Bhattacharyya et al., 2006) and deletion of this region alters the morphology of the aggregates and enhances cytotoxicity in yeast models of HD (Dehay and Bertolotti, 2006).

In order to investigate whether deletion of the N-terminal amino acids adjacent to the polyQ tract alters the mechanism by which fibrillar amyloids are formed a mutant version of the Ex1Q49 protein was generated (Δ NEx1Q49) that lacked the N-terminal 15 amino acids of Htt. In agreement with previously published studies (Lakhani et al., 2010; Sivanandam et al., 2011; Tam et al., 2009) deletion of the N-terminal region dramatically reduced the spontaneous aggregation rate of the Ex1Q49 protein (Figure 2.40). The fragment Δ NEx1Q49 formed SDS-resistant aggregates after 20 h while such aggregates were detectable after 4 h with the Ex1Q49 protein (Figure 2.40 and Figure 2.5).

Digestion of the GST-Ex1Q49 fusion protein with trypsin leads to the formation of a Htt fragment with a similar size than the Δ NEx1Q49 fragment (Δ NTEEx1Q49) (Figure 2.14 and Figure 2.39). Both fragments formed SDS-resistant protein aggregates with a similar time-course analyzed by filter retardation assay. However, digestion with trypsin led to an enhanced formation of oligomeric structures with a broad size distribution (Figure 2.24), suggesting that the cleavage of the fusion protein influences the mechanism of Htt aggregation. Alternatively, it could be that the deletion of amino acids at the C-terminus of Ex1Q49 by trypsin digestion is responsible for the stabilization of intermediate oligomeric Htt structures. The results obtained with trypsin in this study are in agreement with previously published data, indicating that Δ NEx1Q49 spontaneously forms fibrillar aggregates by a nucleation-dependent polymerization reaction (Scherzinger et al., 1999).

The slower formation of SDS-stable Δ NEx1Q49 aggregates monitored by filter retardation assay has been accompanied by the formation of SDS-resistant oligomers that can be detected in SDS-PAGE and Western blotting with the HD1 antibody (Figure 2.42). Under denaturing conditions the Δ NEx1Q49 oligomers had a size of 180 kDa, suggesting that they consist of 16 monomers. However, the molecular weight of polyQ-containing proteins in SDS gels is normally higher than theoretically calculated based on the amino acid sequence of the protein (Figure 2.39). Therefore, the oligomers were further analyzed by size exclusion chromatography. Prior to cleavage with PP the GST- Δ NEx1Q49 fusion protein was eluted from the column with a size of 250 kDa, indicating that the protein forms a stable oligomer consisting of multiple monomers. After 4 h of incubation in the presence of PP no uncleaved GST- Δ NEx1Q49 oligomer peak with a size of 250 kDa was detected. Interestingly, about 30% of the recovered protein has been found in a peak fraction with a size of 46 kDa, corresponding to a tetrameric oligomer of Δ NEx1Q49 monomers. Another 30% of the Δ NEx1Q49 protein was recovered as high molecular weight structures with a size of 700 kDa. After 48 h of incubation 76% of the recovered Δ NEx1Q49 protein has been found in this fraction. This indicates that over time the amount of large aggregates increases in Δ NEx1Q49 aggregation reactions, whereas the relative amount of small oligomers with a size of 46 kDa was decreased to 5% in spontaneous aggregation reactions (Figure 2.44). This is in agreement with results from SDS-PAGE experiments, indicating that after 48 h the oligomeric Δ NEx1Q49 band migrating at 180 kDa is undetectable (Figure 2.42).

To further analyze the early events in the aggregation cascade of Δ NEx1Q49, dot blot assays were performed using the monoclonal antibodies MW1, 3B5H10 and MW8. The signal for MW1 decreased to less than 20% after 4 h and remained constant over time. The immunoreactivity for MW8 decreased to less than 10% after 4 h and increased again with the

formation of SDS-resistant aggregates detected by filter retardation assay (Figure 2.47). After 4 h of incubation the 3B5H10 immunoreactivity was reduced to 40% and slowly decreased further over time, suggesting that the mutant protein Δ NEx1Q49 follows a similar aggregation mechanism than the Ex1Q49 protein. However, the reduced Δ NEx1Q49 aggregation rate allows a better investigation of potential aggregation intermediates.

Analysis of the aggregates detected in size exclusion chromatography experiments revealed that the oligomeric species with a size of 46 kDa are recognized by the antibody 3B5H10. This suggests that the Δ NEx1Q49 protein forms SDS-resistant β -sheet-rich aggregates in a slow polymerization reaction via a stable tetrameric intermediate that can be recognized by the antibody 3B5H10. However, such a well-defined structure was not detected in spontaneous Ex1Q49 aggregation reactions (Figure 2.12), indicating that the presence of N-terminal amino acids in Htt prevent the assembly of SDS-stable aggregation intermediates.

Addition of the chemical compound O4 to the Δ NEx1Q49 aggregation reaction delayed the formation of SDS-resistant aggregates detected by filter retardation assay and by dot blot assay with the monoclonal antibody MW8. The delay of aggregation was accompanied by the stabilization of the polyQ conformation recognized by the 3B5H10 antibody, while no stabilization of the MW1 immunoreactivity has been observed (Figure 2.47). This supports the view that the polyQ conformation recognized by the 3B5H10 antibody is critical for the assembly of SDS-stable Δ NEx1Q49 aggregates.

The antibody MW1 most likely recognizes an open, α -helical polyQ conformation in the GST-Ex1Q49 fusion protein that converts spontaneously into a more compact, β -sheet structure upon removal of the GST-tag with PP. The results indicate that in the protein Δ NEx1Q49 lacking the N-terminal 15 amino acids a similar conformational change occurs that can be followed by a decrease in MW1 or 3B5H10 immunoreactivity. In the presence of O4 a soluble, tetrameric Δ NEx1Q49 conformation recognized by the 3B5H10 antibody is most likely stabilized, which leads to a delayed onset of SDS-stable Htt aggregates. However, additional experiments are necessary to investigate the biochemical and structural properties of the oligomeric Δ N15Ex1Q49-O4 protein complexes.

In the context of the Htt-exon 1 protein the first 17 amino acids adopt an α -helical conformation (Kim et al., 2009). It has been further proposed that this region is also helical in the fibrillar aggregates, in which the polyQ tract is in the core of the amyloid and the N-terminus is exposed to the medium (Sivanandam et al., 2011). In another study it has been shown that the core of Htt-exon 1 aggregates is composed of both the polyQ tract and the N-terminal amino acids of the Htt protein (Thakur et al., 2009). It has been suggested that the first 17 amino acids at the N-terminus of Htt enhance the spontaneous aggregation of the

Htt-exon 1 protein because they stabilize the association of monomers via protein-protein interactions. The chaperonin TRiC has been shown to bind to the N-terminal amino acids in Htt thereby preventing the intermolecular association of polyQ-containing Htt molecules (Tam et al., 2009). Thus, the destabilization of Htt oligomers with compounds or antibodies appears to be a promising strategy to prevent the toxicity of mutant Htt in cells (Takahashi et al., 2008).

The aggregation of Δ NEx1Q49 in cell-free aggregation reactions reflects the autocatalytic mechanism shown for Ex1Q49. The results further indicate that the polyQ tract facilitates the assembly of fibrillar amyloids and that the N-terminal amino acids adjacent to the polyQ tract indeed have a modulating influence on the rate of aggregation.

3.3 Structural characterization of Htt conformations and aggregates

The full-length Htt protein is a 3144 amino acid long protein containing multiple HEAT repeat sequences. These regions are probably responsible for the high helical content of the protein (Li et al., 2006). Recently, the crystal structure of the first exon of Htt containing 17 glutamines fused to a maltose-binding protein has been published (Kim et al., 2009). In this structure the first 17 amino acids of Htt adopt an α -helical conformation, whereas the polyQ tract can adopt α -helical and random coil conformations.

Here, CD experiments have shown that the Htt-exon 1 fragment fused N-terminally to GST most likely has an α -helical conformation (Figure 2.46). Interestingly, a similar α -helical secondary structure was also obtained for the Δ NEx1Q49 protein fused to GST, indicating that the absence of the first 15 amino acids does not significantly influence the structure of the polyQ tract in the GST- Δ NEx1Q49 fusion protein. It has been published previously that the polyQ tract in a TRX Htt fusion protein has a random-coil structure (Bennett et al., 2002). Furthermore, a crystal structure of this fusion protein bound to the antibody MW1 has been obtained (Bennett et al., 2002), indicating that the polyQ tract in the TRX Htt fusion protein adopts a coil-like structure. In contrast, the conformation recognized by the monoclonal antibody 3B5H10 most likely has a compact β -sheet-rich structure (Zhang et al., 2011). A mutational analysis also suggested that aggregation-prone N-terminal Htt fragments form a compact β -sheet-rich structure with alternating β -strand/ β -turn structures containing seven glutamine residues per strand (Thakur et al., 2009). This is in agreement with my results with the Δ NEx1Q49 fragment obtained from ThT assays, showing that spontaneous aggregation is accompanied with an increase in β -sheet-rich amyloid fibrils (Figure 2.40).

Analysis of the insoluble Ex1Q49 aggregates by atomic force microscopy and transmission electron microscopy revealed that these structures have a fibrillar morphology. Most fibrils had a diameter of 10-15 nm and lengths of $>500 \mu\text{m}$. Moreover, they associated to large

bundled aggregates, suggesting that they form by fusion of two or more fibrils that are connected with each other. A second possibility is that the Ex1Q49 bundles are formed from one initial amyloid fibril by branching off new fibrils. In some cases knot-like structures were observed in EM pictures that could represent potential branching points. This is in agreement with the above presented model (Figure 2.10), as branching represents a secondary process that can explain an autocatalytic aggregation mechanism (Andersen et al., 2009).

In the absence of the 15 N-terminal amino acids (Δ NEx1Q49) polyQ-mediated Htt aggregation was much slower compared to the full-length Ex1Q49 protein. However, the resulting Δ NEx1Q49 aggregates showed a fibrillar morphology similar to the Ex1Q49 aggregates. Interestingly, in the presence of O4 no fibrillar aggregates were detected by atomic force microscopy. However, relatively large numbers of spherical Δ NEx1Q49 oligomers with a diameter of 100 nm were detected in spontaneous aggregation reactions after 24 h, indicating that the compound stabilizes aggregation intermediates. Oligomers were also observed for Ex1Q49 after 24 h in the presence of O4, but to a lesser extent. The detection of Δ NEx1Q49 oligomers by atomic force microscopy is in agreement with the results from size exclusion chromatography and SDS-PAGE.

3.4 Implications of O4-mediated effects on Ex1Q49 aggregation for Huntington's disease pathogenesis

In a previous study the natural dye orcein has been discovered as a modulator of spontaneous Htt-exon 1 aggregation (Heiser et al., 2002). Orcein is a mixture of 14 closely related substances that can be grouped into three structural classes, including the compounds 7-amino-2-phenoxazone, 7-hydroxyl-2-phenoxazone (resorufin) and 7-amino-4,5-dimethyl-2-phenoxazone. Orcein has been used in the Middle Ages as a dye for coloring clothes. Today, it is still used as a food dye and for staining elastic fibers in histology. It can be produced by extraction as orcinol (5-Methylbenzene-1,3-diol) from several types of lichen, which then can be converted by oxygen and ammonia into orcein (Beecken et al., 2003).

In this study the effect of the chemically related substance O4 on Htt aggregation has been analyzed. The substance 2,8-bis-(2,4-dihydroxy-phenyl)-7-phenoxazin-3-one, termed O4, can be synthesized by incubation of resorcinol (Benzene-1,3-diol) in aqueous ammonia (Beecken et al., 2003). The compound has a large conjugated π -system and contains

several H-bond acceptors and donors that potentially could interact with the polar polyQ tract in Ex1Q49 or other regions in the Htt protein.

Binding of O4 to A β peptides has been previously monitored by photoimaging of the blue color of the dye (Bieschke, 2011). However, no binding of O4 to Htt monomers or aggregates could be detected in immunoprecipitation experiments or dot blot color-detection assays in this study. This indicates that the affinity of O4 for Ex1Q49 peptides is relatively low and the compound has a high on- and off-rate. Transient drug target interactions are associated with reduced side effects, as the targeted protein remains functional (Ohlson, 2008). Htt is involved in many processes in the cell and loss of Htt function has been linked to increased apoptosis in knock-out HD mice (Zeitlin et al., 1995). As a potential drug for modulating Htt aggregation needs to be administered for many decades, a transient drug interaction that keeps the Htt protein in an active state would be beneficial.

It has been shown recently that the compound O4 is a potent enhancer of spontaneous A β_{42} aggregation (Bieschke, 2011). In that study, it has been demonstrated that O4 directly binds to small A β_{42} oligomers and accelerated their conversion into fibrillar β -sheet-rich aggregates probably by accelerating nucleation. Mechanistic studies indicated that the hydroxyl groups in O4 might induce the formation of additional hydrogen bonds and thereby unmasked the zipper-forming β -sheet-rich segment in the A β_{42} peptide (Bieschke, 2011). The reduction of A β_{42} oligomers in the presence of O4 led to increased cell survival in cells expressing the A β precursor protein APP. In addition, inhibition of long-term potentiation (LTP) by A β oligomers was suppressed by O4 treatment in rat brain slices (Bieschke, 2011). The effect of O4 on A β_{42} aggregation is different to the effect on Ex1Q49 aggregation. Instead of enhancing fibrillogenesis the spontaneous aggregation of N-terminal Htt fragments in the presence of O4 was delayed and a potential β -sheet-rich polyQ conformation, which is recognized by the monoclonal antibody 3B5H10, was stabilized. Increasing evidence suggests that small, soluble Htt intermediates that are formed early in the aggregation cascade are the cause of the HD phenotype and are more toxic than large, mature fibrillar aggregates with a characteristic cross- β sheet structure (Saudou et al., 1998). However, the transient nature of these Htt conformations and the difficulty to purify and characterize Htt intermediates made it impossible to establish a clear relationship between the size and the structure of amyloid species and their cellular toxicity.

The data suggest that O4 stabilizes a monomeric Ex1Q49 conformation that can be recognized by the monoclonal antibody 3B5H10 (Figure 2.31). This antibody has been previously found to recognize a soluble, toxic Htt species in cell culture models (Zhang et al., 2011). However, the results presented in this study do not fully support these results. O4

treatment of a human neuroblastoma cell line (SH-EP) transiently expressing an YFP-Ex1Q73 fusion protein significantly increased the immunoreactivity of the 3B5H10 antibody. This effect, however, did not result in significant increase in cytotoxicity. This suggests that the stabilization of 3B5H10-reactive YFP-Ex1Q73 oligomers is non-toxic for mammalian cells. However, further studies with other cell models are necessary to substantiate these initial findings.

However, O4 treatment of mammalian cells did not alter the total amount of soluble YFP-Ex1Q73 protein, suggesting that the increase in polyQ reactivity monitored by the 3B5H10 and MW1 antibodies is not caused by an increase in protein expression or a decrease in protein degradation. Additional experiments quantifying the proteasome activity of cells expressing mutant Htt in the presence and absence of O4 are needed to further elucidate whether processing of YFP-Ex1Q73 is impaired in these cells.

In SH-EP cells overexpressing the YFP-Ex1Q73 protein, O4 treatment did not influence the formation of inclusion bodies with insoluble Htt aggregates. Lysates of cells expressing YFP-Ex1Q73 for 48 h were filtered through cellulose acetate membranes and formation of aggregates has been monitored by filter retardation assay. Interestingly, the amount of insoluble YFP-Ex1Q73 aggregates did not change upon O4 treatment, suggesting that the compound does not alter the formation of Htt inclusions in SH-EP cells. Therefore, the increase of soluble, 3B5H10-reactive YFP-Ex1Q73 protein in O4 treated cells is most likely not caused by a reduced aggregation of the YFP-tagged Htt fusion protein with a pathogenic polyQ tract.

Taken together, the results indicate that O4 treatment of cells overexpressing the YFP-Ex1Q73 protein increases the amount of soluble 3B5H10 and MW1 reactive Htt conformations without affecting aggregation or toxicity. These results suggest that the conformation stabilized by O4 is nontoxic for mammalian cells. One possible mechanism of O4 action could be that O4 prevents Htt from forming aberrant protein-protein interactions with other polyQ proteins such as the transcription factor CBP (Schaffar et al., 2004; Steffan et al., 2000).

Preliminary results have shown that O4 can cross the blood brain barrier. Further studies to elucidate the mechanism of O4 action in other cell culture models are necessary to evaluate the potential of this compound as a drug candidate for the treatment of Huntington's disease patients. Further *in vivo* studies in transgenic mice and flies will be necessary.

Today's medication for HD is only focused on symptomatic treatment (Walker, 2007). The compound tetrabenazine that is available in the US and in Canada for treatment of chorea,

promotes the degradation of dopamine, but the compound does not change the progression of the disease (Poon et al., 2010). Preventing or slowing down of the progression of aggregation in patients is a very ambitious aim. Therefore, more detailed experiments are necessary in order to investigate the mechanism of Htt misfolding and aggregation *in vivo* and to develop new therapeutic strategies for polyQ diseases.

3.5 Outlook

In order to elucidate the mechanism of action of the compound O4 in cells additional studies with other cell models are necessary. A PC12 cell line stably expressing a Ex1Q103-GFP fusion protein has been shown to be a highly valuable model for studying Htt aggregation and toxicity (Aiken CT, 2004). Using this cell line it would be possible to further investigate the effect of O4 on soluble polyQ conformations, which are recognized by antibodies such as MW1 or 3B5H10.

The *in vitro* results presented above indicate that Ex1Q49 aggregates are formed by an autocatalytic mechanism. The nucleation rate of Ex1Q49 aggregates can be reduced by addition of the chemical compound O4. The results presented for the Δ NEx1Q49 protein lacking the first 15 amino acids suggest that this fragment follows a similar aggregation mechanism. Further experiments with different concentrations of GST- Δ NEx1Q49 fusion protein and O4 are necessary to confirm the initial results.

The results in this study indicate that O4 treatment increases the relative amount of a soluble, non-toxic Htt conformation in cells. However, similar effects can also be obtained when molecular chaperones such as Hsp70 and Hsp40 target polyQ disease proteins (Lotz, Tam). Therefore, it would be interesting to investigate the *in vitro* and *in vivo* effects of different chaperones on Htt conformations using dot blot assays and compare the results with data obtained from studies with O4.

4. Materials and Methods

4.1 Materials

4.1.1 Bacterial strains

Mach1™ T1®	<i>E. coli</i> / F ⁻ Φ80lacZΔM15 ΔlacX74 hsdR(r _k ⁺ , m _k ⁺) ΔrecA1398 endA1 tonA (Invitrogen), recommended strain for use with the Gateway® Cloning System.
DH10B	<i>E. coli</i> / F ⁻ mcrA Δ-(mrr hsd RMS-mcr BC) φ80dlacZΔM15 ΔlacX74 deoR recA1 araD139 Δ(ara leu)7697 galU galK λ-rpsL endA1 nupG (Invitrogen).
BL21-CodonPlus(DE3)-RP	<i>E. coli</i> B F ⁻ ompT hsdS(rB ⁻ mB ⁻) dcm ⁺ Tet ^r gal λ(DE3) endA Hte [argU proL Cam ^r] strain (Statagene); for high level protein expression following IPTG (Isopropyl-1-thio-β-D-galactopyranoside) induction of T7 polymerase driven by lacUV5 promoter.

4.1.2 Cell lines

SH-EP	Human neuroblastoma cell line. Clonal subline of the neuro-epithelioma cell line SK-N-SH. Epithelial-/neuronal-like elongated cells growing as monolayer and in cell cluster.
-------	---

4.1.3 Expression vectors and plasmids

pGEX-6P1	Expression vector with the synthetic tac-promoter for the IPTG-inducible expression of glutathione S-transferase (GST)-fusion proteins. The vector contains an internal lacI q repressor gene for the repression of expression in every strain of <i>E. coli</i> . Fusion proteins contain a restriction site for PreScission™ protease directly after the GST-protein sequence, which allows the cleavage of the GST-tag (Amersham Biotech Europe GmbH).
----------	---

pdEYFP-attR	Expression vectors for EYFP-fusion proteins based on pcDNA3.1 (+) (Clontec). The vector is a Gateway-adapted destination vector, containing the ccdB gene flanked by the attR recombination sites. pdEYFP-attR is designed for fusing a gene of interest to an N-terminal EYFP-tag according to the Gateway Cloning Technology (Invitrogen) and for expression of this gene in mammalian cells under control of the human CMV-IE promoter and enhancer.
pDONR TM 221	A Gateway® vector containing attP sites. This vector is used for cloning PCR products and genes of interest flanked by attB sites (expression clones) to generate entry clones. It contains the ccdB gene for negative selection and the kanamycin resistance gene for selection in <i>E.coli</i> (Invitrogen).

4.1.4 Microbiological media and buffers

1000x Ampicillin	stock 100 mg/ml dissolved in 50% ethanol, stored at -20 °C
AttoPhos TM buffer	50 mM Tris-HCl pH 9.0, 500 mM NaCl, 1 mM MgCl ₂
AttoPhos TM reagent	10 mM AttoPhos reagent dissolved in 100 mM Tris pH 9.0
1% BSA	Bovine serum albumin was dissolved in 1x PBS to a final concentration of 1% (w/v)
Coomassie destaining solution	45% methanol, 10% acetic acid
Coomassie staining Solution	45% methanol, 10% acetic acid, 0.05% Coomassie brilliant blue R250
Dialysis buffer	50mM NaCl, 10mM Tris-HCl pH 7.4, 0.1mM EDTA
4x DNA sample buffer	0.25% bromophenol blue, 0.25% xylene cyanole FF, 30% glycerol
GST-P1 buffer	50 mM NaH ₂ PO ₄ , 5 mM Tris-HCl pH 8.0, 150 mM NaCl, 1mM EDTA
1000x Kanamycin	stock 25 mg/ml dissolved in distilled water, stored at -20 °C
Lysis buffer for mammalian cells	50 mM HEPES pH 7.4, 150 mM NaCl, 1.5 mM MgCl ₂ , 0.1% NP-40, 1 mM EDTA, stored at 4 °C,

	add 1 mM DTT, 1x protease inhibitors Complete™ and 25 U/ml benzonase fresh before use
LB-(Luria Bertani) medium	10 g/l Bacto Pepton, 5g/l yeast-extract, 10 g/l NaCl, pH7.2
MTT-stop buffer	47.75% DMF, 20% SDS, 2% acetic acid, 25 mM HCl
4% paraformaldehyde	4 g of paraformaldehyde dissolved in 100 ml PBS and heated at 50°C for 5 minutes to reach a clear solution, stored at -20°C
25x Protease inhibitors	One tablet of Complete™ protease inhibitor (Roche) dissolved in 2 ml distilled water, stored at -20°C
10x PBS	80 g NaCl, 2 g KCl, 14.4 g Na ₂ HPO ₄ , 2.4 g KH ₂ PO ₄ , to 1 l with distilled water
10x PBS	80 g NaCl, 2 g KCl, 14.4 g Na ₂ HPO ₄ , 2.4 g KH ₂ PO ₄ , to 1 l with distilled water
PMSF	100 mM PMSF dissolved in isopropanol, stored at -20.
10x PP buffer	500 mM Tris-HCl, 1.5 M NaCl, 10 mM EDTA, 10 mM DTT (add immediately before use), pH 7, stored (without DTT) at 4°C
1x SDD running buffer	1x TAE, 1,5% agarose, 0.1% SDS
4x SDD sample buffer	2x TAE, 20% glycerol, 4% SDS, bromphenolblue
10 % SDS resolving gel	2.5 ml of 40% Bisacrylamide, 2.5 ml of 1.5 M Tris-HCl (pH8.8), 100 µl of 10% SDS, 4.9 ml ddH ₂ O, 100 µl of 10% APS, 10 µl TEMED
5% SDS stacking gel	0.75 ml of 40% acrylamide, 1.5 ml of 0.5 M Tris-HCl (pH6.8), 60 µl of 10% SDS, 3.6 ml ddH ₂ O, 60 µl of 10% APS, 6µl TEMED
4x SDS loading buffer	200 mM Tris-HCl pH 6.8, 400 mM DTT, 8% SDS, 4 mg/ml bromophenol blue, 40% glycerol, store at -20°C
1x SDS running buffer	1x WB-buffer, 0.1% SDS
5% skim milk	skim milk powder was dissolved in TBS-T to a final concentration of 5% (w/v)
S.O.C. Medium	2% Tryptone, 0.5% Yeast Extract, 10 mM NaCl, 2.5 mM KCl, 10 mM MgCl ₂ , 10 mM MgSO ₄ , 20 mM glucose
1x TAE	40 mM Tris-Acetate, 1 mM EDTA, pH 8.0
1x TBE	45 mM Tris-Borate, 1 mM EDTA, pH 8.0
1x TBS	20 mM Tris-HCl pH 7.5, 150 mM NaCl
1x TBS-T	20 mM Tris-HCl pH 7.5, 150 mM NaCl, 0.05% Triton X-100
1x TE	10 mM Tris-HCl, pH 7.4, 1 mM EDTA, pH 8.0
1x TNEC	20 mM Tris-HCl pH 8, 150 mM NaCl, 0.1 mM EDTA pH 8.0, 2 mM CaCl ₂
10 x WB buffer	30 g/l Tris, 144 g/l Glycin

Western blot buffer	1 x WB-buffer, 10 % Ethanol
2x YT	16 g/l Bacto Trypton, 10 g/l yeast-extract, 5 g/l NaCl, pH 7.2

4.1.5 Media and supplements for cell culture

Dulbecco's modified Eagle medium (DMEM) with 4.5 g/L	Gibco
D-Glucose, Sodium Pyruvate, without L-Glutamine	Gibco
0.5% Trypsin and 0.53mM Na-EDTA in Hanks' B.S.S.	Gibco
Fetal calf serum (FBS) from E.G. approved countries	Gibco
Dulbecco's phosphate buffered saline (D-PBS) without calcium, magnesium	Gibco

4.1.6 Antibodies

Table 4.1: Primary antibodies

Primary antibody	Species	Dilution	Supplier
Anti-CAG53b	rabbit	1:2000	own production by E. Scherzinger
Anti-HD1	rabbit	1:2000	own production by E. Scherzinger
MW1	mouse	1:2000	Developmental Studies Hybridoma Bank (University of Iowa)
MW7	mouse	1:2000	Developmental Studies Hybridoma Bank (University of Iowa)
MW8	mouse	1:2000	Developmental Studies Hybridoma Bank (University of Iowa)
3B5H10	mouse	1:5000	Sigma-Aldrich
Anti-GST-HRP	mouse	1:5000	Sigma-Aldrich
Anti-actin (AC-15)	mouse	1:2000	Sigma-Aldrich
Anti-GFP	mouse	1:2000	Abgent

Table 4.2: Secondary antibodies

Primary antibody	Conjugate	Species	Dilution	Supplier
Anti-rabbit IgG	Alkaline Phosphatase	goat	1:10,000	Sigma
Anti-mouse IgG	Alkaline Phosphatase	goat	1:10,000	Sigma
Cy5 IgG		goat	1:300	Invitrogen
Anti-rabbit IgG	Peroxidase	goat	1:10,000	Chemicon

4.1.7 Oligonucleotides

Table 4.3: Primer

Name	Sequence 5' -> 3'
Ex1_EcoRI_fwd	TGGAATTCATGGCGACCCTGGAAAAGCT
Ex1_NotI_rev	TTGCGGCCGCTCATGGTCGGTGCAGCGGCTC
delta1-17_fwd_EcoRI	TGGAATTCTCCTTCCAGCAG
deltaP_rev_NotI	TTGCGGCCGCTCATGGCGGCTGCTG
attB_Ex1_fwd	GGGGACAAGTTTGTACAAAAAAGCAGGCTTCATGGCGACCCTG GAAAAGCTGATG
attB_Ex1_rev	GGGGACCACTTTGTACAAGAAAGCTGGGTCACTACAGGGATCC AGGTCGGTGCA

Oligonucleotides have HPLC purification grade and were synthesized by BioTeZ Berlin-Buch GmbH in a quantity of 10 nmol. Primers and probe have been resolved in nuclease-free water and diluted to a concentration of 10 pmol/μl.

4.1.8 Enzymes, proteins and markers

Benchmark pre-stained protein ladder	Invitrogen
Benzonase purity grade II	Merck
BSA 10 mg/ml	NEB
Herrings Sperm Carrier DNA	Clontech
BP Clonase® II enzyme mix	Invitrogen
LR Clonase® II enzyme mix	Invitrogen
Precision protease™	Amersham Biosciences
Ready-Load™ 1 Kb Plus DNA ladder	Invitrogen
Restriction enzymes	New England Biolabs
Shrimp alkaline phosphatase	Roche Applied Science
T4 DNA Ligase	Fermentas
Lysozyme	Sigma-Aldrich
GoTaq polymerase	Promega
PWO SuperYield DNA polymerase	Roche Applied Science
Gel filtration calibration kit LMW	GE Healthcare
Gel filtration calibration kit HMW	GE Healthcare
Trypsin Sequencing Grade, modified	Roche Applied Science
NativeMark™ Unstained Protein Standard	Invitrogen

4.1.9 Kits

BCA Protein assay reagent	Pierce
Chemi Glow West	Cell Biosciences
Lipofectamine Plus™ transfection reagent	Invitrogen
NativePAGE™ Novex® Bis-Tris gel system	Invitrogen
NuPAGE MES SDS running buffer	Invitrogen
Qiaprep spin miniprep kit	Qiagen
Qiagen plasmid midi kit	Qiagen
Qiaquick gel extraction kit	Qiagen

4.1.10 Chemicals and consumables

3-(4,5-dimethylthiazol-2-yl)-2,5-diphenyltetrazolium bromide (MTT)	Promega
Agarose	Invitrogen
Amicon™ centrifugal filter units, cutoff 10 kDa	Millipore
Amicon™ Ultra-15 centrifugal filter units	Millipore
Ammoniumpersulfate	BioRad
Ampicillin-sodium salt	Sigma-Aldrich
Attophos powder	Europa Bioproducts Ltd.
Bacto peptone	Becton Dickinson
Bacto tryptone	Becton Dickinson
Bacto yeast	Becton Dickinson
Bromophenol blue	Merck Eurolab GmbH
Cell culture dishes	DB Falcon
Cellulose acetate membrane 0.2µm	Schleicher and Schuell
Chloramphenicol	Sigma-Aldrich
Complete™ protease inhibitor cocktail	Roche Applied Science
Congo Red, analytical standard	Sigma-Aldrich
Coomassie brilliant blue G-250	Merck
Curcumin, analytical standard	Sigma-Aldrich
Dialysis membrane, 10.000 kDa cutoff	SpectraPor® Dialysis
Deoxyribonucleotides (dNTPs)	Fermentas
Dithiothreitol (DTT)	Serva
Dimethylsulfoxide (DMSO)	Sigma-Aldrich

Materials and Methods

(-)-Epigallocatechin gallate from green tea	Sigma-Aldrich
Ethidium bromide solution 10mg/ml	Sigma-Aldrich
Ethylenediamine tetraacetic acid	Merck Eurolab GmbH
Filter paper GB005	Schleicher and Schuell
Fluoronunc 96-well plates	Nunc
Glutathione-agarose	Sigma-Aldrich
Glutathione, reduced	Sigma-Aldrich
Glycerol	Merck Eurolab GmbH
Hoechst 33342	Invitrogen
IPTG	Apply Chem
Kanamycin A monosulfate	Sigma-Aldrich
Methylene blue	Sigma-Aldrich
Nitrocellulose membrane 0.2µm	Schleicher and Schuell
NP-40 (IGEPAL CA 630)	Sigma-Aldrich
Orcein	Merck
Paraformaldehyde	Sigma-Aldrich
p-t-Octylphenyl-polyoxyethylen (Triton X-100)	Sigma-Aldrich
PGL-034	Merck
Phenylmethylsulfonylfluoride (PMSF)	Sigma-Aldrich
Polyoxyethylensorbitan-Monolaureat (Tween 20)	Sigma-Aldrich
Ponceau S-solution, 0.1%	Sigma-Aldrich
Pro long gold anti-fade reagent	Invitrogen
Protein LoBind tubes	Eppendorf
Quartz glass cuvettes	Hellmer
Quartz glass cuvettes 100-QS	neoLab
Resorufin	Sigma-Aldrich
Sodium glycinate	Sigma-Aldrich
TEMED	Life Technologies
Tetracycline	Sigma-Aldrich
Thiamine	Sigma-Aldrich
Thioflavin T	Merck
Trichloroacetic acid	Merck
TrypanBlue solution (0.4 %)	Sigma-Aldrich
Uranyl acetate dehydrate	Serva
Whatman chromatography paper 3MM	Whatman

All other chemicals, salts, buffer substances, solvents, acids and bases were purchased from Carl Roth GmbH.

4.1.11 Laboratory equipment

Äkta purifier	Amersham Biosciences
ArrayScan VTI	Thermo Scientific
Biophotometer	Eppendorf
Criterion cell for SDS-PAGE	BioRad
DNA electrophoresis chamber	BioRad
EM910	Zeiss
Gene Genius UV imager	Bio Imaging Systems
HybriDot Manifold vacuum filtration unit	Whatman
Infinite M200 microplate reader	TECAN
LAS-3000 photo imager	Fujifilm
Leica TCS SP2	Leica
Micro 22R centrifuge	Hettich
NanoDROP 8000	peQlab
Nanowizard AFM with Zeiss Axiovert 200	JPK Instruments AG
Optima TLX Ultracentrifuge	Beckman Coulter
PTC200 Peltier Thermal Cycler	MJ Research
Shaking Incubator	Infors Unitron
Thermomixer comfort	Eppendorf
Trans-blot semi-dry transfer cell	BioRad
Zetasizer Nano	Malvern Instruments

4.1.12 Software

AIDA 1.0	AIDA, Deutschland
CDNN 2.1 software	(http://bioinformatik.biochemtech.uni-halle.de/cdnn)
Lasergene	DNA star Inc
Generunner	http://www.generunner.com
JPK Data Processing software	JPK Instruments AG
ProtParam	http://au.expasy.org/tools/protparam.html
Unicorn 5.11	Amersham Biosciences

4.2 Methods

4.2.1 Molecular biology

Plasmid preparation from E.coli

For plasmid amplification, LB medium containing the appropriate antibiotics was inoculated with *E. coli* colonies harboring the plasmid of interest and grown to saturation over night at 37°C in an incubator-shaker. Cells were harvested by centrifugation and plasmids were purified using the Qiaprep Spin Miniprep Kit for small quantities or the Qiagen Midi Kit for larger quantities of DNA according to manufacturer's instructions.

Determination of DNA concentration

DNA concentration of purified plasmid DNA was measured by UV absorption spectroscopy at a wavelength of 260 nm. In H₂O, a solution of 50 µg/ml of double stranded DNA exhibits an absorbance of 1.0.

Restriction digest of DNA

Restriction digests were performed as recommended by the manufacturer. Reactions were incubated at 37°C for 1-2 h. Reactions were stopped by adding 4x DNA loading buffer and separated by agarose gel electrophoresis for DNA fragment analysis. For further cloning the enzymes were heat-inactivated for 20 min at 65°C.

DNA agarose gel electrophoreses

For separation of DNA fragments loading buffer was added to the samples and samples were loaded to a 0.8- 1.2% (w/v) agarose gel, depending on the size of the DNA fragment. 0.5x TBE was used as running buffer. The gels were supplemented with 0.5 g/ml ethidiumbromide to visualize the DNA under UV light after separation. A DNA mass standard was used for identification of DNA length.

Creating cDNA entries using the BP recombination reaction (BP reaction)

150 ng of polymerase chain reaction product containing the attB cloning sites were mixed with 75 ng of pDONR221. The volume was adjusted to 8 μ l with TE buffer at pH 8.0 and 2 μ l BP clonase was added. The reaction was incubated at 25°C for 2 h and transformed into 12 μ l commercial Mach1 cells (Invitrogen).

Gateway shuttling of cDNA into expression vectors (LR reaction)

cDNA was integrated into expression vectors using the Gateway technology (Invitrogen). 1 μ l of the entry clone (25 ng/ μ l), 1 μ l of destination vector (150 ng/ μ l) and 2 μ l of TE-buffer at pH 8.0 were incubated with 1 μ l of LR clonase at 25°C for 3 h. The DNA was transformed in 10 μ l commercial Mach1 cells (Invitrogen), for selection of positive clones.

Polymerase chain reaction

The amplification of DNA fragments was performed using the PWO SuperYield DNA Polymerase system (Roche). The PWO polymerase has a proof-reading activity and the system has a buffer for GC-rich DNA fragments. The PCR mix was prepared, containing the following: 0.25 mM of each dNTP, 0.375 μ M of forward and reverse primer, 2.5 U polymerase, 1x PCR buffer, 1x GC-rich solution and 50-100 ng template DNA. Elongation time and annealing temperature were determined for each PCR reaction. The annealing temperature depends on the melting temperature of the primers and the elongation time depends on the length of target to be amplified. The PCR was performed according to the following protocol:

1 st cycle	Denaturing	95 °C	2 min
30 cycles	Denaturing	95 °C	30 sec
	Annealing	60-80 °C	30 sec
	Elongation	72 °C	1 min/ kb
Last cycle	Elongation	72 °C	5 min
		4 °C	

Colony-Polymerase chain reaction

To verify that the fragments were inserted into the plasmid after ligation, colony polymerase chain reaction was performed using the GoTaq polymerase from Promega. The PCR mix was prepared, containing the following: 0.25 mM of each dNTP, 0.375 μ M of forward and reverse primer and 1x green PCR buffer. Then single colonies of transformants were picked with sterile toothpicks, stirred briefly in the PCR mix and the rest of the picked colony was struck out on LB agar plates containing the appropriate antibiotics. Samples were denatured at 96 °C for 10 min and cooled to room temperature before 1 U of polymerase was added to the sample. Taq polymerase was diluted in 10 mM Tris pH 7.0 to a concentration of 1U / μ l. The PCR was performed according to the following protocol:

1 st cycle	Denaturing	95 °C	2 min
30 cycles	Denaturing	95 °C	30 sec
	Annealing	55 °C	30 sec
	Elongation	72 °C	1 min/ kb
Last cycle	Elongation	72 °C	5 min
		4 °C	

DNA extraction from agarose gels

After separation by agarose gel electrophoreses bands of interest were excises with a scalpel and purified with the QIAquick gel extraction kit according to the manufacturer's instructions.

Dephosphorylation of DNA fragments

To prevent vector DNA recircularization during ligation 5' phosphate groups were removed using the Shrimp alkaline phosphatase (SAP; Roche). 1 μ g of digested vector DNA were incubated with 1 U SAP and supplied buffer for 10 min at 37 °C. Subsequently, the enzyme was heat inactivated by incubation at 65 °C for 15 min.

Ligation of DNA fragments

To insert a DNA fragment into a vector with compatible cohesive ends, vector and DNA fragment were mixed at a molar ratio of 3:1 in a volume of 20 μ l. 5 U of T4 DNA ligase and ligase buffer to a final concentration of 1x were added, and the reaction was incubated at room temperature for 1 h. Afterwards the reaction was transformed into chemical competent DH10B *E. coli* cells.

Preparation of chemical competent E. coli

50 ml of LB medium were inoculated with a single colony and grown over night to saturation at 37°C with shaking at 200 rpm. 10 ml of this over night culture were used to inoculate 1 l of LB medium. The culture was grown at 37°C to an optical density of 0.4-0.6 at measured at 600 nm. All the following steps were performed on ice and with pre-chilled solutions. Cells were centrifuged at 2500 rpm for 20 min, washed with 500 ml 0.1 M MgCl₂ solution, again centrifuged and washed with 250 ml 0.1 M CaCl₂ solution. After another centrifugation step the cells were resuspended in 10 ml 0.07 M CaCl₂ solution containing 30 % glycerol. Aliquots were frozen in liquid nitrogen and stored at -80°C.

Chemical transformation of E. Coli

Frozen chemically competent cells were thawed on ice for 5 min. For transformation 30 μ l of DH10B or BL21-RP *E. coli* strains were mixed with 1 μ l of plasmid DNA and incubated on ice for 30 min. The cells were then heat-shocked at 42°C for 45 sec and cooled on ice for 5 min. After addition of 1 ml pre-warmed SOC the cells were incubated at 37°C for 1 h with shaking. Subsequently aliquots of cells were plated on LB agar plates containing the appropriate antibiotics and incubated over night at 37°C. In case of BP or LR reactions, the reaction mix was transformed into 10 μ l of Mach1 cells, heat shocked as described before and grown in 100 μ l SOC media. All cells were plated on LB agar plates containing the appropriate antibiotics.

4.2.2 Protein biochemistry

Expression of GST-fusion proteins in E.coli

For the expression of GST-tagged fusion proteins a single colony of *E. coli* containing the expression vector was inoculated in 100 ml LB media containing the appropriate antibiotics. The culture was grown over night in an incubator-shaker at 37°C. The optical density was measured at 600 nm and 2 l of (3/2) TY/LB media with the appropriate antibiotics and 20 mM MOPS-KOH pH 7.0, 20 µg/ml thiamine and 0.2 % glucose (all final concentrations) were inoculated with over night culture to a final concentration of 0.2 OD₆₀₀. The main culture was grown until an optical density of 0.4- 0.6 measured at 600 nm was reached. Then expression was induced by adding 1 mM isopropyl-1-thio-β-D-galactoside (IPTG) and cells were incubated at 37°C. After 3 h, the cells were harvested by centrifugation at 4000 rpm for 15 min at 4°C. The resulting pellet was frozen at -80°C.

Purification of GST-fusion proteins

For the purification of GST-fusion protein from a 2 l culture, the pellet was resuspended in 34 ml GST-P1 buffer supplied with 1x Complete[®] protease inhibitor and 50 µg/ml lysozym. Lysis was allowed to proceed for 45 min on ice, before the lysate was sonicated two times for 45 sec. Triton-X100 was added to a final concentration of 0.1% (v/v) and the lysate was cleared by centrifugation at 15000 rpm for 30 min at 4 °C. The supernatant was added to 4 ml of Glutathione Sepharose 4B, which have been equilibrated in GST-P1 buffer according to the manufacturer's instructions, and incubated for at least 1 h at 4 °C on a rotating wheel. Two polypropylene columns were equilibrated with 10 ml GST-P1 buffer. The suspension was then poured onto the column, washed three times with 10 ml GST-P1 buffer containing 1x complete[®] protease inhibitor and 0.1% Triton-X100 and 6 times with 10 ml GST-P1 buffer alone. Elution was achieved by adding 5 ml GST-P1 buffer containing 15 mM reduced Glutathione onto the column and incubating for 15 min. The protein was eluted from the column and the elution was repeated with 3 ml elution buffer. The two fractions were pooled and dialysed over night against 10 l of dialysis buffer using a dialysis membrane with a molecular weight cutoff of 10,000 kDa. Dialysis was repeated against 3 l dialysis buffer containing 5% glycerol. Protein concentration of the resulting solution was determined and, if necessary, the solution was concentrated by centrifugation through an Amicon concentrating device with a molecular weight cutoff at 2000 x g, until a final concentration greater than 1 was reached. The protein solution was then aliquoted, snap frozen in liquid nitrogen and stored at -80°C.

Determination of the protein concentration

The protein concentration of GST-fusion proteins was determined spectrophotometrically by measuring the absorption at 280 nm. In order to calculate the concentration from the measured absorbance the theoretical extinction coefficients were calculated for the respective amino acid sequence (<http://au.expasy.org/tools/protparam.html>).

The protein concentration of crude cell lysats was determined using a BCA protein assay kit. The assay was performed according to the microplate procedure in the manufacturer's instructions.

Protein Precipitation by TCA

TCA was added to a final concentration of 13% to the protein solution, incubated at -20°C for 5 min and 15 min at 4°C. Samples were centrifuged for 15 min at 13500 rpm in a Hettich mikro 22 at 4°C. Pellets were dried and resuspended in loading buffer.

SDS-polyacrylamide gel electrophoresis (SDS-PAGE)

Proteins were separated by SDS-PAGE using a discontinuous buffer system under denaturing and reducing conditions according to Laemmli (Laemmli 1970). Prior to loading the samples onto the gel 4x loading buffer was added and proteins were denatured at 96°C for 5 min. SDS-PAGE was performed following the instructions by Sambrook and Russel (Sambrook and Russel, 2001), with gels containing 10% polyacrylamide. As protein standard Benchmark™ pre-stained protein ladder from Invitrogen was used. Gels were run in SDS running buffer for 15 min at 120 V, followed by 40 min at 180 V.

Western blotting

Proteins, separated by SDS-PAGE, were transferred to nitrocellulose membrane in a semi-dry Transblot Apparatus at 20 V for 1 h. The gel was placed on a nitrocellulose membrane and assembled in a sandwich of two layers of Schleicher and Schuell GB005 Whatman paper. The membrane was placed on the side of the gel facing the anode.

Immunodetection of proteins on nitrocellulose or cellulose acetate membranes

Membranes were blocked in 5% milk in TBS-T for 30 min at room temperature or over night at 4°C. The first antibody was diluted in 5% milk in TBS-T, if not stated otherwise, and incubated with the membrane at room temperature for 50 min or over night at 4°C. After washing the membranes three times with TBS-T for 5 min the secondary antibody, also diluted in 5% milk in TBS-T was added and the membranes were incubated for 35 min at room temperature.

For alkaline phosphatase conjugated secondary antibodies the membranes were washed twice with TBS-T, once with TBS and finally once with attophos buffer each for 5 min. The membranes were then incubated for 1 min in a 200-fold dilution of AttoPhos reagent in attophos buffer. Protein bands or dots were visualized by fluorescence under 460 nm UV-light in an LAS3000 Image reader and quantified using the AIDA software.

If the secondary antibody was conjugated to peroxidase the membranes were washed twice with TBS-T and once with TBS each for 5 min. Chemiluminescence was measured using the Western Lightning TM kit from PerkinElmer using a LAS300 Image reader according to the manufacturer's protocol.

If a membrane had to be developed more than twice the membrane was incubated with stripping buffer for at least 30 min, washed three times with TBS-T and once with TBS each for 5 min before the membrane was blocked again in 5% milk in TBS-T.

Coomassie staining of SDS gels

Coomassie Brilliant Blue is a dye that forms strong non-covalent complexes with proteins. The dye is used to stain proteins in SDS-polyacrylamide gels. After SDS-PAGE the gels were incubated for 1 h in Coomassie staining solution on a horizontal shaker at room temperature. To reduce background staining the gels were then washed in destaining solution until the bands were clearly visible. For documentation the gel was scanned using a tabletop scanner.

Semi-denaturing detergent-agarose gel electrophoresis (SDD-AGE)

SDD-AGE is a technique to detect and characterize amyloid conformational variants based on size and detergent insolubility. The technique was first reported by Kryndushkin et al. (Kryndushkin et al., 2003) and has been modified by Halfmann and Lindquist in 2008 (Halfmann et al., 2008). The proteins and aggregates are separated on an agarose gel containing 0.1 % SDS and subsequent downward capillary transfer to a membrane.

A 1.5% agarose solution in 1x TAE was boiled in a microwave until the agarose was completely dissolved. After melting, the solution was stirred and SDS was added to a final concentration of 0.1%. The solution was poured into the casting tray and any bubbles were removed. 4x sample buffer was added to the samples to generate lysats containing 1x loading buffer and incubated for 5 min at room temperature. 1 µg of GST-fusion protein or 50 µg of protein lysate were loaded on the gel. Purified proteins were loaded as size markers: Catalase (232 kDa), ferritin (440 kDa), thyroglobulin (669 kDa) and Blue dextran (2000 kDa). Electrophoresis was performed in 1x TAE containing 0.1% SDS at 90 V for 1 h 30 min at 4°C. For transfer a PVDF membrane was placed on a stack of 2 cm of tissue, 10 pieces of GB005 and 1 piece of GB005, which has been pre-wet in TBS. The agarose gel was rinsed in TBS transferred onto the membrane. After removing bubbles 3 pre-wet GB005 were placed on the stack and a pre-wet tissue was draped across the stack such that either end was submerged in trays containing TBS. A glass plate bearing the extra weight of a 500 ml bottle was put on top. Transfer was processed for 5 h 30 min at 4°C. After transfer the membrane was stained with Ponceau-S for 5 min and subsequently washed with distilled water to remove background staining. Standard proteins were marked and after washing the membrane 3 times with TBS-T the standard immunodetection protocol was carried out.

in vitro GST-fusion protein aggregation reactions

Cleavage with PreScission protease (PP)

Aggregation of GST-fusion proteins was initiated by addition of 0.28 U PreScission protease per µg fusion protein in PP-buffer at 20 °C and 300 rpm shaking in a Thermomixer. If not stated otherwise, aggregation was performed at a concentration of 2 µM. For kinetics, samples were taken before PP protease was added and at indicated time points, frozen on dry ice and stored at -80°C. Samples that were processed under native conditions were transferred to protein Lobind tubes.

Cleavage with Trypsin

GST-fusion proteins at a concentration of 10 µM were cleaved with 0.1 µg trypsin per µg fusion protein in TNEC-buffer. The reactions were incubated at 37°C without shaking. Kinetics were performed as described for PP protease cleavage.

Filter retardation assay

To detect SDS-insoluble aggregates, 50 µg of cell extracts or 500 ng of *in vitro* aggregation reactions were mixed with an equal volume denaturing buffer containing 0.4% SDS and 100 mM DTT and denatured at 96°C for 5 min, followed by filtration through a cellulose acetate membrane with a pore size of 0.2 µm. Slots were washed twice with 100 µl 0.2% SDS solution. Aggregates were detected with the CAG53b antibody using the standard immunodetection protocol (Scherzinger et al., 2000).

Dot blot assay

To analyze the epitope accessibility of aggregation intermediates, 40 µl of PBS were added to aliquots of 250 ng of *in vitro* aggregation reactions and samples were thaw on ice, followed immediately by filtration through a nitrocellulose membrane. Samples were washed twice with PBS and immunodetected as described before. For the detection of epitopes in cell lysates, 30 µg of proteins were transferred directly to the filter device.

Preparation of seeds

Seeds were prepared using the standard *in vitro* aggregation protocol. Seeds were incubated for 3 h at a concentration of 2 µM at 20°C and were added immediately to the aggregation reactions.

ThT assay

ThT fluorescence was recorded from triplicate experiments at 1 or 10 µM aggregation reactions. The ThT kinetics were recorded as described before (Bieschke et al., 2005) using a fluorescence plate reader (Infinite M200, Tecan) with 10 or 20 min reading intervals and 5 s shaking before each read. 2 µM ThT were added to aggregation reactions and the shift in fluorescence was monitored continuously at an excitation wavelength of 450 nm and an emission wavelength of 485 nm.

4.2.3 Analytical methods

Electron microscopy (EM)

Small aliquots of 1 μg *in vitro* aggregation reactions were applied to formvar-carbon-coated grids for 1 min, washed 4 times and stained with 5 % aqueous uranyl acetate. Images were taken with a Zeiss 910 electron microscope equipped with a 1kx1k high speed slow scan CCD camera and the iTEM software (Olympus Soft Imaging Solutions, Münster, Germany).

Atomic force microscopy (AFM)

Aliquots of 2 μg of *in vitro* aggregation reactions were spotted immediately on freshly cleaved mica, allowed to adhere for 5 min and then washed four times with 40 μl distilled water. The samples were dried over night at room temperature. The samples were then imaged in air with a digital multimode Nano Wizard® II atomic force microscope operating in intermittent contact mode.

CD spectroscopy

Huntingtin fragments (0.1 $\mu\text{g}/\mu\text{l}$) were cleaved with PP and aggregated for 0 or 4 h as described above and CD spectra were recorded on a Chiroscan CD Spectrometer (Applied Photophysics limited). Solutions containing corresponding amounts of buffer only were incubated in parallel. Reference CD spectra of GST were recorded and subtracted from the CD signals to isolate the huntingtin-specific changes in the CD spectra.

Size-exclusion chromatography

Protein samples were loaded to a Superdex 30/100_GL column fitted to a Äkta purifier system. The proteins were eluted in PP buffer at a flow rate of 300 $\mu\text{l}/\text{min}$ at 4°C. Eluted peaks were detected by measuring the absorbance at 280 nm. The eluate was collected in fractions of 400 μl for further analysis.

Dynamic light scattering

The size of aggregates was measured at 20°C without agitation using dynamic light scattering (Malvern Nano Zetasizer ZS, with a green laser $\lambda = 532 \text{ nm}$, and backscattered detection at an angle $\theta = 173 \text{ deg}$). The GST-Ex1Q49 sample was centrifuged at 208,000xg

and 4 °C for 20 min (Beckman Coulter, Optima TL, rotor TLA100.3), to remove dust, probes were centrifuged at 4 °C using a table-top centrifuge (18000 rpm) prior to transfer to a quartz cuvette for light scattering measurements. Dynamic light scattering yields the normalized time autocorrelation function of the intensity of the scattered light $g^{(2)}(\tau)$ at time τ

$$g^{(2)}(\tau) = \frac{\langle I(t)I(t+\tau) \rangle}{\langle I(t) \rangle^2}. \quad (1)$$

Each correlation spectra is the average of 10 traces à 3 sec each. The z-averaged diffusion coefficient D_z of the aggregates in solution was computed as described in Frisken (2001). Briefly, the autocorrelation function is expanded in terms of the moments around the mean of the decay rate distribution. An expansion up to order two in τ gives the approximation

$$g^{(2)}(\tau) \approx B + \beta \exp(-2\mu_1) \left(1 + \frac{\mu_2 \tau^2}{2!} \right)^2. \quad (2)$$

Where μ_1 is i -th moment around the mean, β a factor that depends on the experimental geometry and B the baseline, which can differ from its theoretical value of 1 due to noise. The first moment relates to the z-averaged diffusion constant

$$D_z = \mu_1 / q^2, \text{ with } q = \frac{4\pi n}{\lambda} \sin\left(\frac{\theta}{2}\right). \quad (3)$$

For the setup and a refractive index $n = 1.333$ the scattering wave vector was $q = 31.4281 \mu\text{m}^{-1}$. Equation 1 was fitted to the autocorrelation data, using the non-linear fitting routine `lsqnonlin` from matlab to obtain μ_1 , μ_2 , B and β . The z-averaged radius R_z is calculated from the Einstein-Stokes equation

$$R_z = \frac{kT}{6 \pi \eta D_z}. \quad (4)$$

Where k is the Boltzmann-constant, T the temperature, and the viscosity $\eta = 1.0324$ cP. The particle size distribution by intensity is obtained using the general purpose algorithm from the Malvern Zetasizer software version 6.12.

4.2.4 Methods in cell biology

Cultivation of mammalian cells

SH-EP cells were grown in Dulbecco's modified Eagle medium (DMEM) without L-Glutamine and with 4,5 g/l D-Glucose supplemented with 5% FBS, 100 U/ml penicillin and 100 $\mu\text{g/ml}$ streptomycin at 37 °C and 5% CO_2 . Cells were grown up to 90% confluence and split down to 10% confluence as described before.

Long term storage of mammalian cells

Cells were grown to 80% confluence in a 75 cm² culture flask. The medium was removed, washed with D-PBS, the detached using trypsin and pelleted by centrifugation at 1000 g for 10 min. Cells were resuspended in 1 ml of culture medium with 20% FBS, and DMSO was added slowly to a final concentration of 10%. Subsequently the cells were aliquoted in two tubes and slowly cooled down to -80 °C in a cryo-tube placed in a box filled with isopropanol. Finally the tubes were transferred to the liquid nitrogen tank for long term storage at -180 °C.

Determination of cell number by TrypanBlue staining

To determine numbers of living cells within a population, a Neubauer counting chamber was used. 10 µl of cell suspension was mixed with 10 µl of 0.4% Trypanblue staining solution. The cells were counted in 4 counting squares and the number of living cells was calculated according to the formula below.

$$\text{Total cell number} = \frac{\text{number of counted cells}}{4} \times 2 \times 10^4$$

Transient transfection of SH-EP cells

SH-EP cells were transfected with plasmid DNA using Lipofectamine 2000 reagent (Invitrogen) according to the manufacturer's instructions. 20,000 cells were plated per 96 well plate or 100,000 per 48 well plate one day prior to transfection. Cells were transfected with 0.2 µg DNA in case of 96 well plates or 0.5 µg in 48-well plates and incubated for 24-48 h at 37 °C and 5% CO₂.

Preparation of cell lysats

Cell lysats were prepared 24 or 48 h after transfection. Cells were washed once with D-PBS and scraped of in 50 µl D-PBS. Cells were centrifuged at 1000 g for 5 min and the pellets were frozen at -80 °C until lysis. The cells were thaw in 30 µl lysis buffer and cells were disrupted by pulling five times through a syringe with a 1.2 gauge needle attached.

Determination of cell survival

The MTT assay is a colorimetric assay for cellular growth and survival. It is based on the reduction of the tetrazole MTT to formazan by cellular redox enzymes in living cells. Following lysis of the cells, the absorption of the formazan solution at 570 nm can be analyzed spectrometrically.

After 2 days, 15 μ l of MTT reagent (Methylthiazolyldiphenyl-tetrazolium bromide) was added to each well and the plates were incubated for 2 hours at 37°C. The cells were then lysed by adding 100 μ l MTT stop solution per well and incubating for another 2 h at 37°C. The absorption of the formazan solution at 570 nm was then measured using the Tecan Infinite M200 plate reader. P-values were calculated using the two-tailed t-test.

Immunofluorescence microscopy

To investigate the localization of distinct Htt conformations directly in mammalian cells immunofluorescence staining experiments were performed. For immunofluorescence staining SH-EP cells were grown on sterile coverslips. Cells were transfected with plasmid DNA coding for YFP-Ex1Q73. After 48 h of incubation the cells were washed carefully with D-PBS and fixed with 4% paraformaldehyde (PFA) in 1x PBS for 15 min at room temperature. Subsequently, cells were washed once with PBS. Cells were then permeabilized with 0.2% TritonX-100 for 2 min. Permeabilized cells were blocked in 1 % bovine serum albumin (BSA) in 1x PBS for 1 h, followed by incubation for 1 h with a primary antibody recognizing the protein of interest diluted in 1% BSA. After 3 washing steps to remove unbound primary antibody the samples were incubated with a suitable fluorescence-labelled secondary antibody for 1 h at room temperature. The coverslips were washed 3 times and incubated with Hoechst 33342 for 15 min. After 3 washing steps coverslips carrying the stained cells were mounted upside down on glass plates using ProLong® Gold antifade reagent (Invitrogen).

The mounted samples were stored over night at RT and subsequently examined using a SP2 confocal microscope (Leica).

Automated high-throughput fluorescence microscopy

For quantification of Htt conformations in individual cells, SH-EP cells were analyzed with an automated fluorescence microscope. The cells were transfected with plasmids expressing either Ex1Q73-EYFP or YFP alone. Six hours after the transfection the medium was exchanged with media containing O4 or DMSO. After 48 h of incubation the cells were washed carefully with D-PBS and fixed with 4% paraformaldehyde (PFA) in 1x PBS

containing Hoechst 33342 to a final concentration of 1:2500 for 15 min at room temperature. Subsequently, cells were washed once with PBS. Cells were then permeabilized with 0.2% TritonX-100 for 2 min. Permeabilized cells were blocked in 1 % bovine serum albumin (BSA) in 1x PBS for 1 h, followed by incubation for 1 h with a primary antibody recognizing the protein of interest diluted in 1% BSA. After 3 washing steps to remove unbound primary antibody the samples were incubated with a suitable fluorescence-labelled secondary antibody for 1 h at room temperature. After 3 washing steps PBS containing 0.1% NaN₃ was added to the cells and plates were stored at 4°C and subsequently examined using a ArrayScan VTI (Thermo Scientific) with the ArrayScan VTI software.

5. Literature

- Andersen, C.B., H. Yagi, M. Manno, V. Martorana, T. Ban, G. Christiansen, D.E. Otzen, Y. Goto, and C. Rischel. 2009. Branching in amyloid fibril growth. *Biophys J.* 96:1529-36.
- Andrade, M.A., and P. Bork. 1995. HEAT repeats in the Huntington's disease protein. *Nat Genet.* 11:115-6.
- Andrew, S.E., Y.P. Goldberg, B. Kremer, H. Telenius, J. Theilmann, S. Adam, E. Starr, F. Squitieri, B. Lin, M.A. Kalchman, and et al. 1993. The relationship between trinucleotide (CAG) repeat length and clinical features of Huntington's disease. *Nat Genet.* 4:398-403.
- Anfinsen, C.B. 1973. Principles that govern the folding of protein chains. *Science.* 181:223-30.
- Arango, M., S. Holbert, D. Zala, E. Brouillet, J. Pearson, E. Regulier, A.K. Thakur, P. Aebischer, R. Wetzel, N. Deglon, and C. Neri. 2006. CA150 expression delays striatal cell death in overexpression and knock-in conditions for mutant huntingtin neurotoxicity. *J Neurosci.* 26:4649-59.
- Arrasate, M., S. Mitra, E.S. Schweitzer, M.R. Segal, and S. Finkbeiner. 2004. Inclusion body formation reduces levels of mutant huntingtin and the risk of neuronal death. *Nature.* 431:805-10.
- Atwal, R.S., J. Xia, D. Pinchev, J. Taylor, R.M. Eppard, and R. Truant. 2007. Huntingtin has a membrane association signal that can modulate huntingtin aggregation, nuclear entry and toxicity. *Hum Mol Genet.* 16:2600-15.
- Bachoud-Levi, A., C. Bourdet, P. Brugieres, J.P. Nguyen, T. Grandmougin, B. Haddad, R. Jeny, P. Bartolomeo, M.F. Boisse, G.D. Barba, J.D. Degos, A.M. Ergis, J.P. Lefaucheur, F. Lisovoski, E. Pailhous, P. Remy, S. Palfi, G.L. Defer, P. Cesaro, P. Hantraye, and M. Peschanski. 2000. Safety and tolerability assessment of intra-striatal neural allografts in five patients with Huntington's disease. *Exp Neurol.* 161:194-202.
- Balch, W.E., R.I. Morimoto, A. Dillin, and J.W. Kelly. 2008. Adapting proteostasis for disease intervention. *Science.* 319:916-9.
- Bates, G. 2003. Huntingtin aggregation and toxicity in Huntington's disease. *Lancet.* 361:1642-4.
- Bates, G., S.P. Harper, and L. Jones. 2002. Huntington's Disease. Oxford University Press.
- Beecken, H., E.M. Gottschalk, U. v Gizycki, H. Kramer, D. Maassen, H.G. Matthies, H. Musso, C. Rathjen, and U. Zdhorszky. 2003. Orcein and litmus. *Biotech Histochem.* 78:289-302.
- Bence, N.F., R.M. Sampat, and R.R. Kopito. 2001. Impairment of the ubiquitin-proteasome system by protein aggregation. *Science.* 292:1552-5.
- Bennett, M.J., K.E. Huey-Tubman, A.B. Herr, A.P. West, Jr., S.A. Ross, and P.J. Bjorkman. 2002. A linear lattice model for polyglutamine in CAG-expansion diseases. *Proc Natl Acad Sci U S A.* 99:11634-9.
- Bernacki, J.P., and R.M. Murphy. 2009. Model discrimination and mechanistic interpretation of kinetic data in protein aggregation studies. *Biophys J.* 96:2871-87.
- Bertoncini, C.W., C.O. Fernandez, C. Griesinger, T.M. Jovin, and M. Zweckstetter. 2005. Familial mutants of alpha-synuclein with increased neurotoxicity have a destabilized conformation. *J Biol Chem.* 280:30649-52.
- Bhattacharyya, A., A.K. Thakur, V.M. Chellgren, G. Thiagarajan, A.D. Williams, B.W. Chellgren, T.P. Creamer, and R. Wetzel. 2006. Oligoproline effects on polyglutamine conformation and aggregation. *J Mol Biol.* 355:524-35.
- Bieschke, J., Wanker, E. E. . 2011. *Nat Chem Biol.* accepted.
- Bodner, R.A., T.F. Outeiro, S. Altmann, M.M. Maxwell, S.H. Cho, B.T. Hyman, P.J. McLean, A.B. Young, D.E. Housman, and A.G. Kazantsev. 2006. Pharmacological promotion of inclusion formation: a therapeutic approach for Huntington's and Parkinson's diseases. *Proc Natl Acad Sci U S A.* 103:4246-51.

- Busch, A., S. Engemann, R. Lurz, H. Okazawa, H. Lehrach, and E.E. Wanker. 2003. Mutant huntingtin promotes the fibrillogenesis of wild-type huntingtin: a potential mechanism for loss of huntingtin function in Huntington's disease. *J Biol Chem.* 278:41452-61.
- Chen, S., F.A. Ferrone, and R. Wetzel. 2002. Huntington's disease age-of-onset linked to polyglutamine aggregation nucleation. *Proc Natl Acad Sci U S A.* 99:11884-9.
- Chen, Y., F. Ding, H. Nie, A.W. Serohijos, S. Sharma, K.C. Wilcox, S. Yin, and N.V. Dokholyan. 2008. Protein folding: then and now. *Arch Biochem Biophys.* 469:4-19.
- Chiti, F., and C.M. Dobson. 2006. Protein misfolding, functional amyloid, and human disease. *Annu Rev Biochem.* 75:333-66.
- Cornett, J., F. Cao, C.E. Wang, C.A. Ross, G.P. Bates, S.H. Li, and X.J. Li. 2005. Polyglutamine expansion of huntingtin impairs its nuclear export. *Nat Genet.* 37:198-204.
- Davies, S.W., M. Turmaine, B.A. Cozens, M. DiFiglia, A.H. Sharp, C.A. Ross, E. Scherzinger, E.E. Wanker, L. Mangiarini, and G.P. Bates. 1997. Formation of neuronal intranuclear inclusions underlies the neurological dysfunction in mice transgenic for the HD mutation. *Cell.* 90:537-48.
- Dehay, B., and A. Bertolotti. 2006. Critical role of the proline-rich region in Huntingtin for aggregation and cytotoxicity in yeast. *J Biol Chem.* 281:35608-15.
- Desai, U.A., J. Pallos, A.A. Ma, B.R. Stockwell, L.M. Thompson, J.L. Marsh, and M.I. Diamond. 2006. Biologically active molecules that reduce polyglutamine aggregation and toxicity. *Hum Mol Genet.* 15:2114-24.
- DiFiglia, M., E. Sapp, K.O. Chase, S.W. Davies, G.P. Bates, J.P. Vonsattel, and N. Aronin. 1997. Aggregation of huntingtin in neuronal intranuclear inclusions and dystrophic neurites in brain. *Science.* 277:1990-3.
- Dikshit, P., A. Goswami, A. Mishra, N. Nukina, and N.R. Jana. 2006. Curcumin enhances the polyglutamine-expanded truncated N-terminal huntingtin-induced cell death by promoting proteasomal malfunction. *Biochem Biophys Res Commun.* 342:1323-8.
- Dill, K.A., and H.S. Chan. 1997. From Levinthal to pathways to funnels. *Nat Struct Biol.* 4:10-9.
- Dinner, A.R., A. Sali, L.J. Smith, C.M. Dobson, and M. Karplus. 2000. Understanding protein folding via free-energy surfaces from theory and experiment. *Trends Biochem Sci.* 25:331-9.
- Dobson, C.M. 2003. Protein folding and misfolding. *Nature.* 426:884-90.
- Dobson, C.M., and M. Karplus. 1999. The fundamentals of protein folding: bringing together theory and experiment. *Curr Opin Struct Biol.* 9:92-101.
- Dorval, V., and P.E. Fraser. 2007. SUMO on the road to neurodegeneration. *Biochim Biophys Acta.* 1773:694-706.
- Douglas, P.M., and A. Dillin. 2010. Protein homeostasis and aging in neurodegeneration. *J Cell Biol.* 190:719-29.
- Duennwald, M.L., S. Jagadish, P.J. Muchowski, and S. Lindquist. 2006. Flanking sequences profoundly alter polyglutamine toxicity in yeast. *Proc Natl Acad Sci U S A.* 103:11045-50.
- Dunah, A.W., H. Jeong, A. Griffin, Y.M. Kim, D.G. Standaert, S.M. Hersch, M.M. Mouradian, A.B. Young, N. Tanese, and D. Krainc. 2002. Sp1 and TAFII130 transcriptional activity disrupted in early Huntington's disease. *Science.* 296:2238-43.
- Dunker, A.K., J.D. Lawson, C.J. Brown, R.M. Williams, P. Romero, J.S. Oh, C.J. Oldfield, A.M. Campen, C.M. Ratliff, K.W. Hipps, J. Ausio, M.S. Nissen, R. Reeves, C. Kang, C.R. Kissinger, R.W. Bailey, M.D. Griswold, W. Chiu, E.C. Garner, and Z. Obradovic. 2001. Intrinsically disordered protein. *J Mol Graph Model.* 19:26-59.
- Duyao, M.P., A.B. Auerbach, A. Ryan, F. Persichetti, G.T. Barnes, S.M. McNeil, P. Ge, J.P. Vonsattel, J.F. Gusella, A.L. Joyner, and et al. 1995. Inactivation of the mouse Huntington's disease gene homolog Hdh. *Science.* 269:407-10.
- Ehrnhoefer, D.E., J. Bieschke, A. Boeddrich, M. Herbst, L. Masino, R. Lurz, S. Engemann, A. Pastore, and E.E. Wanker. 2008. EGCG redirects amyloidogenic polypeptides into unstructured, off-pathway oligomers. *Nat Struct Mol Biol.* 15:558-66.

- Ehrnhoefer, D.E., S.L. Butland, M.A. Pouladi, and M.R. Hayden. 2009. Mouse models of Huntington disease: variations on a theme. *Dis Model Mech.* 2:123-9.
- Ehrnhoefer, D.E., M. Duennwald, P. Markovic, J.L. Wacker, S. Engemann, M. Roark, J. Legleiter, J.L. Marsh, L.M. Thompson, S. Lindquist, P.J. Muchowski, and E.E. Wanker. 2006. Green tea (-)-epigallocatechin-gallate modulates early events in huntingtin misfolding and reduces toxicity in Huntington's disease models. *Hum Mol Genet.* 15:2743-51.
- Ellis, R.J., and A.P. Minton. 2003. Cell biology: join the crowd. *Nature.* 425:27-8.
- Fabrini, R., A. De Luca, L. Stella, G. Mei, B. Orioni, S. Ciccone, G. Federici, M. Lo Bello, and G. Ricci. 2009. Monomer-dimer equilibrium in glutathione transferases: a critical re-examination. *Biochemistry.* 48:10473-82.
- Ferrone, F. 1999. Analysis of protein aggregation kinetics. *Methods Enzymol.* 309:256-74.
- Ferrone, F.A., M. Ivanova, and R. Jasuja. 2002. Heterogeneous nucleation and crowding in sickle hemoglobin: an analytic approach. *Biophys J.* 82:399-406.
- Fersht, A.R. 2000. Transition-state structure as a unifying basis in protein-folding mechanisms: contact order, chain topology, stability, and the extended nucleus mechanism. *Proc Natl Acad Sci U S A.* 97:1525-9.
- Fersht, A.R., A. Matouschek, J. Sancho, L. Serrano, and S. Vuilleumier. 1992. Pathway of protein folding. *Faraday Discuss:*183-93.
- Georgalis, Y., E.B. Starikov, B. Hollenbach, R. Lurz, E. Scherzinger, W. Saenger, H. Lehrach, and E.E. Wanker. 1998. Huntingtin aggregation monitored by dynamic light scattering. *Proc Natl Acad Sci U S A.* 95:6118-21.
- Gerber, H.P., K. Seipel, O. Georgiev, M. Hofferer, M. Hug, S. Rusconi, and W. Schaffner. 1994. Transcriptional activation modulated by homopolymeric glutamine and proline stretches. *Science.* 263:808-11.
- Glabe, C.G. 2004. Conformation-dependent antibodies target diseases of protein misfolding. *Trends Biochem Sci.* 29:542-7.
- Graham, R.K., Y. Deng, J. Carroll, K. Vaid, C. Cowan, M.A. Pouladi, M. Metzler, N. Bissada, L. Wang, R.L. Faull, M. Gray, X.W. Yang, L.A. Raymond, and M.R. Hayden. 2010. Cleavage at the 586 amino acid caspase-6 site in mutant huntingtin influences caspase-6 activation in vivo. *J Neurosci.* 30:15019-29.
- Gu, X., E.R. Greiner, R. Mishra, R. Kodali, A. Osmand, S. Finkbeiner, J.S. Steffan, L.M. Thompson, R. Wetzel, and X.W. Yang. 2009. Serines 13 and 16 are critical determinants of full-length human mutant huntingtin induced disease pathogenesis in HD mice. *Neuron.* 64:828-40.
- Gutekunst, C.A., S.H. Li, H. Yi, J.S. Mulroy, S. Kuemmerle, R. Jones, D. Rye, R.J. Ferrante, S.M. Hersch, and X.J. Li. 1999. Nuclear and neuropil aggregates in Huntington's disease: relationship to neuropathology. *J Neurosci.* 19:2522-34.
- Halfmann, R., and S. Lindquist. 2008. Screening for amyloid aggregation by Semi-Denaturing Detergent-Agarose Gel Electrophoresis. *J Vis Exp.*
- Han, I., Y. You, J.H. Kordower, S.T. Brady, and G.A. Morfini. 2010. Differential vulnerability of neurons in Huntington's disease: the role of cell type-specific features. *J Neurochem.* 113:1073-91.
- Harjes, P., and E.E. Wanker. 2003. The hunt for huntingtin function: interaction partners tell many different stories. *Trends Biochem Sci.* 28:425-33.
- Harper, J.D., and P.T. Lansbury, Jr. 1997. Models of amyloid seeding in Alzheimer's disease and scrapie: mechanistic truths and physiological consequences of the time-dependent solubility of amyloid proteins. *Annu Rev Biochem.* 66:385-407.
- Harper, J.D., C.M. Lieber, and P.T. Lansbury, Jr. 1997. Atomic force microscopic imaging of seeded fibril formation and fibril branching by the Alzheimer's disease amyloid-beta protein. *Chem Biol.* 4:951-9.
- HDCRG. 1993. A novel gene containing a trinucleotide repeat that is expanded and unstable on Huntington's disease chromosomes. The Huntington's Disease Collaborative Research Group. *Cell.* 72:971-83.

- Heiser, V., S. Engemann, W. Brocker, I. Dunkel, A. Boeddrich, S. Waelter, E. Nordhoff, R. Lurz, N. Schugardt, S. Rautenberg, C. Herhaus, G. Barnickel, H. Bottcher, H. Lehrach, and E.E. Wanker. 2002. Identification of benzothiazoles as potential polyglutamine aggregation inhibitors of Huntington's disease by using an automated filter retardation assay. *Proc Natl Acad Sci U S A*. 99 Suppl 4:16400-6.
- Hersch, S.M., and H.D. Rosas. 2001. Neuroprotective therapy for Huntington's disease: new prospects and challenges. *Expert Rev Neurother*. 1:111-8.
- Hol, E.M., and W. Scheper. 2008. Protein quality control in neurodegeneration: walking the tight rope between health and disease. *J Mol Neurosci*. 34:23-33.
- Jahn, T.R., O.S. Makin, K.L. Morris, K.E. Marshall, P. Tian, P. Sikorski, and L.C. Serpell. 2010. The common architecture of cross-beta amyloid. *J Mol Biol*. 395:717-27.
- Jana, N.R., E.A. Zemskov, G. Wang, and N. Nukina. 2001. Altered proteasomal function due to the expression of polyglutamine-expanded truncated N-terminal huntingtin induces apoptosis by caspase activation through mitochondrial cytochrome c release. *Hum Mol Genet*. 10:1049-59.
- Johnston, J.A., C.L. Ward, and R.R. Kopito. 1998. Aggresomes: a cellular response to misfolded proteins. *J Cell Biol*. 143:1883-98.
- Kayed, R., E. Head, J.L. Thompson, T.M. McIntire, S.C. Milton, C.W. Cotman, and C.G. Glabe. 2003. Common structure of soluble amyloid oligomers implies common mechanism of pathogenesis. *Science*. 300:486-9.
- Kazantsev, A., E. Preisinger, A. Dranovsky, D. Goldgaber, and D. Housman. 1999. Insoluble detergent-resistant aggregates form between pathological and nonpathological lengths of polyglutamine in mammalian cells. *Proc Natl Acad Sci U S A*. 96:11404-9.
- Kegel, K.B., E. Sapp, J. Alexander, P. Reeves, D. Bleckmann, L. Sobin, N. Masso, A. Valencia, H. Jeong, D. Krainc, J. Palacino, D. Curtis, R. Kuhn, C. Betschart, M. Sena-Esteves, N. Aronin, P. Paganetti, and M. Difiglia. 2010. Huntingtin cleavage product A forms in neurons and is reduced by gamma-secretase inhibitors. *Mol Neurodegener*. 5:58.
- Kelly, J.W., and W.E. Balch. 2003. Amyloid as a natural product. *J Cell Biol*. 161:461-2.
- Khoshnan, A., J. Ko, and P.H. Patterson. 2002. Effects of intracellular expression of anti-huntingtin antibodies of various specificities on mutant huntingtin aggregation and toxicity. *Proc Natl Acad Sci U S A*. 99:1002-7.
- Kim, M.W., Y. Chelliah, S.W. Kim, Z. Otwinowski, and I. Bezprozvanny. 2009. Secondary structure of Huntingtin amino-terminal region. *Structure*. 17:1205-12.
- Klunk, W.E., J.W. Pettegrew, and D.J. Abraham. 1989. Quantitative evaluation of congo red binding to amyloid-like proteins with a beta-pleated sheet conformation. *J Histochem Cytochem*. 37:1273-81.
- Krebs, M.R., L.A. Morozova-Roche, K. Daniel, C.V. Robinson, and C.M. Dobson. 2004. Observation of sequence specificity in the seeding of protein amyloid fibrils. *Protein Sci*. 13:1933-8.
- Lajoie, P., and E.L. Snapp. 2010. Formation and toxicity of soluble polyglutamine oligomers in living cells. *PLoS One*. 5:e15245.
- Lakhani, V.V., F. Ding, and N.V. Dokholyan. 2010. Polyglutamine induced misfolding of huntingtin exon1 is modulated by the flanking sequences. *PLoS Comput Biol*. 6:e1000772.
- Landles, C., and G.P. Bates. 2004. Huntingtin and the molecular pathogenesis of Huntington's disease. Fourth in molecular medicine review series. *EMBO Rep*. 5:958-63.
- Landles, C., K. Sathasivam, A. Weiss, B. Woodman, H. Moffitt, S. Finkbeiner, B. Sun, J. Gafni, L.M. Ellerby, Y. Trottier, W.G. Richards, A. Osmand, P. Paganetti, and G.P. Bates. 2010. Proteolysis of mutant huntingtin produces an exon 1 fragment that accumulates as an aggregated protein in neuronal nuclei in Huntington disease. *J Biol Chem*. 285:8808-23.

- Lashuel, H.A., D. Hartley, B.M. Petre, T. Walz, and P.T. Lansbury, Jr. 2002. Neurodegenerative disease: amyloid pores from pathogenic mutations. *Nature*. 418:291.
- Lee, C.C., R.H. Walters, and R.M. Murphy. 2007. Reconsidering the mechanism of polyglutamine peptide aggregation. *Biochemistry*. 46:12810-20.
- Legleiter, J., G.P. Lotz, J. Miller, J. Ko, C. Ng, G.L. Williams, S. Finkbeiner, P.H. Patterson, and P.J. Muchowski. 2009. Monoclonal antibodies recognize distinct conformational epitopes formed by polyglutamine in a mutant huntingtin fragment. *J Biol Chem*. 284:21647-58.
- Legleiter, J., E. Mitchell, G.P. Lotz, E. Sapp, C. Ng, M. DiFiglia, L.M. Thompson, and P.J. Muchowski. 2010. Mutant huntingtin fragments form oligomers in a polyglutamine length-dependent manner in vitro and in vivo. *J Biol Chem*. 285:14777-90.
- LeVine, H., 3rd. 1999. Quantification of beta-sheet amyloid fibril structures with thioflavin T. *Methods Enzymol*. 309:274-84.
- Li, P., K.E. Huey-Tubman, T. Gao, X. Li, A.P. West, Jr., M.J. Bennett, and P.J. Bjorkman. 2007. The structure of a polyQ-anti-polyQ complex reveals binding according to a linear lattice model. *Nat Struct Mol Biol*. 14:381-7.
- Li, W., L.C. Serpell, W.J. Carter, D.C. Rubinsztein, and J.A. Huntington. 2006. Expression and characterization of full-length human huntingtin, an elongated HEAT repeat protein. *J Biol Chem*. 281:15916-22.
- Lin, M.T., and M.F. Beal. 2006. Mitochondrial dysfunction and oxidative stress in neurodegenerative diseases. *Nature*. 443:787-95.
- Lotz, G.P., J. Legleiter, R. Aron, E.J. Mitchell, S.Y. Huang, C. Ng, C. Glabe, L.M. Thompson, and P.J. Muchowski. 2010. Hsp70 and Hsp40 functionally interact with soluble mutant huntingtin oligomers in a classic ATP-dependent reaction cycle. *J Biol Chem*. 285:38183-93.
- Lunkes, A., K.S. Lindenberg, L. Ben-Haiem, C. Weber, D. Devys, G.B. Landwehrmeyer, J.L. Mandel, and Y. Trottier. 2002. Proteases acting on mutant huntingtin generate cleaved products that differentially build up cytoplasmic and nuclear inclusions. *Mol Cell*. 10:259-69.
- Mangiarini, L., K. Sathasivam, M. Seller, B. Cozens, A. Harper, C. Hetherington, M. Lawton, Y. Trottier, H. Lehrach, S.W. Davies, and G.P. Bates. 1996. Exon 1 of the HD gene with an expanded CAG repeat is sufficient to cause a progressive neurological phenotype in transgenic mice. *Cell*. 87:493-506.
- Marsh, J.L., J. Pallos, and L.M. Thompson. 2003. Fly models of Huntington's disease. *Hum Mol Genet*. 12 Spec No 2:R187-93.
- Morimoto, R.I. 2008. Proteotoxic stress and inducible chaperone networks in neurodegenerative disease and aging. *Genes Dev*. 22:1427-38.
- Morris, A.M., M.A. Watzky, J.N. Agar, and R.G. Finke. 2008. Fitting neurological protein aggregation kinetic data via a 2-step, minimal/"Ockham's razor" model: the Finke-Watzky mechanism of nucleation followed by autocatalytic surface growth. *Biochemistry*. 47:2413-27.
- Morris, A.M., M.A. Watzky, and R.G. Finke. 2009. Protein aggregation kinetics, mechanism, and curve-fitting: a review of the literature. *Biochim Biophys Acta*. 1794:375-97.
- Muchowski, P.J. 2002. Protein misfolding, amyloid formation, and neurodegeneration: a critical role for molecular chaperones? *Neuron*. 35:9-12.
- Muchowski, P.J., G. Schaffar, A. Sittler, E.E. Wanker, M.K. Hayer-Hartl, and F.U. Hartl. 2000. Hsp70 and hsp40 chaperones can inhibit self-assembly of polyglutamine proteins into amyloid-like fibrils. *Proc Natl Acad Sci U S A*. 97:7841-6.
- Nagai, Y., T. Inui, H.A. Popiel, N. Fujikake, K. Hasegawa, Y. Urade, Y. Goto, H. Naiki, and T. Toda. 2007. A toxic monomeric conformer of the polyglutamine protein. *Nat Struct Mol Biol*. 14:332-40.
- Nasir, J., S.B. Floresco, J.R. O'Kusky, V.M. Diewert, J.M. Richman, J. Zeisler, A. Borowski, J.D. Marth, A.G. Phillips, and M.R. Hayden. 1995. Targeted disruption of the

- Huntington's disease gene results in embryonic lethality and behavioral and morphological changes in heterozygotes. *Cell*. 81:811-23.
- Nekooki-Machida, Y., M. Kurosawa, N. Nukina, K. Ito, T. Oda, and M. Tanaka. 2009. Distinct conformations of in vitro and in vivo amyloids of huntingtin-exon1 show different cytotoxicity. *Proc Natl Acad Sci U S A*. 106:9679-84.
- Nguyen, J., M.A. Baldwin, F.E. Cohen, and S.B. Prusiner. 1995. Prion protein peptides induce alpha-helix to beta-sheet conformational transitions. *Biochemistry*. 34:4186-92.
- O'Nuallain, B., and R. Wetzel. 2002. Conformational Abs recognizing a generic amyloid fibril epitope. *Proc Natl Acad Sci U S A*. 99:1485-90.
- Ohlson, S. 2008. Designing transient binding drugs: a new concept for drug discovery. *Drug Discov Today*. 13:433-9.
- Oz, M., D.E. Lorke, and G.A. Petroianu. 2009. Methylene blue and Alzheimer's disease. *Biochem Pharmacol*. 78:927-32.
- Pauling, L., R.B. Corey, and H.R. Branson. 1951. The structure of proteins; two hydrogen-bonded helical configurations of the polypeptide chain. *Proc Natl Acad Sci U S A*. 37:205-11.
- Perutz, M.F., J.T. Finch, J. Berriman, and A. Lesk. 2002. Amyloid fibers are water-filled nanotubes. *Proc Natl Acad Sci U S A*. 99:5591-5.
- Perutz, M.F., T. Johnson, M. Suzuki, and J.T. Finch. 1994. Glutamine repeats as polar zippers: their possible role in inherited neurodegenerative diseases. *Proc Natl Acad Sci U S A*. 91:5355-8.
- Poirier, M.A., H. Jiang, and C.A. Ross. 2005. A structure-based analysis of huntingtin mutant polyglutamine aggregation and toxicity: evidence for a compact beta-sheet structure. *Hum Mol Genet*. 14:765-74.
- Poirier, M.A., H. Li, J. Macosko, S. Cai, M. Amzel, and C.A. Ross. 2002. Huntingtin spheroids and protofibrils as precursors in polyglutamine fibrillization. *J Biol Chem*. 277:41032-7.
- Poon, L.H., G.A. Kang, and A.J. Lee. 2010. Role of tetrabenazine for Huntington's disease-associated chorea. *Ann Pharmacother*. 44:1080-9.
- Powers, E.T., and D.L. Powers. 2008. Mechanisms of protein fibril formation: nucleated polymerization with competing off-pathway aggregation. *Biophys J*. 94:379-91.
- Preisinger, E., B.M. Jordan, A. Kazantsev, and D. Housman. 1999. Evidence for a recruitment and sequestration mechanism in Huntington's disease. *Philos Trans R Soc Lond B Biol Sci*. 354:1029-34.
- Ptitsyn, O.B. 1995. Molten globule and protein folding. *Adv Protein Chem*. 47:83-229.
- Ptitsyn, O.B., and A.A. Rashin. 1975. A model of myoglobin self-organization. *Biophys Chem*. 3:1-20.
- Qiu, Z., F. Norflus, B. Singh, M.K. Swindell, R. Buzescu, M. Bejarano, R. Chopra, B. Zucker, C.L. Benn, D.P. DiRocco, J.H. Cha, R.J. Ferrante, and S.M. Hersch. 2006. Sp1 is up-regulated in cellular and transgenic models of Huntington disease, and its reduction is neuroprotective. *J Biol Chem*. 281:16672-80.
- Ramshini, H., C. Parrini, A. Relini, M. Zampagni, B. Mannini, A. Pesce, A.A. Saboury, M. Nemat-Gorgani, and F. Chiti. 2011. Large proteins have a great tendency to aggregate but a low propensity to form amyloid fibrils. *PLoS One*. 6:e16075.
- Rochet, J.C., and P.T. Lansbury, Jr. 2000. Amyloid fibrillogenesis: themes and variations. *Curr Opin Struct Biol*. 10:60-8.
- Ross, C.A., and M.A. Poirier. 2004. Protein aggregation and neurodegenerative disease. *Nat Med*. 10 Suppl:S10-7.
- Rubinsztein, D.C., J. Leggo, R. Coles, E. Almqvist, V. Biancalana, J.J. Cassiman, K. Chotai, M. Connarty, D. Crauford, A. Curtis, D. Curtis, M.J. Davidson, A.M. Differ, C. Dode, A. Dodge, M. Frontali, N.G. Ranen, O.C. Stine, M. Sherr, M.H. Abbott, M.L. Franz, C.A. Graham, P.S. Harper, J.C. Hedreen, M.R. Hayden, and et al. 1996. Phenotypic characterization of individuals with 30-40 CAG repeats in the Huntington disease (HD) gene reveals HD cases with 36 repeats and apparently normal elderly individuals with 36-39 repeats. *Am J Hum Genet*. 59:16-22.

- Sassone, J., C. Colciago, G. Cislighi, V. Silani, and A. Ciammola. 2009. Huntington's disease: the current state of research with peripheral tissues. *Exp Neurol.* 219:385-97.
- Sathasivam, K., A. Lane, J. Legleiter, A. Warley, B. Woodman, S. Finkbeiner, P. Paganetti, P.J. Muchowski, S. Wilson, and G.P. Bates. 2010. Identical oligomeric and fibrillar structures captured from the brains of R6/2 and knock-in mouse models of Huntington's disease. *Hum Mol Genet.* 19:65-78.
- Saudou, F., S. Finkbeiner, D. Devys, and M.E. Greenberg. 1998. Huntingtin acts in the nucleus to induce apoptosis but death does not correlate with the formation of intranuclear inclusions. *Cell.* 95:55-66.
- Sawaya, M.R., S. Sambashivan, R. Nelson, M.I. Ivanova, S.A. Sievers, M.I. Apostol, M.J. Thompson, M. Balbirnie, J.J. Wiltzius, H.T. McFarlane, A.O. Madsen, C. Riek, and D. Eisenberg. 2007. Atomic structures of amyloid cross-beta spines reveal varied steric zippers. *Nature.* 447:453-7.
- Schaffar, G., P. Breuer, R. Boteva, C. Behrends, N. Tzvetkov, N. Strippel, H. Sakahira, K. Siegers, M. Hayer-Hartl, and F.U. Hartl. 2004. Cellular toxicity of polyglutamine expansion proteins: mechanism of transcription factor deactivation. *Mol Cell.* 15:95-105.
- Scherzinger, E., R. Lurz, M. Turmaine, L. Mangiarini, B. Hollenbach, R. Hasenbank, G.P. Bates, S.W. Davies, H. Lehrach, and E.E. Wanker. 1997. Huntingtin-encoded polyglutamine expansions form amyloid-like protein aggregates in vitro and in vivo. *Cell.* 90:549-58.
- Scherzinger, E., A. Sittler, K. Schweiger, V. Heiser, R. Lurz, R. Hasenbank, G.P. Bates, H. Lehrach, and E.E. Wanker. 1999. Self-assembly of polyglutamine-containing huntingtin fragments into amyloid-like fibrils: implications for Huntington's disease pathology. *Proc Natl Acad Sci U S A.* 96:4604-9.
- Scheuner, D., C. Eckman, M. Jensen, X. Song, M. Citron, N. Suzuki, T.D. Bird, J. Hardy, M. Hutton, W. Kukull, E. Larson, E. Levy-Lahad, M. Viitanen, E. Peskind, P. Poorkaj, G. Schellenberg, R. Tanzi, W. Wasco, L. Lannfelt, D. Selkoe, and S. Younkin. 1996. Secreted amyloid beta-protein similar to that in the senile plaques of Alzheimer's disease is increased in vivo by the presenilin 1 and 2 and APP mutations linked to familial Alzheimer's disease. *Nat Med.* 2:864-70.
- Serio, T.R., A.G. Cashikar, A.S. Kowal, G.J. Sawicki, J.J. Moslehi, L. Serpell, M.F. Arnsdorf, and S.L. Lindquist. 2000. Nucleated conformational conversion and the replication of conformational information by a prion determinant. *Science.* 289:1317-21.
- Sharma, D., L.M. Shinchuk, H. Inouye, R. Wetzel, and D.A. Kirschner. 2005. Polyglutamine homopolymers having 8-45 residues form slablike beta-crystallite assemblies. *Proteins.* 61:398-411.
- Shirahama, T., and A.S. Cohen. 1967. High-resolution electron microscopic analysis of the amyloid fibril. *J Cell Biol.* 33:679-708.
- Sikorski, P., and E. Atkins. 2005. New model for crystalline polyglutamine assemblies and their connection with amyloid fibrils. *Biomacromolecules.* 6:425-32.
- Sivanandam, V.N., M. Jayaraman, C.L. Hoop, R. Kodali, R. Wetzel, and P.C. van der Wel. 2011. The aggregation-enhancing huntingtin N-terminus is helical in amyloid fibrils. *J Am Chem Soc.* 133:4558-66.
- Soto, C. 2003. Unfolding the role of protein misfolding in neurodegenerative diseases. *Nat Rev Neurosci.* 4:49-60.
- Squitieri, F., C. Gellera, M. Cannella, C. Mariotti, G. Cislighi, D.C. Rubinsztein, E.W. Almqvist, D. Turner, A.C. Bachoud-Levi, S.A. Simpson, M. Delatycki, V. Maglione, M.R. Hayden, and S.D. Donato. 2003. Homozygosity for CAG mutation in Huntington disease is associated with a more severe clinical course. *Brain.* 126:946-55.
- Steffan, J.S., A. Kazantsev, O. Spasic-Boskovic, M. Greenwald, Y.Z. Zhu, H. Gohler, E.E. Wanker, G.P. Bates, D.E. Housman, and L.M. Thompson. 2000. The Huntington's disease protein interacts with p53 and CREB-binding protein and represses transcription. *Proc Natl Acad Sci U S A.* 97:6763-8.

- Strong, T.V., D.A. Tagle, J.M. Valdes, L.W. Elmer, K. Boehm, M. Swaroop, K.W. Kaatz, F.S. Collins, and R.L. Albin. 1993. Widespread expression of the human and rat Huntington's disease gene in brain and nonneural tissues. *Nat Genet.* 5:259-65.
- Sunde, M., and C. Blake. 1997. The structure of amyloid fibrils by electron microscopy and X-ray diffraction. *Adv Protein Chem.* 50:123-59.
- Takahashi, T., S. Kikuchi, S. Katada, Y. Nagai, M. Nishizawa, and O. Onodera. 2008. Soluble polyglutamine oligomers formed prior to inclusion body formation are cytotoxic. *Hum Mol Genet.* 17:345-56.
- Tam, S., C. Spiess, W. Auyeung, L. Joachimiak, B. Chen, M.A. Poirier, and J. Frydman. 2009. The chaperonin TRiC blocks a huntingtin sequence element that promotes the conformational switch to aggregation. *Nat Struct Mol Biol.* 16:1279-85.
- Taylor, J.P., J. Hardy, and K.H. Fischbeck. 2002. Toxic proteins in neurodegenerative disease. *Science.* 296:1991-5.
- Terry, R.D., E. Masliah, D.P. Salmon, N. Butters, R. DeTeresa, R. Hill, L.A. Hansen, and R. Katzman. 1991. Physical basis of cognitive alterations in Alzheimer's disease: synapse loss is the major correlate of cognitive impairment. *Ann Neurol.* 30:572-80.
- Thakur, A.K., M. Jayaraman, R. Mishra, M. Thakur, V.M. Chellgren, I.J. Byeon, D.H. Anjum, R. Kodali, T.P. Creamer, J.F. Conway, A.M. Gronenborn, and R. Wetzel. 2009. Polyglutamine disruption of the huntingtin exon 1 N terminus triggers a complex aggregation mechanism. *Nat Struct Mol Biol.* 16:380-9.
- Thakur, A.K., and R. Wetzel. 2002. Mutational analysis of the structural organization of polyglutamine aggregates. *Proc Natl Acad Sci U S A.* 99:17014-9.
- Thompson, P.D., A. Berardelli, J.C. Rothwell, B.L. Day, J.P. Dick, R. Benecke, and C.D. Marsden. 1988. The coexistence of bradykinesia and chorea in Huntington's disease and its implications for theories of basal ganglia control of movement. *Brain.* 111 (Pt 2):223-44.
- Tompa, P. 2002. Intrinsically unstructured proteins. *Trends Biochem Sci.* 27:527-33.
- Tompkins, M.M., and W.D. Hill. 1997. Contribution of somal Lewy bodies to neuronal death. *Brain Res.* 775:24-9.
- Vonsattel, J.P., R.H. Myers, T.J. Stevens, R.J. Ferrante, E.D. Bird, and E.P. Richardson, Jr. 1985. Neuropathological classification of Huntington's disease. *J Neuropathol Exp Neurol.* 44:559-77.
- Wacker, J.L., M.H. Zareie, H. Fong, M. Sarikaya, and P.J. Muchowski. 2004. Hsp70 and Hsp40 attenuate formation of spherical and annular polyglutamine oligomers by partitioning monomer. *Nat Struct Mol Biol.* 11:1215-22.
- Waelter, S., A. Boeddrich, R. Lurz, E. Scherzinger, G. Lueder, H. Lehrach, and E.E. Wanker. 2001. Accumulation of mutant huntingtin fragments in aggresome-like inclusion bodies as a result of insufficient protein degradation. *Mol Biol Cell.* 12:1393-407.
- Walker, F.O. 2007. Huntington's disease. *Lancet.* 369:218-28.
- Walsh, D.M., A. Lomakin, G.B. Benedek, M.M. Condron, and D.B. Teplow. 1997. Amyloid beta-protein fibrillogenesis. Detection of a protofibrillar intermediate. *J Biol Chem.* 272:22364-72.
- Warby, S.C., E.Y. Chan, M. Metzler, L. Gan, R.R. Singaraja, S.F. Crocker, H.A. Robertson, and M.R. Hayden. 2005. Huntingtin phosphorylation on serine 421 is significantly reduced in the striatum and by polyglutamine expansion in vivo. *Hum Mol Genet.* 14:1569-77.
- Watzky, M.A., A.M. Morris, E.D. Ross, and R.G. Finke. 2008. Fitting yeast and mammalian prion aggregation kinetic data with the Finke-Watzky two-step model of nucleation and autocatalytic growth. *Biochemistry.* 47:10790-800.
- Wellington, C.L., L.M. Ellerby, C.A. Gutekunst, D. Rogers, S. Warby, R.K. Graham, O. Loubser, J. van Raamsdonk, R. Singaraja, Y.Z. Yang, J. Gafni, D. Bredesen, S.M. Hersch, B.R. Leavitt, S. Roy, D.W. Nicholson, and M.R. Hayden. 2002. Caspase cleavage of mutant huntingtin precedes neurodegeneration in Huntington's disease. *J Neurosci.* 22:7862-72.
- Whitford, D. 2005. *Proteins Structure and Function.* Wiley.

- Williamson, T.E., A. Vitalis, S.L. Crick, and R.V. Pappu. 2010. Modulation of polyglutamine conformations and dimer formation by the N-terminus of huntingtin. *J Mol Biol.* 396:1295-309.
- Wolynes, P.G., J.N. Onuchic, and D. Thirumalai. 1995. Navigating the folding routes. *Science.* 267:1619-20.
- Wytenbach, A., J. Carmichael, J. Swartz, R.A. Furlong, Y. Narain, J. Rankin, and D.C. Rubinsztein. 2000. Effects of heat shock, heat shock protein 40 (HDJ-2), and proteasome inhibition on protein aggregation in cellular models of Huntington's disease. *Proc Natl Acad Sci U S A.* 97:2898-903.
- Xia, J., D.H. Lee, J. Taylor, M. Vandelft, and R. Truant. 2003. Huntingtin contains a highly conserved nuclear export signal. *Hum Mol Genet.* 12:1393-403.
- Xue, W.F., A.L. Hellewell, W.S. Gosal, S.W. Homans, E.W. Hewitt, and S.E. Radford. 2009. Fibril fragmentation enhances amyloid cytotoxicity. *J Biol Chem.* 284:34272-82.
- Yamamoto, A., J.J. Lucas, and R. Hen. 2000. Reversal of neuropathology and motor dysfunction in a conditional model of Huntington's disease. *Cell.* 101:57-66.
- Yanai, A., K. Huang, R. Kang, R.R. Singaraja, P. Arstikaitis, L. Gan, P.C. Orban, A. Mullard, C.M. Cowan, L.A. Raymond, R.C. Drisdell, W.N. Green, B. Ravikumar, D.C. Rubinsztein, A. El-Husseini, and M.R. Hayden. 2006. Palmitoylation of huntingtin by HIP14 is essential for its trafficking and function. *Nat Neurosci.* 9:824-31.
- Yang, F., G.P. Lim, A.N. Begum, O.J. Ubada, M.R. Simmons, S.S. Ambegaokar, P.P. Chen, R. Kaye, C.G. Glabe, S.A. Frautschy, and G.M. Cole. 2005. Curcumin inhibits formation of amyloid beta oligomers and fibrils, binds plaques, and reduces amyloid in vivo. *J Biol Chem.* 280:5892-901.
- Zeitlin, S., J.P. Liu, D.L. Chapman, V.E. Papaioannou, and A. Efstratiadis. 1995. Increased apoptosis and early embryonic lethality in mice nullizygous for the Huntington's disease gene homologue. *Nat Genet.* 11:155-63.
- Zhang, Q.C., T.L. Yeh, A. Leyva, L.G. Frank, J. Miller, Y.E. Kim, R. Langen, S. Finkbeiner, M.L. Amzel, C.A. Ross, and M.A. Poirier. 2011. A compact {beta} model of huntingtin toxicity. *J Biol Chem.*
- Zhang, X., D.L. Smith, A.B. Meriin, S. Engemann, D.E. Russel, M. Roark, S.L. Washington, M.M. Maxwell, J.L. Marsh, L.M. Thompson, E.E. Wanker, A.B. Young, D.E. Housman, G.P. Bates, M.Y. Sherman, and A.G. Kazantsev. 2005. A potent small molecule inhibits polyglutamine aggregation in Huntington's disease neurons and suppresses neurodegeneration in vivo. *Proc Natl Acad Sci U S A.* 102:892-7.
- Zuccato, C., A. Ciammola, D. Rigamonti, B.R. Leavitt, D. Goffredo, L. Conti, M.E. MacDonald, R.M. Friedlander, V. Silani, M.R. Hayden, T. Timmusk, S. Sipione, and E. Cattaneo. 2001. Loss of huntingtin-mediated BDNF gene transcription in Huntington's disease. *Science.* 293:493-8.
- Zuccato, C., M. Tartari, A. Crotti, D. Goffredo, M. Valenza, L. Conti, T. Cataudella, B.R. Leavitt, M.R. Hayden, T. Timmusk, D. Rigamonti, and E. Cattaneo. 2003. Huntingtin interacts with REST/NRSF to modulate the transcription of NRSE-controlled neuronal genes. *Nat Genet.* 35:76-83.

6. List of Abbreviations

AD	Alzheimer's disease
AFM	atomic force microscopy
APS	ammonium persulfate
ATP	adenosine triphosphate
bp	base pairs
BSA	bovine serum albumin
CD	circular dichroism
Curc	Curcumin
DLS	dynamic light scattering
DMEM	Dulbecco's modified Eagle medium
DMSO	dimethylsulfoxide
DNA	deoxyribonucleic acid
EDTA	ethylenediamine tetraacetic acid
EM	electron microscopy
Ex1	exon 1
FRA	filter retardation assay
FRET	fluorescence resonance energy transfer
GST	glutathione-S transferase
HD	Huntington's disease
Htt	Huntingtin
IB	inclusion body
IPTG	isopropyl-3-D-thiogalactopyranoside
IUP	intrinsically unstructured protein
MB	methylene blue
MSN	medium spiny neurons
MTT	3-(4,5-dimethylthiazol-2-yl)-2,5-diphenyltetrazolium bromide
NCC	nucleated conformational conversion
NII	neuronal intranuclear inclusion
Orc	orcein
PBS	phospho-buffered saline
PD	Parkinson's disease
PFA	paraformaldehyde
polyQ	polyglutamine
PP	PreScission Protease
Res	resorufin
SDD-AGE	semi-denaturing detergent agarose gel electrophoreses
SDS-PAGE	sodium dodecyl sulphate polyacrylamide gel electrophoreses
SEC	size exclusion chromatography
TBS	tris-buffered saline
TCA	Trischloroacetic acid
ThT	Thioflavin T
TRX	Thioredoxin
UV	ultraviolet
WT	wildtype
YFP	yellow fluorescent protein